



POLITECNICO
MILANO 1863

SCUOLA DI INGEGNERIA INDUSTRIALE
E DELL'INFORMAZIONE

Unsteady turbine flow analysis by PIV data processing

TESI DI LAUREA MAGISTRALE IN
AERONAUTICAL ENGINEERING - INGEGNERIA AERONAUTICA

Author: **Srinath Srinivasan**

Student ID: 925814 (10687821)

Advisor: Prof. Gaetani Paolo

Co-advisors: Prof. Sergio Lavagnoli

Academic Year: 2022-23

Abstract

In this present work, the flow quantities have been extracted from experimental PIV data obtained in a high-speed high-pressure turbine from the facility of Von Karman Institute of fluid dynamics. The extraction of flow quantities starts from the data that has been obtained in the form of hundreds of images. Before capturing the images, the flow field is injected with the tracer particles and these particles scatter the light when the laser sheet falls on them. These images are captured with the help of a high-speed camera when an endoscope delivers the laser sheet to the region of interest and a plano-concave window that provides the optical access for the measurement in the annular test section. After the acquisition of PIV images, it is found that the image has lot of noise and background reflections. Even the contrast of the images has to be improved. So, for the improvement of contrast, two filters named CLAHE and the Min/Max intensity normalization has been compared and provided with the result. In the case of background removal, Sobel, Temporal and POD have been compared. Both these contrast enhancement filters and the background removal filters are sensitive to noises. In contrast enhancement case, they intensify the local noise and in the case background removal, they allow noise to pass through the filter. It is important to have the denoising filter in order to improve the signal to noise ratio. Hence, the Gaussian filter and the Bilateral filter are compared in this case. After the image pre-processing, the images are then processed for the evaluation of the velocity flow fields. A test matrix with different parameters like initial and final window size, initial and final window overlap percentage, number of passes, peak to peak threshold value etc., are altered or optimized in such a way to have the best output of it. There are few uncertainties that are associated with the PIV evaluation especially the out-of-the-plane (plane that is normal to laser sheet) velocity components are evaluated in the present work. Finally, the PIV result is being compared with the available experimental data (5 hole probe) and the CFD (RANS) predictions.

Keywords: PIV image Enhancement, PIV evaluation, High-speed high-pressure turbine, Highpass filter, Lowpass filter, Contrast Enhancement

Abstract in lingua italiana

In questo lavoro, le quantità di flusso sono state estratte da dati sperimentali PIV ottenuti in una turbina ad alta pressione ad alta velocità dalla struttura del Von Karman Institute of fluidodinamica. L'estrazione delle quantità di flusso parte dai dati che sono stati ottenuti sotto forma di centinaia di immagini. Prima di acquisire le immagini, il campo di flusso viene iniettato con le particelle traccianti e queste particelle disperdono la luce quando il foglio laser cade su di esse. Queste immagini vengono acquisite con l'aiuto di una telecamera ad alta velocità quando un endoscopio fornisce il foglio laser alla regione di interesse e una finestra piano-concava che fornisce l'accesso ottico per la misurazione nella sezione di test anulare. Dopo l'acquisizione delle immagini PIV, si scopre che l'immagine presenta molto rumore e riflessi di sfondo. Anche il contrasto delle immagini deve essere migliorato. Quindi, per il miglioramento del contrasto, sono stati confrontati e forniti con il risultato due filtri denominati CLAHE e la normalizzazione dell'intensità Min/Max. In caso di rimozione dello sfondo sono stati confrontati Sobel, Temporal e POD. Sia questi filtri di miglioramento del contrasto che i filtri di rimozione dello sfondo sono sensibili ai rumori. Nel caso di miglioramento del contrasto, intensificano il rumore locale e nel caso di rimozione dello sfondo, consentono al rumore di passare attraverso il filtro. È importante avere il filtro denoising per migliorare il rapporto segnale/rumore. Quindi, in questo caso, vengono confrontati il filtro gaussiano e il filtro bilaterale. Dopo la pre-elaborazione dell'immagine, le immagini vengono quindi elaborate per la valutazione dei campi di flusso di velocità. Una matrice di test con diversi parametri come la dimensione della finestra iniziale e finale, la percentuale di sovrapposizione della finestra iniziale e finale, il numero di passaggi, il valore di soglia da picco a picco ecc., vengono alterati o ottimizzati in modo tale da ottenere il miglior risultato. Ci sono poche incertezze associate alla valutazione PIV, in particolare le componenti della velocità fuori dal piano (piano che è normale al foglio laser) sono valutate nel presente lavoro. Infine, il risultato PIV viene confrontato con i dati sperimentali disponibili e le previsioni CFD.

Parole chiave: Miglioramento dell'immagine PIV, valutazione PIV, turbina ad alta pressione ad alta velocità, filtro passa alto, filtro passa basso, miglioramento del contrasto

Contents

Abstract	i
Abstract in lingua italiana	iii
Contents	v
1 Introduction to PIV	1
1.1 Historical background	1
1.2 Principles of measuring velocities	3
1.3 Principle of Particle Image Velocimetry (PIV)	4
1.3.1 Multi-pass Filter	7
1.3.2 Initial, final: Window size and the Overlap percentage	7
1.3.3 Peak-to-Peak Ratio	8
1.3.4 Cross-Correlation Map	8
2 Experimental Design and Setup	11
3 Image Pre-Processing	19
3.1 Contrast Enhancement	20
3.1.1 Min/Max intensity Normalization	20
3.1.2 CLAHE	24
3.2 Background Removal	29
3.2.1 Sobel	30
3.2.2 Temporal	35
3.2.3 Proper Orthogonal Decomposition (POD)	37
3.3 Denoising (Smoothing)	41
3.3.1 Bilateral and Gaussian	41
3.4 Combinations of Pre-Processing filters	43
3.4.1 CLAHE+Lowpass(Bilateral)	44

3.4.2	CLAHE + Lowpass (Bilateral) + Highpass (Sobel)	46
3.4.3	CLAHE + POD with 100 percent and 98 percent particle recovery + Lowpass (Bilateral)	49
3.5	Conclusion for Pre-Processing of PIV images	53
4	PIV image Processing	61
4.1	Multi-pass filter	61
4.2	Initial and Final window sizes	62
4.3	Initial and Final overlap percentage	63
4.4	Conclusion for the best PIV settings	64
4.4.1	Conclusion for the Initial and the Final window size	64
4.4.2	Conclusion for the Initial and the Final overlap percentage	65
4.4.3	Conclusion for Peak-to-Peak threshold value	66
5	Uncertainty analysis	69
5.1	Uncertainty due to out-of-the-plane vectors	69
6	Comparison with CFD predictions and available experimental data	77
7	Conclusion	81
	Bibliography	83
A	Appendix A	87
A.1	Code for Contrast Limited Adaptive Histogram Equalization (CLAHE) . .	87
A.2	Code for Bilateral smoothing	88
B	Appendix B	91
B.1	Mathematical modelling of edges in an image	91
B.2	Convolution Operation	92
B.3	Working of sobel operator	94
C	Appendix C	97
C.1	Histogram Equalization	97
C.2	Adaptive Histogram Equalization	98
C.3	Contrast Limited Adaptive Histogram Equalization (CLAHE)	99

List of Figures	101
List of Tables	107
List of Symbols	109
Acknowledgements	111

1 | Introduction to PIV

1.1. Historical background

Human beings give high importance in observing the nature as it is very useful for the survival. Human senses are well adapted to the moving objects because of its promising food and even in some cases they save from danger. A qualitative measurement can be made with a simple experiment like a piece of wood in the flowing water that gives a rough estimate in velocity of the flowing water and also can provide the information regarding the swirls, wakes behind any obstacles (if present), etc. The first necessary step beyond pure qualitative visualization was the ability to record the observed flow patterns. The major breakthrough at qualitative visualization was made in the late 19th century, early 20th century, when it was possible to store pictures or even movies by means of photographic recording techniques. Noteworthy are the efforts of both ETIENNE – JULES MAREY and FRIEDRICH AHLBORN visualizing turbulence in air and water. In particular AHLBORN describes two types of measurements. One with the help of Aluminum powder or lycopodium seeds for surface flow visualization and the other with the help of flash illumination technique where the sub surface particles are visualized in a water tunnel with illumination through a narrow slit window. LUDWING PRANDTL, one of the most prominent representatives of fluid mechanics in the 19th century, a well-known promoter and user of such flow visualization methods, who designed and utilized flow visualization techniques in a water channel to study the unsteady separated flows behind the wings and other objects following the procedures developed by AHLBORN. One of the best examples similar to PIV was done by PRANDTL where in his experiment, with the help of the flash lamp, he illuminated twice the surface of the fluid within a short interval of time to trace the particles at each illumination. Now, simply said, it is possible to determine the local flow velocity from the local displacement of the tracer particles and the time interval between the two illuminations.

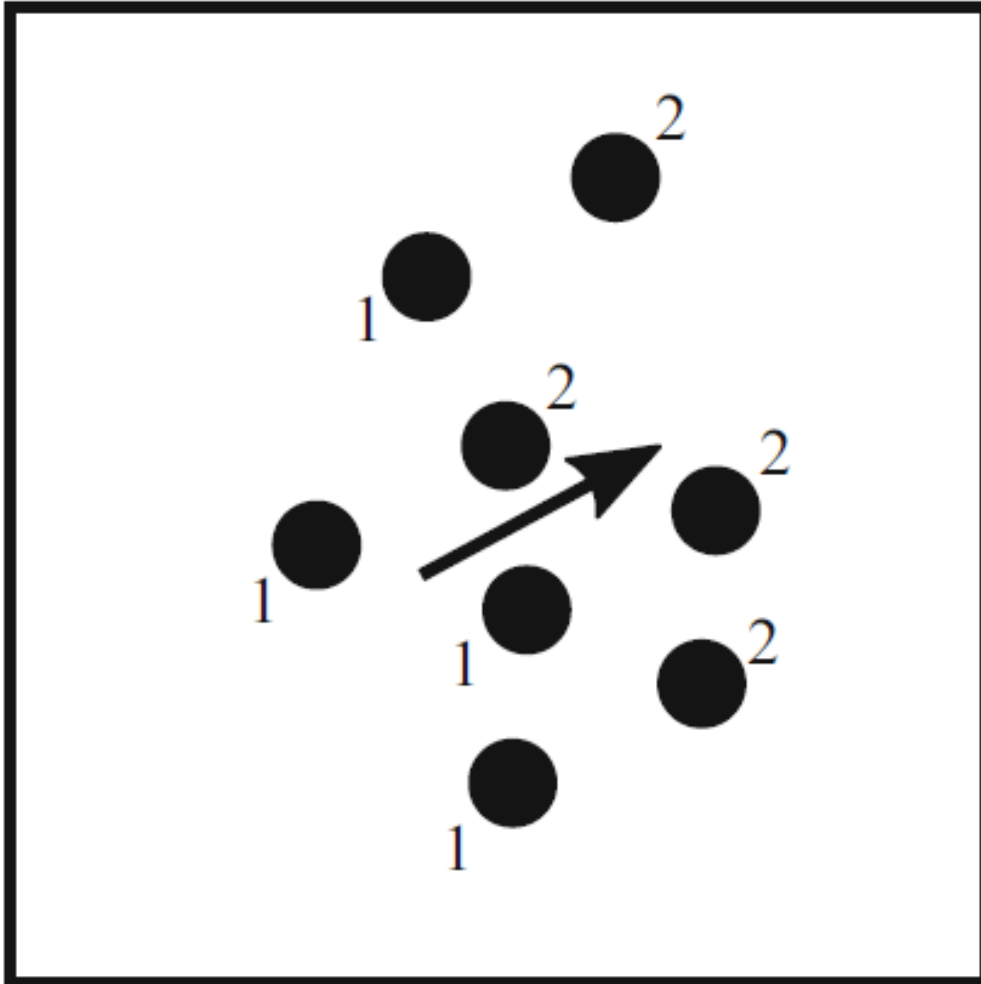


Figure 1.1: Position of tracers particles at two different instants of time, t_1 and t_2 . Picture taken from [19]

The sketch in Figure 1.1 exemplifies this principle. This illustrates that the basic principle underlying the quantitative visualization technique “Particle Image Velocimetry (PIV)” have already been known for a long time [2]. In PIV, the motions of group of particles are evaluated in order to determine the local velocity but it is also possible to track a single particle over a known time interval. This approach is called Particle Tracking Velocimetry (PTV) [14] or Lagrangian Particle Tracking (LPT). Shake-the-box is one of the most advanced 3-dimensional Lagrangian Particle Tracking for densely seeded flows at highest spacial resolution [21] [22]. The scientific and technical progress achieved in

the recent decades in lasers, digital imaging and computer techniques was prerequisite to further develop methods for qualitative flow visualization to such a stage that they can be employed for quantitative measurements of complex instantaneous velocity fields.

1.2. Principles of measuring velocities

If the velocity of a moving object has to be measured, then the distance travelled by the object and the time required to cover that distance is required. This is easy in case of an object but not that easy in case of a flow because the gases as well as the pure liquids do not contain moving objects that reveal the required parameters (distance and time) for measuring the velocity of the fluid.

Thus, many measurement techniques have been developed for addressing this issue such that the flow velocity is measured indirectly using other parameters, such as:

- pressure (pressure probes),
- rotational speed (wind anemometer),
- heat transfer (hot film, hot wire).

Since there are well established relations between the velocity and the above mentioned parameters, the flow velocity can be determined easily. These indirect measurements have their own advantages and disadvantages. The advantage is that these are very easy to use and they are cheap. The major disadvantage is that they may disturb the flow or fluid properties, leading to the measurement errors and also they provide the results only at a single location. In order to obtain the velocity field, the probe must be traversed through the flow field. Since this traversing method requires some time to perform, instead of getting the instantaneous velocity field, only the averaged data is obtained. Therefore, the structure of an unsteady flow field (snapshot) cannot be obtained by such methods.

In order to overcome these difficulties optical measurement techniques have been developed [26]. These optical measurement techniques allow us to place the sensors outside the flow field and capture the images of the whole flow field of interest. These methods are highly expensive in terms of equipment used and the techniques are quite complex. The optical measurement techniques that are widely used needs tracer particles that follow the flow motion faithfully and without disturbing the flow or the flow properties. So, by measuring the position of these tracer particles in time, provides the velocity of the flow field indirectly.

The most important optical measurement techniques for the flow velocity exploit:

- the displacement of tracer particles between two instants of time (Particle Image Velocimetry (PIV), Particle Tracking Velocimetry (PTV)),
- the travelling time of the tracer particles between two light barriers (Laser to focus (L2F)),
- the Doppler effect, that relates the frequency shift of light that is being scattered from the tracer particles and the speed of the moving tracer particles (Laser Doppler Velocimeter(LDV), Doppler Global Velocimeter(DGV)).

1.3. Principle of Particle Image Velocimetry (PIV)

In this section, the basic features of Particle Image Velocimetry (PIV) measurement technique will be discussed briefly [4] [12]. Before that, let's have look at the experimental set for the PIV technique since it has several subsystems.

- Seeding: These are the tracer particles that are added to the flow.
- Illumination: The added tracer particles have to be illuminated twice within a short and known interval of time in a plane or a volume of the flow.
- Recording: During illumination, the light that is being scattered from the tracer particles has to be recorded either on two separate frames or on a sequence of frames of a camera.
- Calibration: Calibration is required in order to obtain a relation between the particle displacement in the recorded image and the actual fluid flow.
- Evaluation: The displacement of particles in the recorded image between the two light pulses has to be determined through PIV evaluation.
- Post-Processing: In order to detect and remove the outliers (invalid measurements) and extract complex flow quantities of interest, sophisticated post-processing is required.

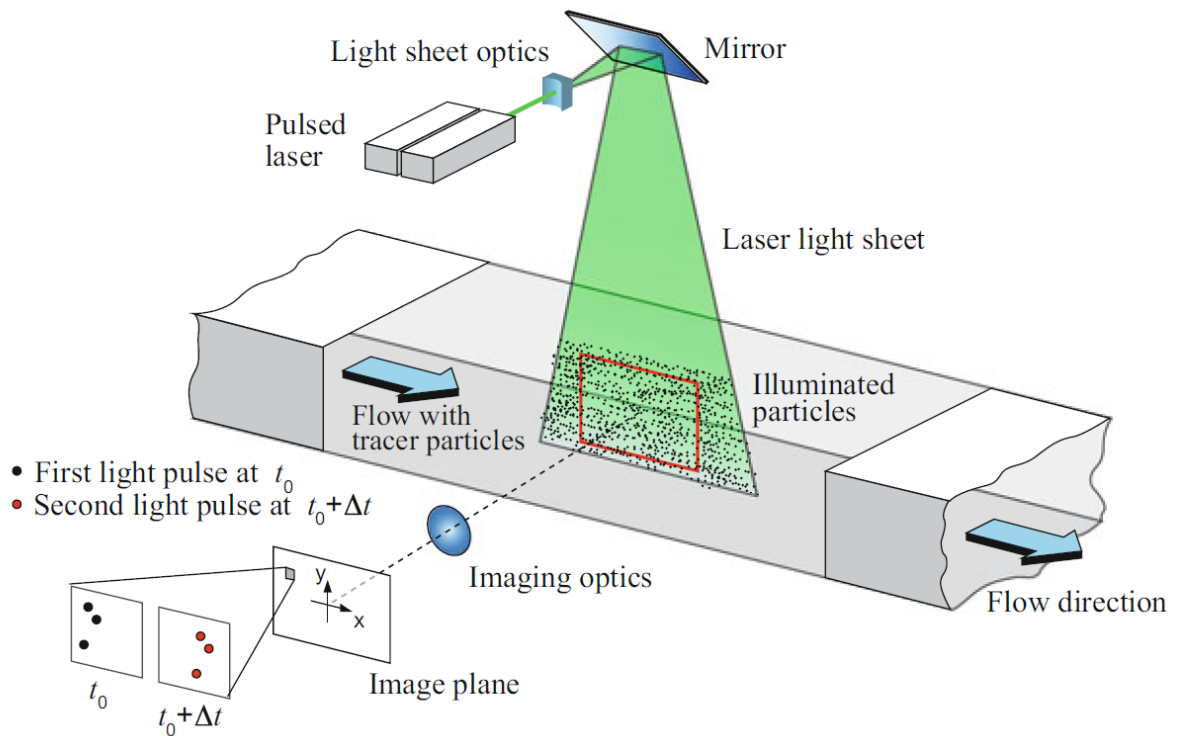


Figure 1.2: Experimental arrangement for planar PIV in a wind tunnel. This image has been taken from [19]

The Figure 1.2 describes the experimental set up for evaluation of two components of velocity in a flow field in the wind tunnel [8] [9]. Before the flow enters the region of interest, the tracer particles are added to the flow without disturbing it. Also the tracer particles shouldn't alter the properties of the flow field. The laser light sheet is illuminated twice in the region for evaluation with short and known time period. The time delay between the two pulses is already fixed so that the only unknown for the evaluation of velocities is the distance travelled by the particles. The light scattered by the tracer particles is recorded via a high quality lens on two separate frames of a dedicated cross-correlation digital camera. The outputs from the digital sensors are stored in the memory of a computer.

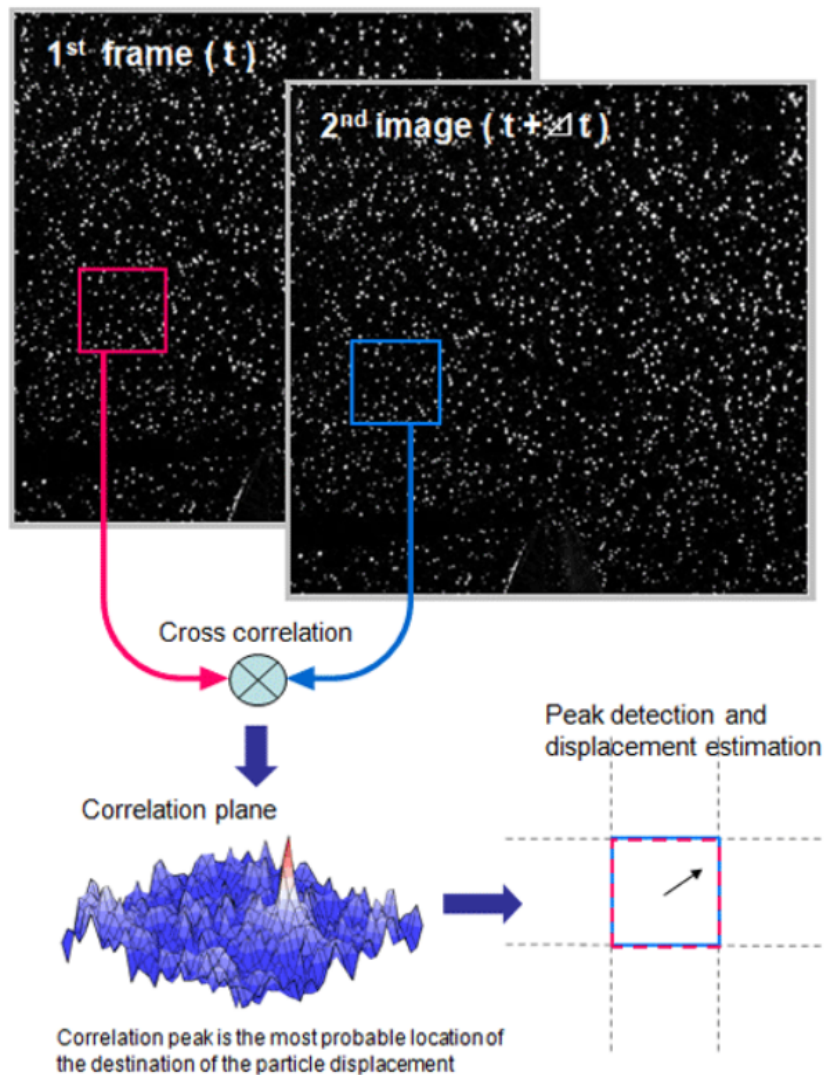


Figure 1.3: Representation of an interrogation window in a complete image and the detection of peak for those two interrogation windows after cross-correlating. (The image has been taken from seika digital images)

During the evaluation, the complete digital image in PIV recording is subdivided into small areas called as “Interrogation windows” or simply “windows” (red and blue square’s in Figure 1.3). The size of the interrogation window depends on the user and the user decides its size on the basis of the problem requirements. The local displacement vector for the images of the tracer particles of the 1st and 2nd illumination is determined for each interrogation area by means of statistical methods (cross-correlation). With the help of the time delay that we fixed between two illuminations and the displacement that we obtained from cross-correlation, the velocity vectors are evaluated locally for that interrogation window. The evaluation is repeated for all the interrogation windows in the

PIV recording. With modern digital cameras, it is possible to capture more than 100 PIV images per minute. If data is required for online monitoring which means that the data is required at a very high rate, there are commercially available software algorithms which perform evaluation at reduced precision within some fractions of seconds.

Before looking further into the context, there are few parameters that are very important in our case. Let's start with the multi-pass.

1.3.1. Multi-pass Filter

Usually there are few reasons for having the multi-pass filter. One of the main reasons for having the multi-pass filter is the requirement of the velocity gradient in the flow. And also very few digital images with extremely high quality without any background noise or reflection, doesn't require the multi-pass filter. Other than that in general all the PIV image evaluation require multi-pass filter. Multi-pass is nothing but number of iteration that are provided by the user such that the instantaneous velocity field (solution) converges. Usually in all most all the cases in the PIV evaluation, 3 to 4 iterations or multi-pass filter would be enough. Since this multi-pass filter is being used during the process, there come few more filters named final window size and final overlap percentage.

1.3.2. Initial, final: Window size and the Overlap percentage

Now let's look into what are these final overlap percentage and the final window size mean. During a single pass filter, the interrogation window is the small area in the complete resolution where the evaluation of PIV occurs between 1st and the 2nd digital PIV image. Due to the usage of multi-pass filter, for the same evaluation, there occur two types of interrogation windows named initial window and the final window. These window sizes are chosen in such a way that the initial window has a larger area than the final window. During the multi-pass filter, the initial iteration occurs with the initial window size and all the remaining iteration is being done with the final window size. In the same way, due to the presence of multi-pass filter, there occurs two overlap percentage named initial overlap percentage and the final overlap percentage. During the PIV evaluation of particles locally, there are two interrogation windows that are used. So, overlap percentage means that the percentage of 2nd interrogation window overlapping on the 1st interrogation window for the better improvement of number of vectors while performing the PIV evaluation. And since the multi-pass filter is being used, the initial overlap percentage is performed on the initial iterations and for all the other iterations, the final overlap percentage will be used.

1.3.3. Peak-to-Peak Ratio

Peak to peak ratio is also one of the important parameter that is being used in the evaluation of PIV results. Basically this filter is used majorly for the elimination of the unwanted vectors or outliers from the result. Other than the extraordinary images that has very least background reflection or noises (Figure 1.4 left image), almost all the PIV images during the cross correlation throws multiple peaks in the considered interrogation window.

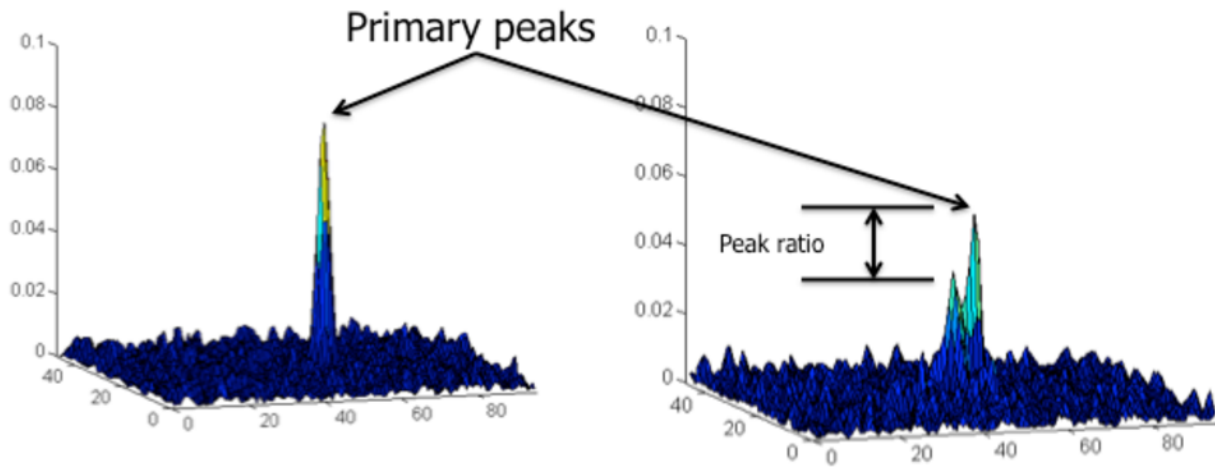


Figure 1.4: Example representing the correlation map for describing the primary peaks and the peak ratio. The image has been taken from [29]

In these multiple peaks, usually one will be having the utmost peak (primary peak in the Figure 1.4) and all other will be having a peak which is less than the highest one. These multiple peaks are formed because of background reflections in the image due to which the cross correlation is happening between the non-same particles. These cross correlation between the non-same particles throws an error in the evaluation of the vectors (known as outliers) that has to be removed for the better results. This is being done by the peak to peak threshold value. This value is provided by the user in the form of ratio between the utmost peak and the peak that the user requires. So, after applying this filter with the value given by the user, all other peaks will be removed other than the provided value from the evaluation which in turn removes all the outliers corresponding to those peaks.

1.3.4. Cross-Correlation Map

Cross-correlation map is one of the important parameter for evaluating the particle displacement in the interrogation window. The instantaneous field that we obtain in the PIV evaluation for each window is the average velocity of that window.

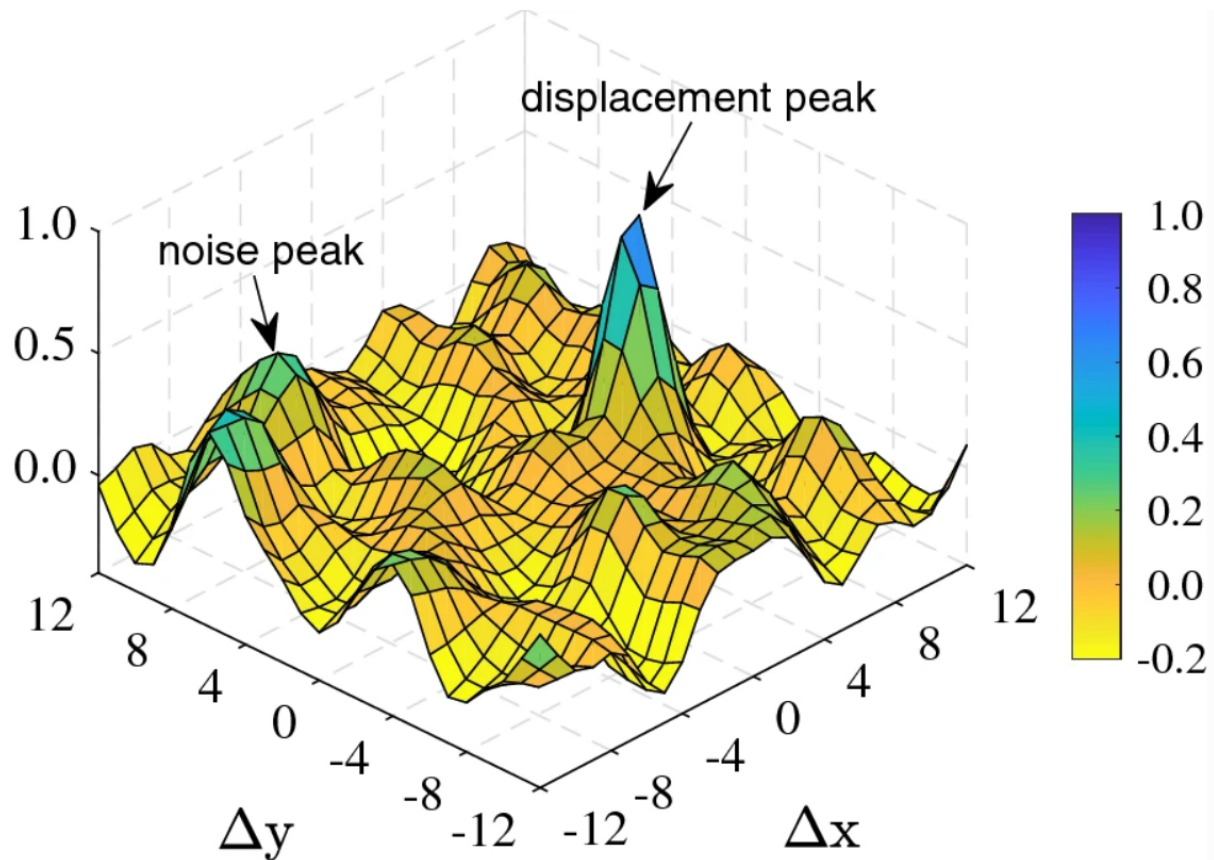


Figure 1.5: Figure representing the displacement peak and the peak due to noise in the raw image. The image has been taken from the article [28]

Hence, a statistical method, usually correlation analysis, is used to acquire the particle displacement. By computing the spatial auto-correlation for double-exposure single-frame images or cross-correlation for double-exposure double-frame images, the location of the displacement-correlation peak yields the average particle displacement. In the case of cross-correlation, there is only one peak, the “true” displacement correlation peak, and no directional ambiguity needs to be resolved. Repeating this procedure for all the interrogation spots and dividing the displacement with the time delay between the two recordings produce a raw velocity vector field. But usually the raw images after capturing doesn’t have the excellent quality. This can be observed in Figure 3.1. The raw images has poor contrast, background reflections etc.,. Due to these types of poor quality, the correlation map forms a wider peak(example Figure 3.5 where the wider peak can be observed in the correlation map of non pre-processed window) due to which there will be a bias in the displacement evaluated. In such case, for obtaining the accurate peak, proper image pre-processing is required. And also, due to the noise in the images, there is a possibility to have multiple peaks in the correlation map. This can be observed in the Figure 1.5 where

one peak corresponds to the displacement peak and the other peak corresponds to the noise. So in order to have an unbiased result for the displacement, proper pre-processing methods should be used to eliminate the unnecessary peaks in the correlation map.

2 | Experimental Design and Setup

In the current thesis work, test facility CT3 at Von Karman Institute for Fluid Dynamics is being used, which is a high-speed short-duration turbine. This test facility can simulate engine representative condition (shown in Table 2.1) [11].

Parameters	Value
<i>Testing time</i>	around 0.3 sec
<i>Rotational speed</i>	5926 RPM
<i>Mach number</i>	0.2 to 0.8
<i>Reynolds number</i>	0.5 to $3.4 * 10^6$

Table 2.1: Parameters and their quantities that the test facility at Von Karman Institute for fluid dynamics can achieve which are similar to the engine operating conditions

In the blow-down tunnel, the PIV measurement technique has been installed so that now it's easier to capture the instantaneous and whole-field flow measurements. A schematic representation of the test facility has been shown in the Figure 2.1. This blow-down tunnel consists of three main components: the compression tube (upstream cylinder, 8m long, 1.6m diameter, including a free moving piston of 70kg), the test section (consisting the research turbine), and the dump tank (downstream reservoir). The compression tube and the test section is separated by a fast opening shutter valve. The dump tank remains downstream of the test section which is connected via an adjustable sonic throat. There exists a settling chamber that is just before the test section used to stabilize and homogenize the turbine inlet flow. The turbine inlet is designed such that it replicates the outlet geometry of the combustion chamber. The test can house one-and-a-half turbine stages with maximum external diameter of nearly 1m.

The shutter valve must be closed initially in order to isolate the test section from the upstream cylindrical reservoir. The piston is at its initial position which is at the rear part of the compression tube set to an initial pressure at ambient temperature. The

test section and the downstream reservoirs are evacuated to vacuum, about 20-30 mbar absolute pressure. With the help of an auxiliary air-driven power turbine, the turbine rotor in the test section is spun upto 90-95 percentage of its nominal speed within about 400 to 500 seconds. The cold air from the high-pressure reservoir (14.4 m^3 at 200-250 bar) will be injected at the back of the compression tube. With the help of number of adjustable sonic throats, the opening of the main automatic valve (valve that injects the cold air mass flow into the cylinder) is being controlled. The high-pressure air is expanded at the back of the piston into a low pressure environment, giving raise to a high supersonic jet. In order to prevent the supersonic jet to interact directly with the piston, a metallic structure is being attached at the tube rear wall. When the pressure at the back of the piston is one differential above the upstream pressure, the piston starts to slide along the tube, and thereby quasi-isentropic compression is performed between the shutter valve and the piston. Once the required pressure is obtained, the shutter valve opens discharging the pressurized and the heated air into the test section. Usually the shutter valve opening time varies between 40 ms to 90 ms depending on the level of differential pressure between the tube and the settling chamber.

After the fluid flow enters the settling chamber, the tracing particles are being inserted into the flow field.

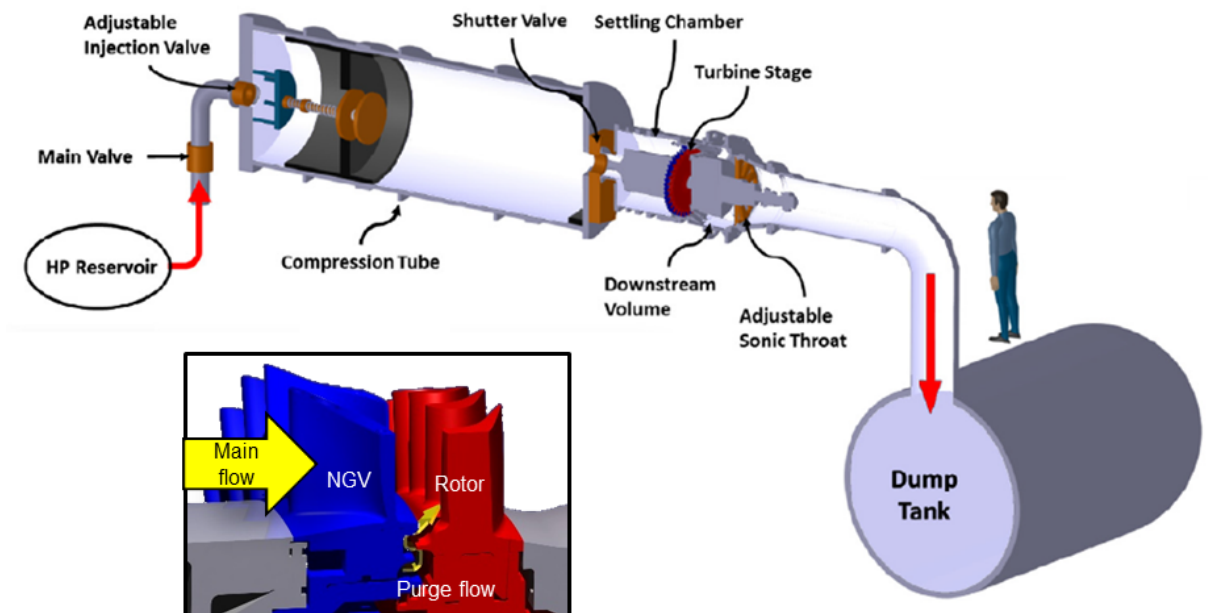


Figure 2.1: Schematic representation of the short-duration compression tube turbine test facility at Von Karman Institute for fluid dynamics. The image has been taken from [3]

As soon as the flow enters the test section, the particles should be able to track the flow

field perfectly. These particles scatter the light from the laser sheet that is present in the test section and provide the opportunity for camera to capture it digitally. After the test section, the flow will be passed into the dump tank which is underneath the floor. The above description was a short overview of the PIV measurement technique.

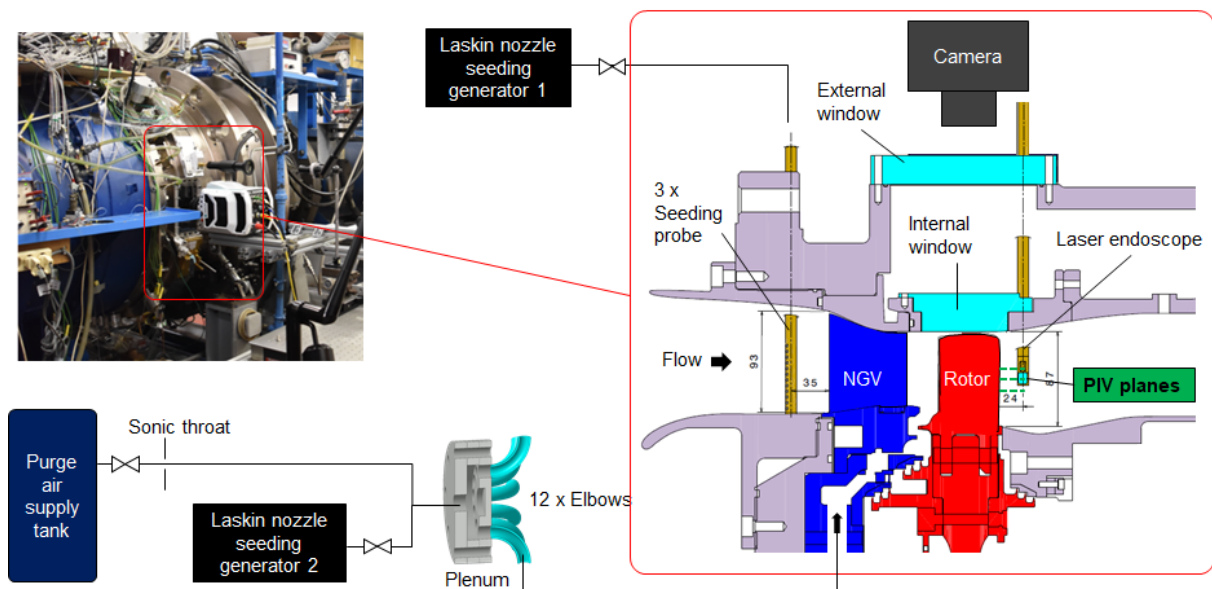


Figure 2.2: Sectional view of the test section that is being marked in the red box

Before looking further, let's look into the sectional view of test section. Figure 2.2 is the sectional view of annular turbine test section. In the figure, it is shown a schematic diagram in the test section for the single stage turbine that consists of a rotor and the nozzle guided vane.

Selecting the appropriate tracer particles and the methodology for seeding these tracer particles into the flow plays one of the major roles in the PIV measurement technique. In order for the particles to trace the flow without or with least lag, the particles should be of small size and density. However, the small diameter has a disadvantage of lower intensity of light that is being scattered from the particles which in turn results in the low signal to noise ratio while processing the image. In general, for a high speed flow, the particles used are DI-Ethyl-Hexyl-Sebacat (DEHS) oil particles with diameter ranging between 0.3 to 1 micro-meter. In the present study, the tracer particles used are DEHS droplets with 0.9 micro-meter. These particles are generated by the Laskin nozzle. The seeding is injected into the main flow with the help of three probes that are inserted in the upstream of the nozzle guide vanes at different circumferential positions. These seeding particles then pass through the test section with the flow resulting in the instantaneous

fields with PIV planes. In addition, the rim sealing cavity flow that is purged between the nozzle guide vanes and the rotor is also seeded as shown in the Figure 2.2. The total mass flow of the seeding particles that are injected into the flow is less than 0.2 percent of the main stream flow.

There exists an internal as well as the external windows that are mounted on the casing in order to provide the optical access for a camera as shown in Figure 2.3. The internal window has a curvature to match the annular flow path. Laser sheet is generated on the tangential plane using the laser endoscope of 8mm external diameter. This endoscope is inserted into the internal casing at the downstream of the laser stage using a slot originally designed for probe measurements. The laser endoscope was designed and manufactured especially for this kind of measurement where there exists an optical curvature during the measurement process. The curved surface of the window causes the image distortion, as it is one of the limitation of PIV [10]. But this limitation can be wiped off in multiple ways.

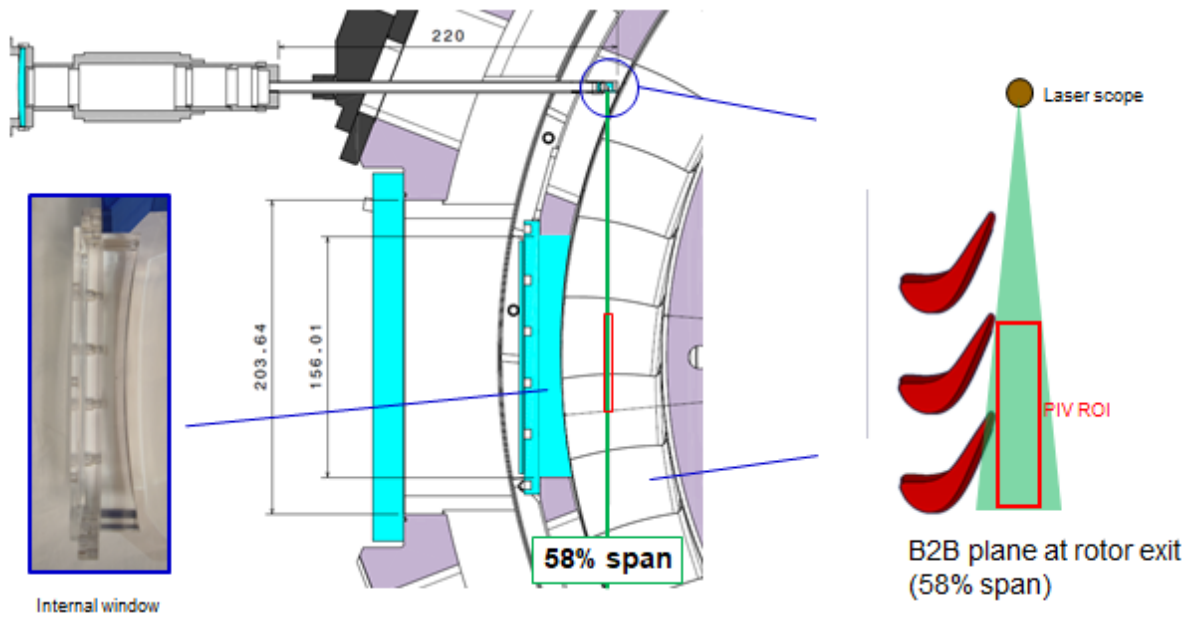


Figure 2.3: Overview of optical access containing test section downstream of rotor row

In the left side of Figure 2.3, it is the diagram representing the optical access. In the right figure, it is observed that the laser which is emerging from the laser scope creates a sheet in the tangential direction. It is also important to note that the laser sheet not only illuminates the tracer particles in the flow but also other components on its path which includes casing surface, the blade at the very end of the sheet. All in turn creates a huge problem as this gives a strong reflections in the digital image which will bias the

displacement while calculating which in turn provides an error in the computed fields or simply these background reflections yields more noise than the light that is being scattered from the tracer particles. This effect is addressed initially by coating the rotor blade and other components with a matte-black paint to minimize the reflections. But yet, it is found that the reflections from the rotor surface are very strong. These sorts of problems and how it is being dealt are discussed in the later sections.

Image calibration is required step for a PIV measurement. This calibration can be done after or even before the image processing. The calibration scale is shown in Figure 2.4. The calibration scale has been captured in the test section. The internal window was covered with a black tape in order to eliminate the capturing of rotor blades in the calibration image. This calibration is important because, this allows the measurement calculated in the digital plane to convert into the real plane. This calibration scale is also used to correct the calculations that have an error due to the image distortion present in the captured images due to the curved internal window. The dots in the calibration scale have a diameter of 1 mm and the distance between two dots is 2 mm. This calibration step in our process is being performed before the image processing in the DAVIS 8.4 software.

In PIV measurement technique, Synchronization has to be done between the PIV systems and the operational test rig. It is one of the difficult task that has to be carried out. A high-speed Phantom v2012 camera and a high-speed Quantronix DarwinDuo dual cavity laser system were synchronized at 1 kHz acquisition frequency (laser output power: 20 - 25 W) by Stanford DG535 digital delay/pulse generators. The camera sensor resolution is 1280 x 800 pixels with 28 micro pixel pitch. The particles to have enough displacement, either it should have greater magnification or it should have larger separation time. Since the larger separation time can't be provided, camera equipped with Nikon AF Micro-Nikkor 60 mm f/2.8D lens, provides an optical magnification of 0.56. The separation time between two light pulses is 1.14 micro-seconds.

Before starting the PIV image processing, Different software has been analyzed for this purpose. There are multiple software such as DAVIS, Dynamic Studio, Insight 4G, PIVLab, OpenPiv etc., which are used for the image pre-processing and processing. Taking into account few parameters like cost, availability, background noise reduction, contrast enhancement, de-blurring, auto-masking, 2D/3D, ability to control camera and laser, post processing etc., these software have different purposes. PIVLab is one of the

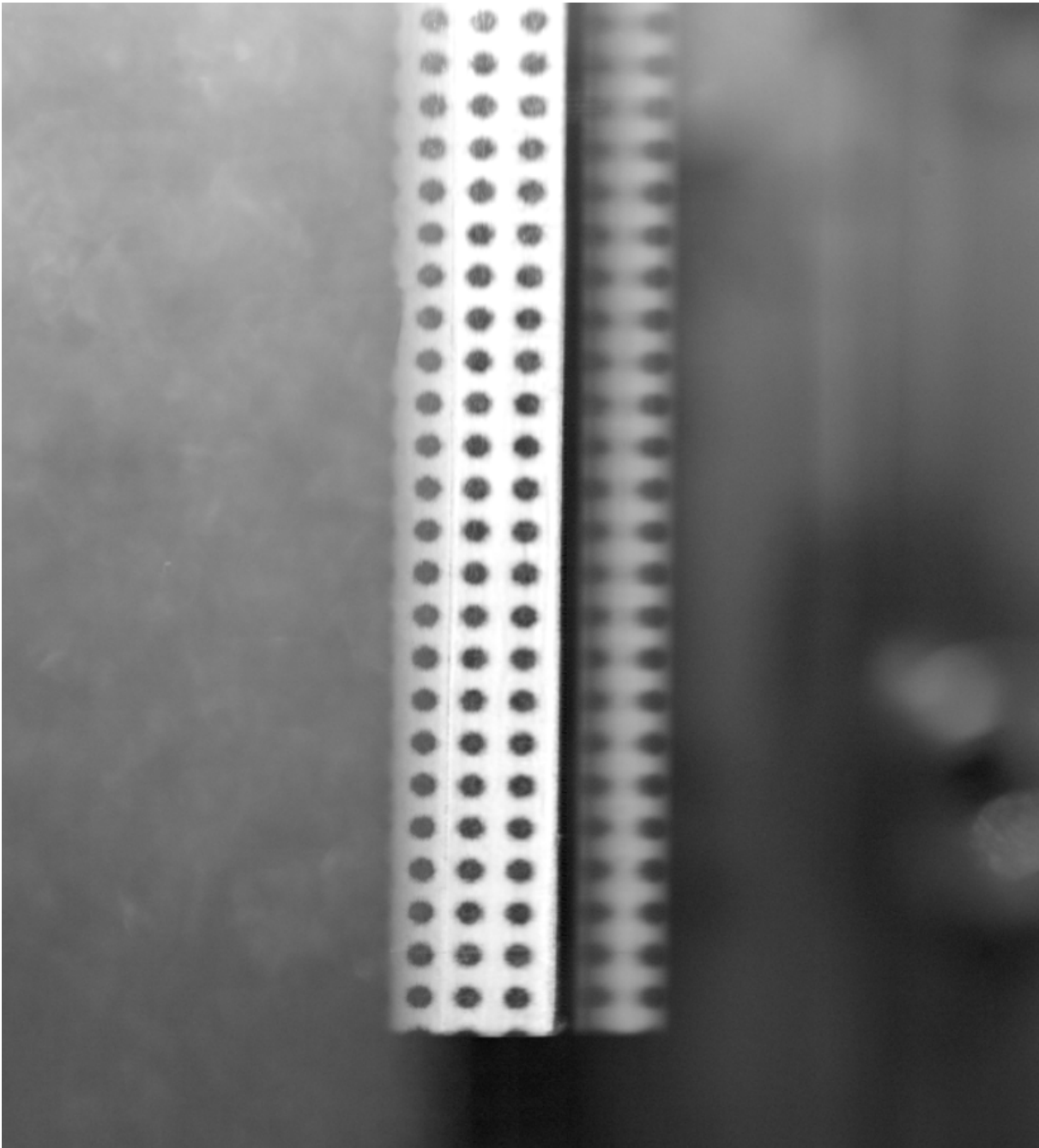


Figure 2.4: Image of the calibration scale used for PIV evaluation

open-source software which is developed for the PIV image processing. But the drawback with PIVLab is that it adds few filters automatically and there is no flexibility with user preferences. So, by comparing the most commonly used commercial software, in our case DAVIS 8.4 has slightly better performance and also there is readily available license at Von Karman Institute for Fluid Dynamics. Package in python known as openCV is also used simultaneously with DAVIS 8.4. There are even bunch of software named FLUERE,

Fluid Image, MPIV, JPIV, UVMAT and PIVMat that has been referred in few papers are used in PIV processing. But there are no clear information about accuracy or reliability of these software compared with the standard ones. So, in this present work, Python (openCV), Matlab and DAVIS 8.4 are being used.

3 | Image Pre-Processing

Over the years, digital particle imaging velocimetry (PIV) has evolved into a technique that can be used in increasingly complex systems. The performance of this technique depends on the quality of the image and post-acquisition signal processing. Image processing is relatively simple if the original image quality is good, i.e. uniform illumination, good contrast, low background noise, few stationary objects, suitable displacement of tracer particles, etc. In practice, however, these conditions are not always satisfied. Due to the difference between the two lasers pulses, the laser intensity may vary between images or image pairs, objects may introduce strong light reflections, and/or reflections from channel walls in confined flows may produce glow. This can be observed with the help of an example. Look into Figure 3.1 where these figures are captured at adjacent time intervals. (here the time series for capturing the images are (1st+2nd),(3rd+4th),(5th+6th),(7th+8th), and so on.. Now the image (a) corresponds to 1st, (b) to 3rd, (c) to 5th and (d) to 7th). In all the images, the background reflections as well as the reflections from the rotor blades can be observed, especially in (a), (b) and (d). It is difficult to observe the particles due to low contrast in the images. There are several approaches in the literature to address these issues. So, the initial way is the Image pre-processing. There are different levels of image pre-processing. The three fundamental image pre-processing includes Contrast Enhancement, Background Removal and Denoising (smoothing). These each pre-processing step involves different sub types which changes with the type of problem that is being addressed.

S.No	Image pre-processing	Name of the filter	Software/library used
1.	<i>Contrast Enhancement</i>	CLAHE	Python (OpenCV)
		Min/Max Intensity Normalization	DAVIS 8.4
2.	<i>Background Removal</i>	Highpass(Sobel)	Python(OpenCV) and DAVIS 8.4
		Highpass (temporal)	Python(OpenCV)
		Proper Orthogonal Decomposition (POD)	Matlab
3.	<i>Denoising (smoothing)</i>	Lowpass (Bilateral)	Python(OpenCV)
		Lowpass (Gaussian)	Python(OpenCV) and DAVIS 8.4

Table 3.1: Table representing different image pre-processing with their respective filters

Here in the present work, for Contrast Enhancement, CLAHE and Min/Max Intensity Normalization are analyzed. Similarly for Background Removal and Denoising, High-pass(Sobel), Highpass(temporal), Proper Orthogonal Decomposition (POD) and Low-pass(Bilateral), Lowpass(Gaussian) are analyzed respectively. After analyzing individual pre-processing methods, their combinations are also analyzed in order to have the best output of the PIV images for Image Processing.

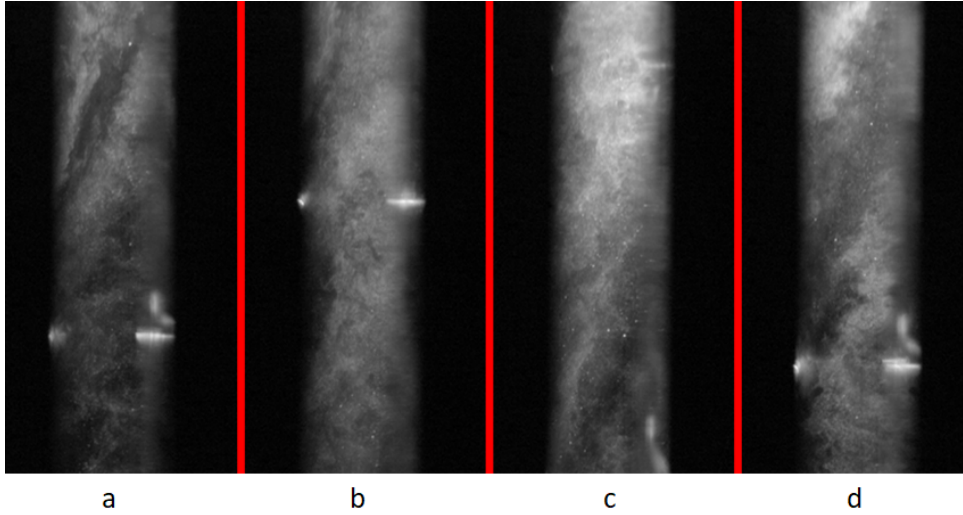


Figure 3.1: Figure representing the raw images(a-d) captured at the first four consecutive time intervals.

3.1. Contrast Enhancement

Contrast enhancement is one of the most required filter in the case of PIV images. In general, the image intensity field should consist of bright particle images, of nearly uniform intensity, over a dark background to deliver an accurate measurement of velocity field. However, one of the common imperfections of PIV images are its weaker illuminations which can affect the accuracy of the measured velocity fields. In order to overcome such imperfections, [2] suggests that there are two possible ways of enhancing the contrast. They are Min/Max intensity Normalization and CLAHE.

3.1.1. Min/Max intensity Normalization

After dividing the image into certain number of windows, the minimum and maximum intensities are identified for each window. Then for each pixel in the image, it is considered a neighboring window through which the minimum and maximum intensities are identified. Now the local pixel intensities are re-scaled with respect to the considered local range

(maximum-minimum), thus both normalizing the particle intensities through the image and increasing locally the contrast with respect to the background. This method of min/max filtering is used in this paper [17].

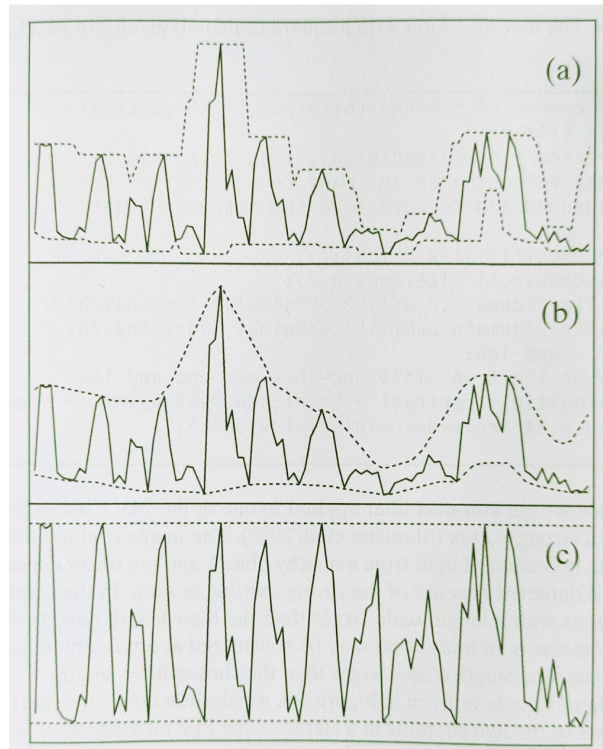


Figure 3.2: Conceptual example of contrast normalization using min/max intensity normalization for a one-dimensional signal. Picture for the PIV book by Adrian and Westerweel (2011).

With this enhancement technique, it is observed that this method not only normalizes the particle intensities but also increases the local contrast with respect to the background. Since it deals with the local contrast, if there is a noise in the image, then the noise also intensifies with this enhancement method. lets observe this normalization in detail.

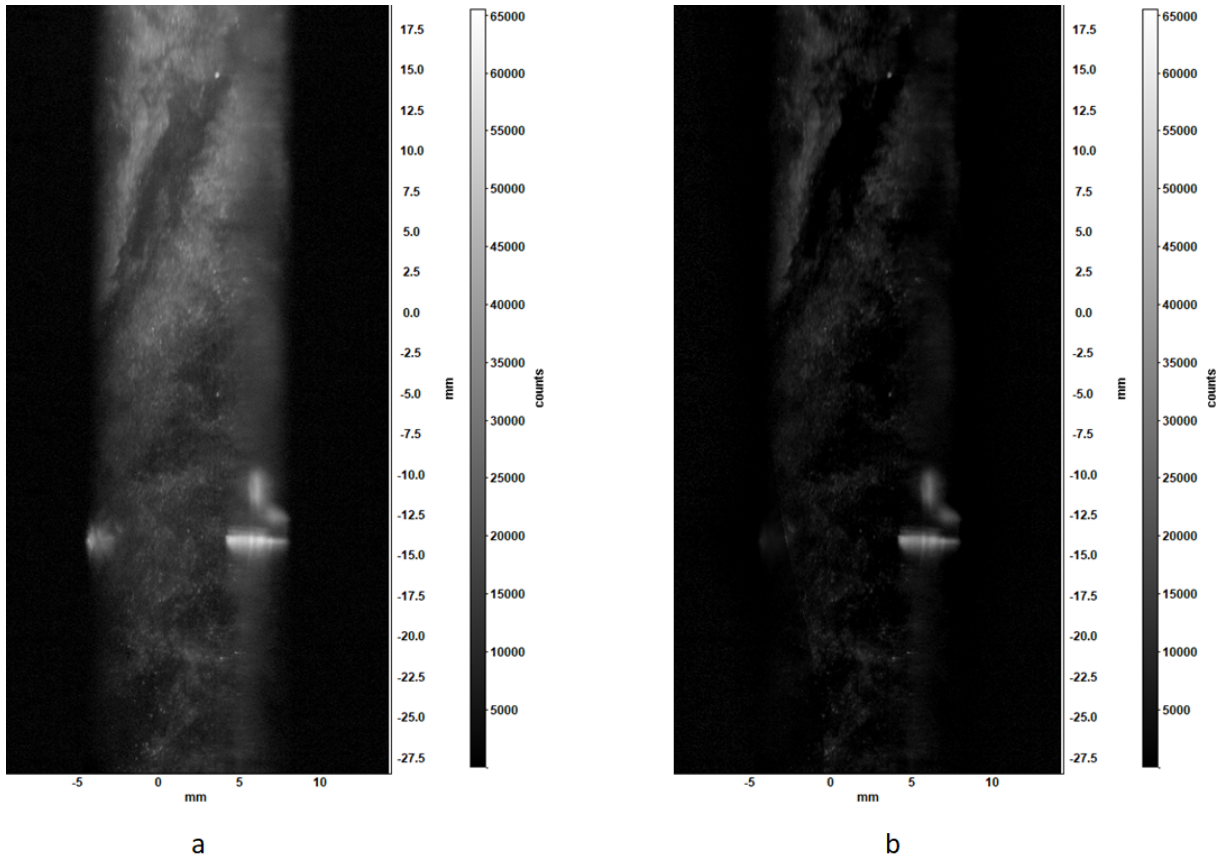


Figure 3.3: image (a) is the raw image captured and image (b) is the image after applying the filter Min/Max intensity Normalization

From the above Figure 3.3, it is observed that, the left image is too bright that it difficult to observe the particles for a PIV image processing. The right-side image is pre-processed with Min/Max intensity normalization with pixel size 28. It can be clearly observed that in the right image, the contrast has been enhanced. Due to this image quality enhancement, it is able to observe the image particles clearly and this would be helpful for the PIV image processing. Further a portion of the raw image has been cropped and zoomed-in in Figure 3.4. From the cropped region it is clearly able to observe the enhancement of the contract after pre-processing the image. The bright spot in the raw image is been normalized and it is able to observe clearly the particles as well as the edges in the pre-processed image.

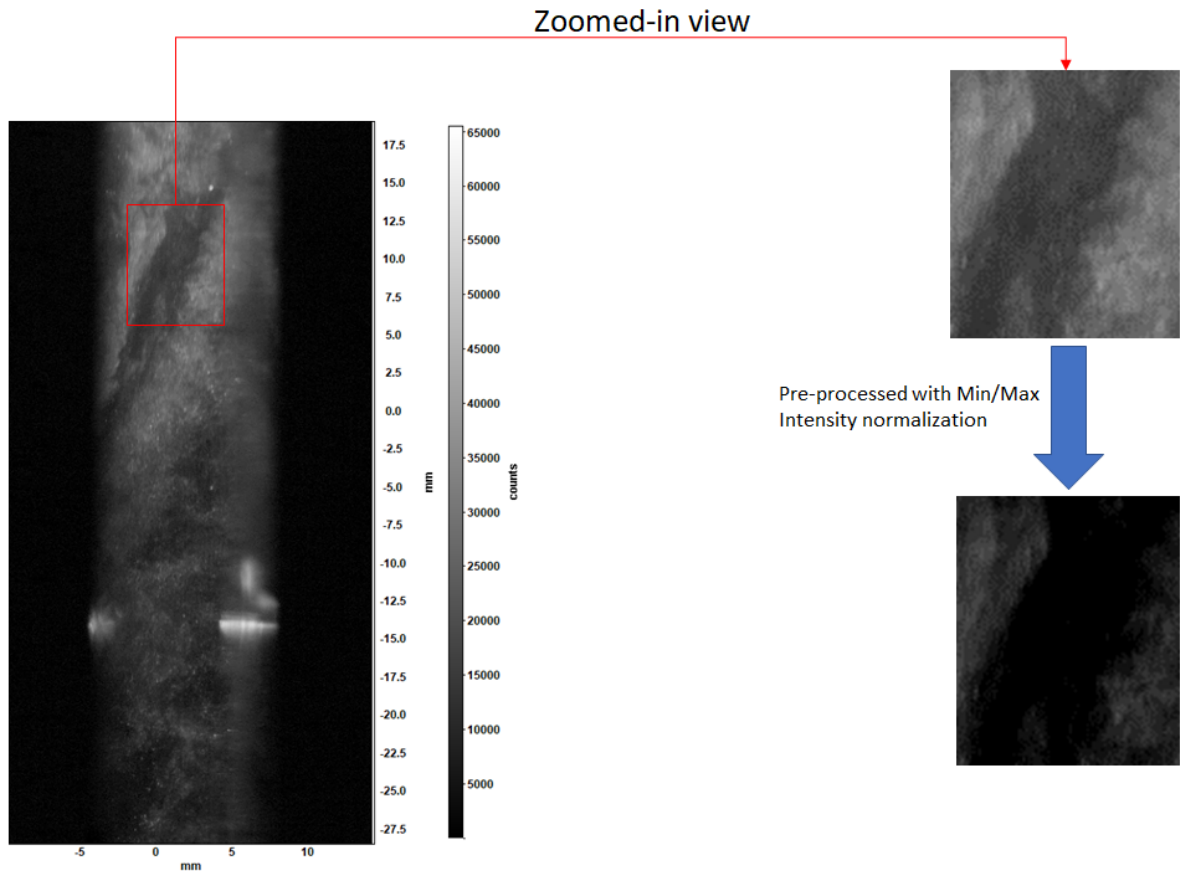


Figure 3.4: The red box drawn on the raw image(left-side figure is the raw image) is observed closely before and after applying the Min/Max intensity Normalization

This pre-processing helps in the enhancement of contrast which in turn helps the proper cross correlation of these images that is being used to calculate the instantaneous velocity. After observing the raw images, it is always better to look at the correlation map for the improvement of the peak that is being formed as discussed in the sub-section 1.3.4. Now to clearly observe the play of correlation map with the enhancement process, another raw image is being considered in Figure 3.5. In Figure 3.5, before the pre-processing, the particles were not able to cross correlate properly. This can be observed with the help of a correlation map. After the pre-processing with Min/Max intensity normalization, the particles in the image were able to cross-correlate properly which resulted in the nice correlation map with good peak. Since this enhancement method happens locally for each window with the help of its neighboring window, if there exists a noise in the image, instead of remaining in the same level or decreasing, the noise gets intensifies. Due to this while using this filter, it should be always kept in mind that the enhancement is happening at the cost of locally intensifying the noise for a certain level. So it is always advisable to use the noise filter later in order to obtain the best output.

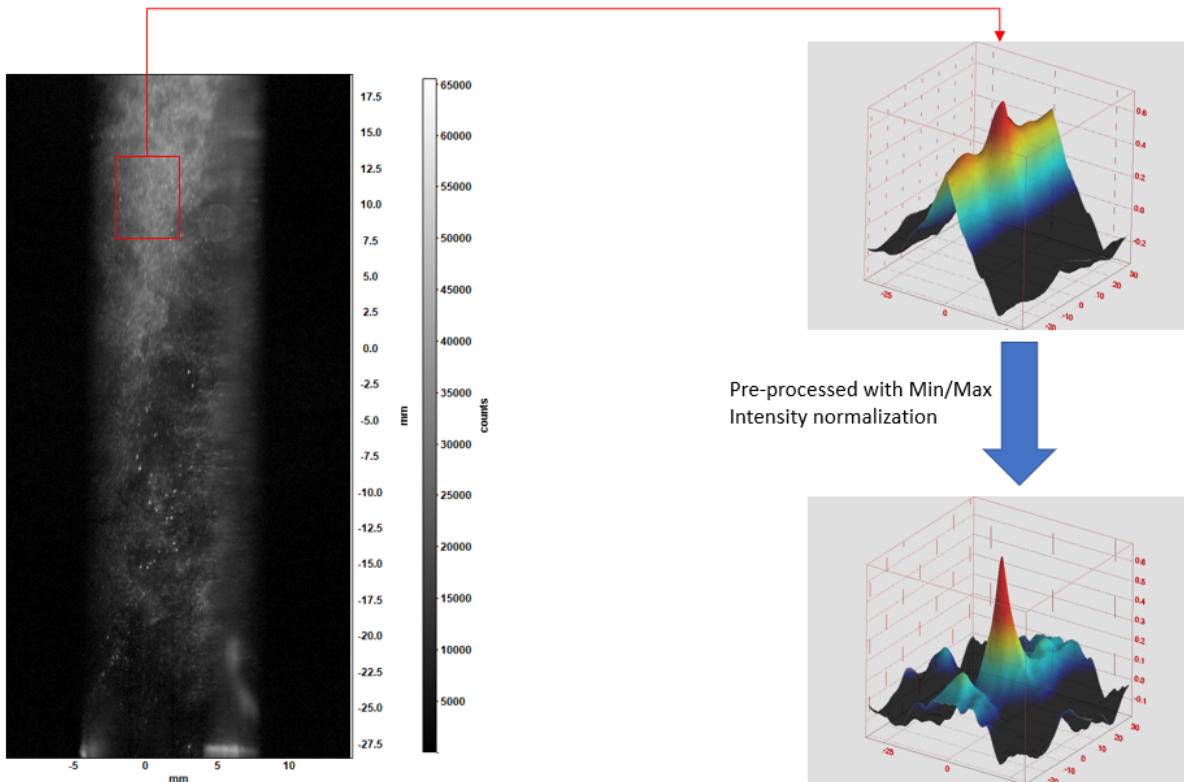


Figure 3.5: Left-side image is the raw image. In the right-side, the correlation map is observed for the marked region with red box before and after applying the filter Min/Max intensity Normalization

Also note that the pixel size of 28 is being chosen after the being analyzed with pixel size of 6 and 12 where the later both pixel sizes shown comparatively poor results than the 28.

3.1.2. CLAHE

Initially Histogram Equalization is a way of stretching the histogram to include all ranges of intensities in the image histogram [18]. For example, a histogram is plotted for an image with different intensities between the intensity and the number of times the intensity is getting repeated. Now if this histogram is stretched in order to include all the ranges of intensities, then it is known as the Histogram Equalization.

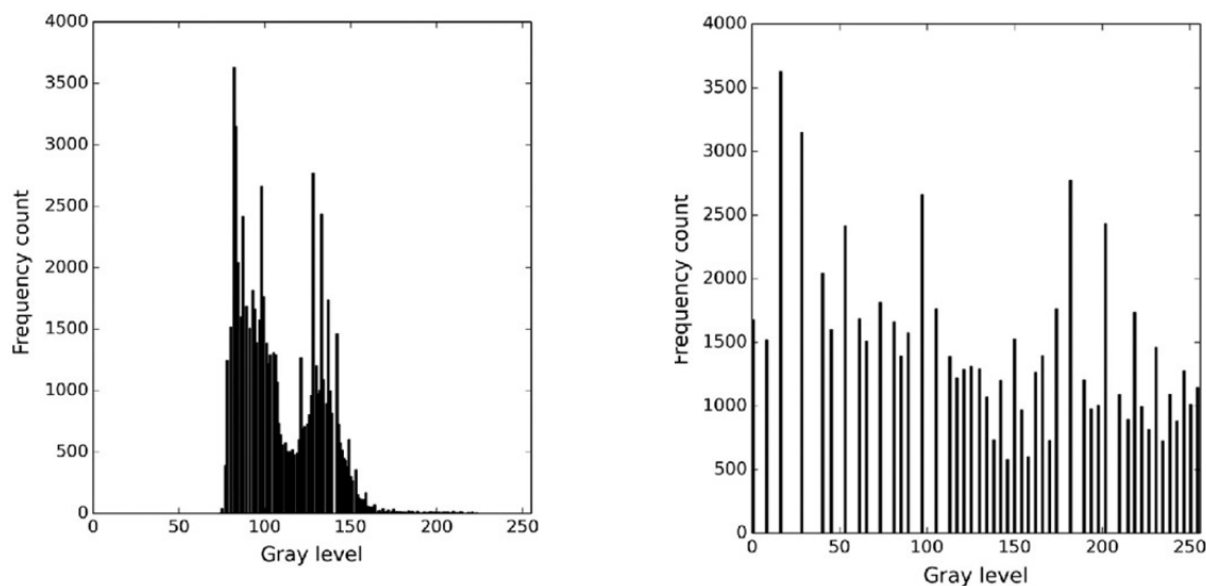


Figure 3.6: Left-image is the histogram drawn for a random image and Right-side image is the histogram equalized plot for the same image. Note that this histogram is randomly chosen just to observe how the histogram equalization works

One of the examples is shown in the Figure 3.6. In the left figure, the histogram is concentrated to the center. In the right figure, the histogram is being equalized to all the range of the grayscale. Because of this there will be an enhancement in the contrast of the image. But the major drawback of this histogram equalization method is that this produces either too bright or too dark sites in the image because this method uses the histogram of the complete image and tries to stretch it. This is being briefly shown in the section appendix C.1

To overcome the limitation of this method, there comes the Adaptive Histogram Equalization [20]. In this method, Instead of using the intensities of the complete image for the histogram, the image is split into multiple pieces known as windows and the histogram of those windows are equalized in this method. Since this method deals with the local histogram, this will not produce bright or dark regions in the pre-processed image because as mentioned this deal with the local windows and not the complete image. But this may amplify the noise or the contrast in the image drastically. So, in order to limit the amplification, the contrast limitation is applied to the Adaptive Histogram Equalization. Hence this method of Contrast enhancement is known as the Contrast Limited Adaptive Histogram Equalization.

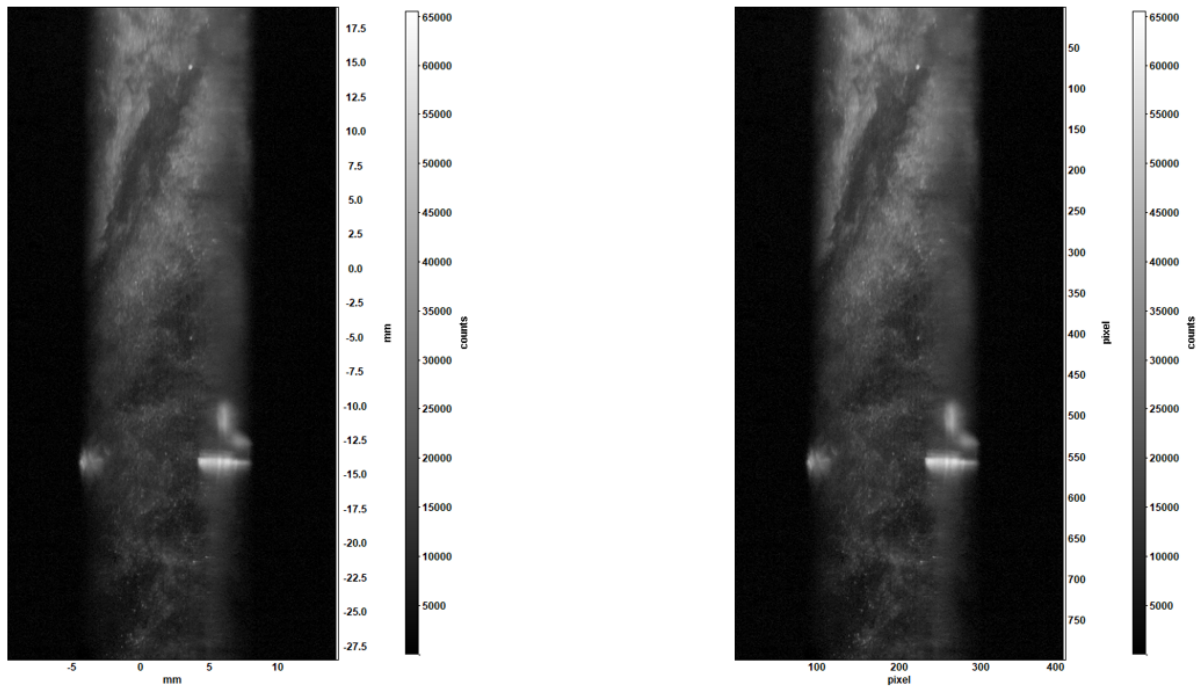


Figure 3.7: The left side image is the raw image and the right side image is the image filtered with CLAHE

In the Figure 3.7, the left image is a non-pre-processed image whereas the right image is a pre-processed Image with CLAHE. The pre-processed might look not much enhanced but if the pre-processed image is observed closely, then the particles as well as the edges in the image are made much clear than a non-pre-processed image. In the zoomed in picture shown in Figure 3.8, it can be clearly observed that few of the edges and particles are not visible in the raw image whereas, in the pre-processed image it can be observed. Since this enhancement is happening locally, the noise in the raw image will be intensified with pre-processing method of CLAHE. This can be observed in the following pages where the correlation map is considered.

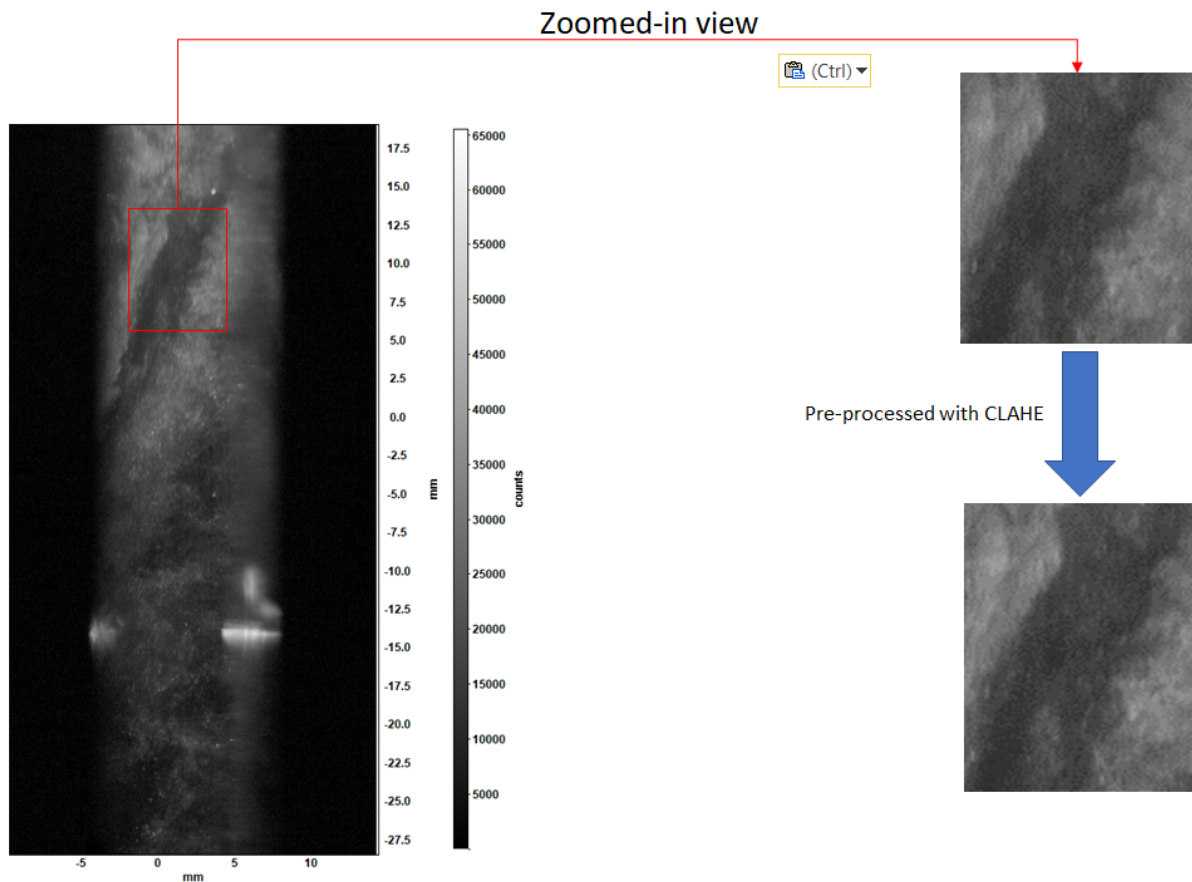


Figure 3.8: Left image is the raw image and the right side images are the raw image and the pre-processed image with CLAHE in the marked region

From Figure 3.9, it is observed that the Correlation map has been improved from raw to pre-processed image. This is because as said in the previous context, due to image enhancement, the particles in the image is able to cross correlate properly with the same particles. It is also observed that due to enhancement of noise in the image there are few other small peaks in the correlation map.

Both the Min/Max intensity normalization as well as the CLAHE are used for the contrast enhancement. Since both the enhancement technique deals with the local contrast and not the global contrast, there will be an intensification in the noise in pre-processed image.

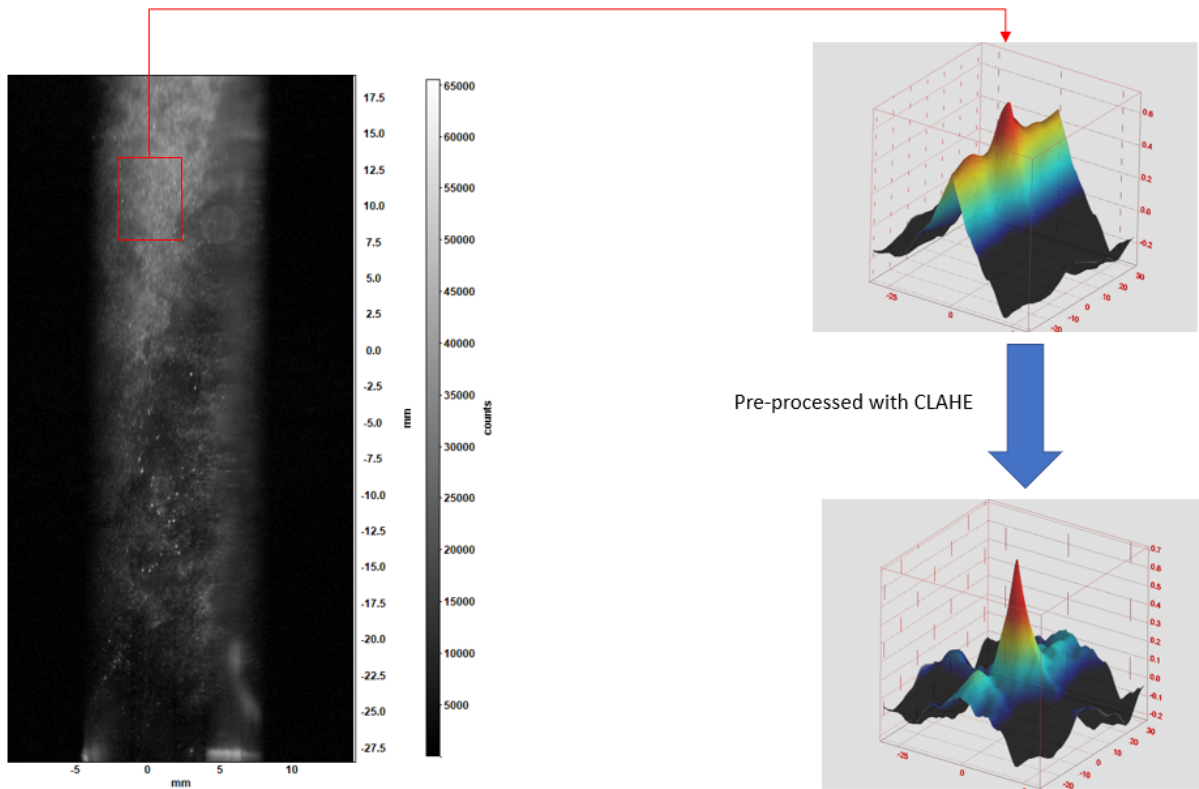


Figure 3.9: Correlation map of the region marked on the raw image(left image is the raw image) and its correlation map after the filter CLAHE

Now if the CLAHE's and the Min/Max intensity normalization's correlation is compared from the Figure 3.9 and the Figure 3.5 respectively, the CLAHE produced better correlation map than the Min/Max intensity normalization in-terms of peak and noise. So before concluding the result, it is better to observe the correlation for any other region. Let's look into Figure 3.10. Since both the contrast enhancements methods have equal amount of advantages and disadvantages, by observing the Figure 3.10, we can further conclude which is better for our case. Both Min/Max intensity normalization 3.10(b) and CLAHE 3.10(c) gave similar kinds of result but 3.10(c) was able to produce better peak than the 3.10(b). Hence, CLAHE was able to cross correlate properly with the same particles whereas Min/Max intensity normalization produced comparatively poor results. This can be observed in 3.10(b)'s cross correlation map which has few unnecessary peaks wherein 3.10(c) has better correlation map than that of the Min/Max intensity normalization.

In conclusion for our case, as seen before, for contrast enhancement, it is preferable to use CLAHE rather than the Min/Max intensity normalization.

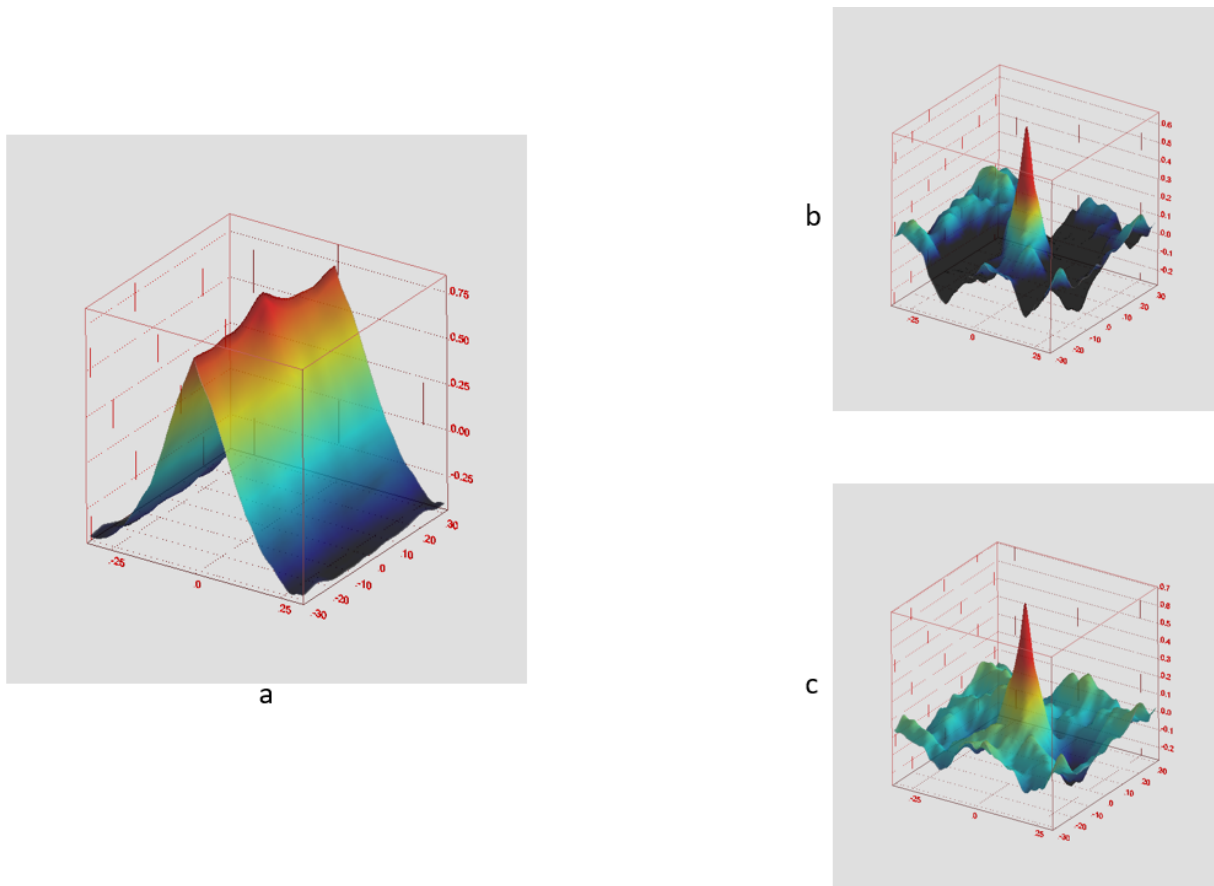


Figure 3.10: (a) correlation map of the raw image. (b) correlation map of the image pre-processed with Min/Max intensity Normalization. (c) Correlation map of the image pre-processed with CLAHE

3.2. Background Removal

Similar to the contrast enhancement mentioned in the previous section, the other major filter required in the PIV field is the background removal. PIV images in realistic conditions include sharp particle images, ideally of gaussian shape and with a diameter of few pixels plus a background illumination, typically ascribed to laser reflection over solid objects. If the wall has little displacements or if the number of samples are large enough, then there exhibits a coherence and will have an intensity varying slowly over time. Also the typical characteristic size of light reflections is significantly larger than particle images and is perceived as a low-pass signal. When dealing with time varying reflections or vibrating objects (moving objects), the elimination of background requires more complex approaches. Here in this section, the highpass filter and its few types are discussed.

Highpass Filter

A Highpass filter is one that attenuates low frequencies and passes high frequencies unattenuated [15]. Usually the low frequency signals are bright spots or areas in the image and these are generally caused due to unwanted reflections. Here in this context there are three highpass filters are discussed. They are Sobel, Temporal and Proper Orthogonal Decomposition (POD). This POD filter falls as a highpass filter in our case because the major modes that are being removed during the process eliminates the low frequency signal and this filter is insensitive to the high frequency signals (This POD filter is insensitive to high frequency signal is being mentioned in the article [16] and also in our Sub-Section 3.4.3). Each mentioned filters for the background removal works on different principles. They are discussed as follows.

3.2.1. Sobel

Sobel filter is one of the best filters for background removal and edge detection [6]. Usually, bright areas or spots in the image are considered to be low frequency signals and edges as well as noise are considered to be high frequency signals in the image. So, this filter is able to remove the low frequency signals and allows the high frequency signals to pass through. Point to be noted is that this sobel filter is sensitive to the noise in the image. If there are any noises in the image before pre-processing, then those noises in the image are not being filtered by this sobel operation.

This filter works on a pair of convolution kernels (known to be two matrices) that is being shown in Figure 3.11. Both the kernels are made in such a way that they individually used to detect the edges in an image vertically 3.11 (left kernel) and horizontally 3.11 (right kernel). These kernels can be combined together to find the absolute magnitude of the gradient at each point and the orientation of that gradient. These kernels runs over the images locally and applies the filter. This working of sobel and how the convolution works mathematically are briefly discussed in the appendix B. In our case, this sobel filter with diagonal kernel shown in Figure 3.12 is compared between the OpenCV and the DAVIS 8.4 (comparison has been done in the current sub-section) and has been used in the present work.

-1	0	+1
-2	0	+2
-1	0	+1

+1	+2	+1
0	0	0
-1	-2	-1

Figure 3.11: The two convolution kernels that the sobel filter depends on.

-2	-1	0
-1	0	1
0	1	2

Sobel kernel – Diagonal

Figure 3.12: Diagonal kernel that is being used for the sobel filter in our case. Data has been taken from the DAVIS user manual

In the left image of the Figure 3.13, it can be observed that there are lot of bright areas or spots. In this case, these bright spots are due to the high density of particles present in the test section. In this experiment due to very small test timing, instead of only relying on the particles, the patterns of the high density regions are also observed in order to calculate the displacement in the image. But these high density regions present in the image can bias the displacements while cross-correlation between two image pairs. So this is reason it is very important to eliminate the bright regions in the image.

So, after applying the filter sobel, this was able to remove all the bright regions in the image. This filter was able to retain all the edges in the image as these edges also falls under the high frequency signal. For example, if there are particles in the image, then this filter tries to remove the bright region in the particle and was able to retain the edges of that particle. Hence these edges are very important in the case of cross correlation.

In the Figure 3.14, in the zoomed-in portion, before pre-processing the image, there were lot of lot of high density regions of particles as well as reflections in few regions. After applying the highpass sobel, the particles are clearly visible and the bright regions has been completely removed by retaining the patterns or edges.

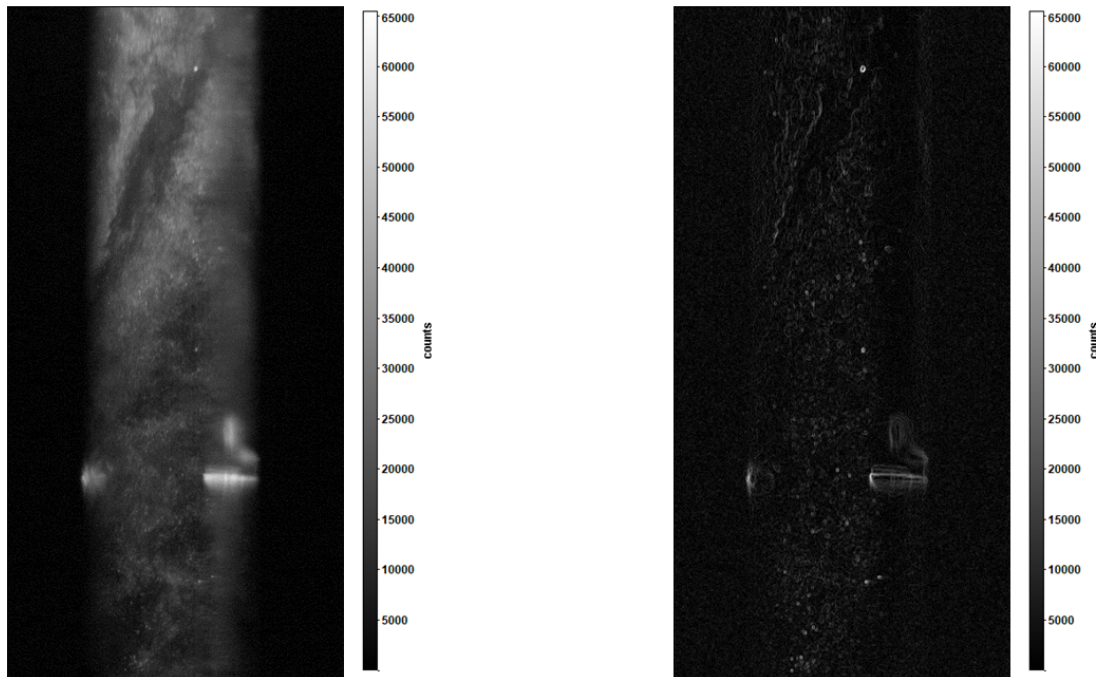


Figure 3.13: Left side image is the raw image and the right side image is pre-processed with the sobel filter

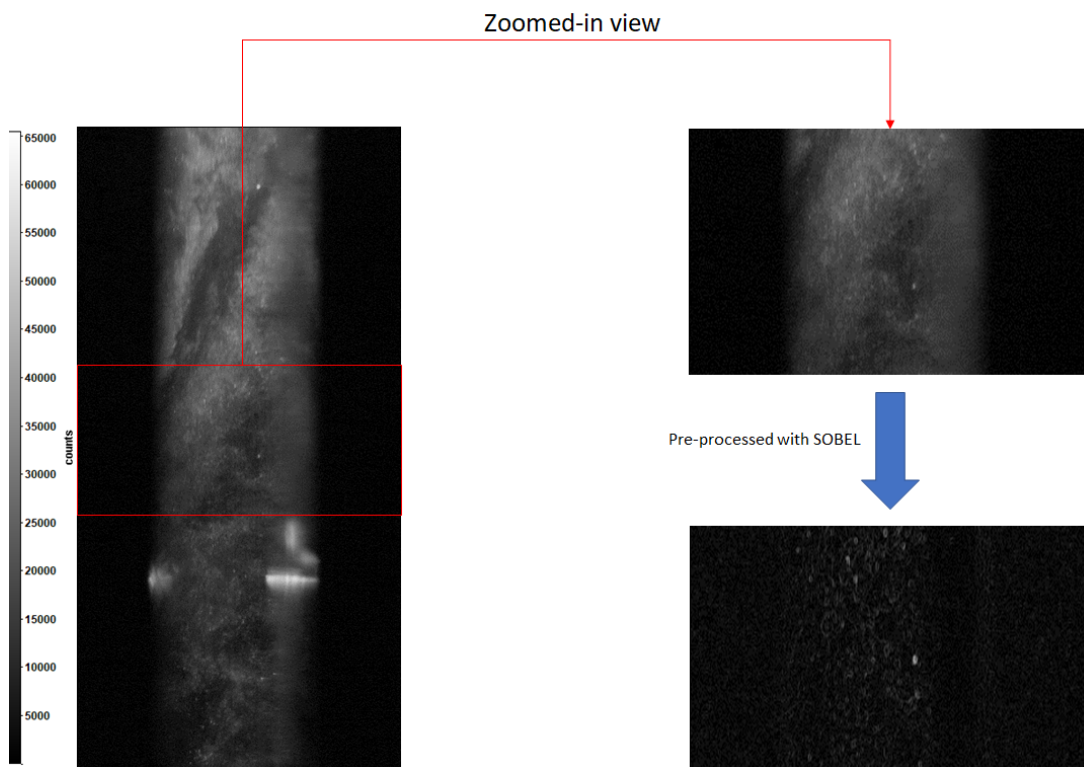


Figure 3.14: left image is the raw image and the right side images are the images before and after the sobel filter is applied for the region mention with red box

Before going further, it's seen that, this sobel filter is present in both OpenCV (Python) and the DAVIS 8.4. Let's quickly compare the results from these two software and conclude which one to be used.

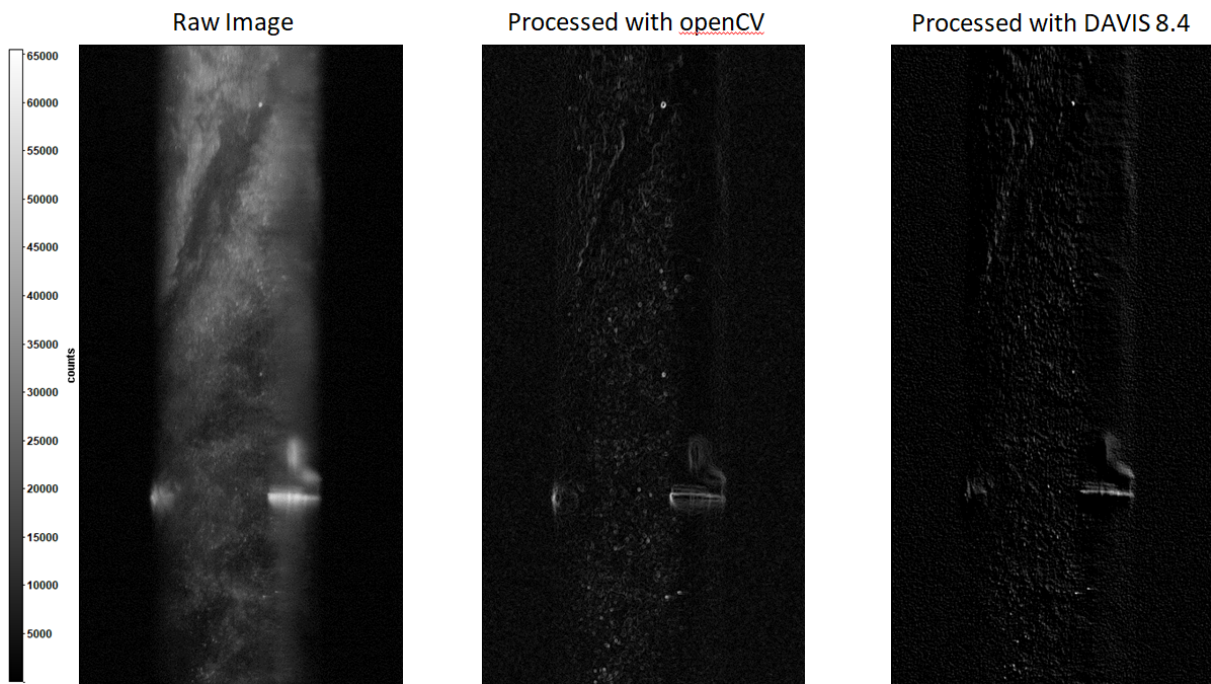


Figure 3.15: left image is the raw image, middle image is the pre-processed image with SOBEL (OpenCV) and the right most image is the image pre-processed with SOBEL (DAVIS 8.4)

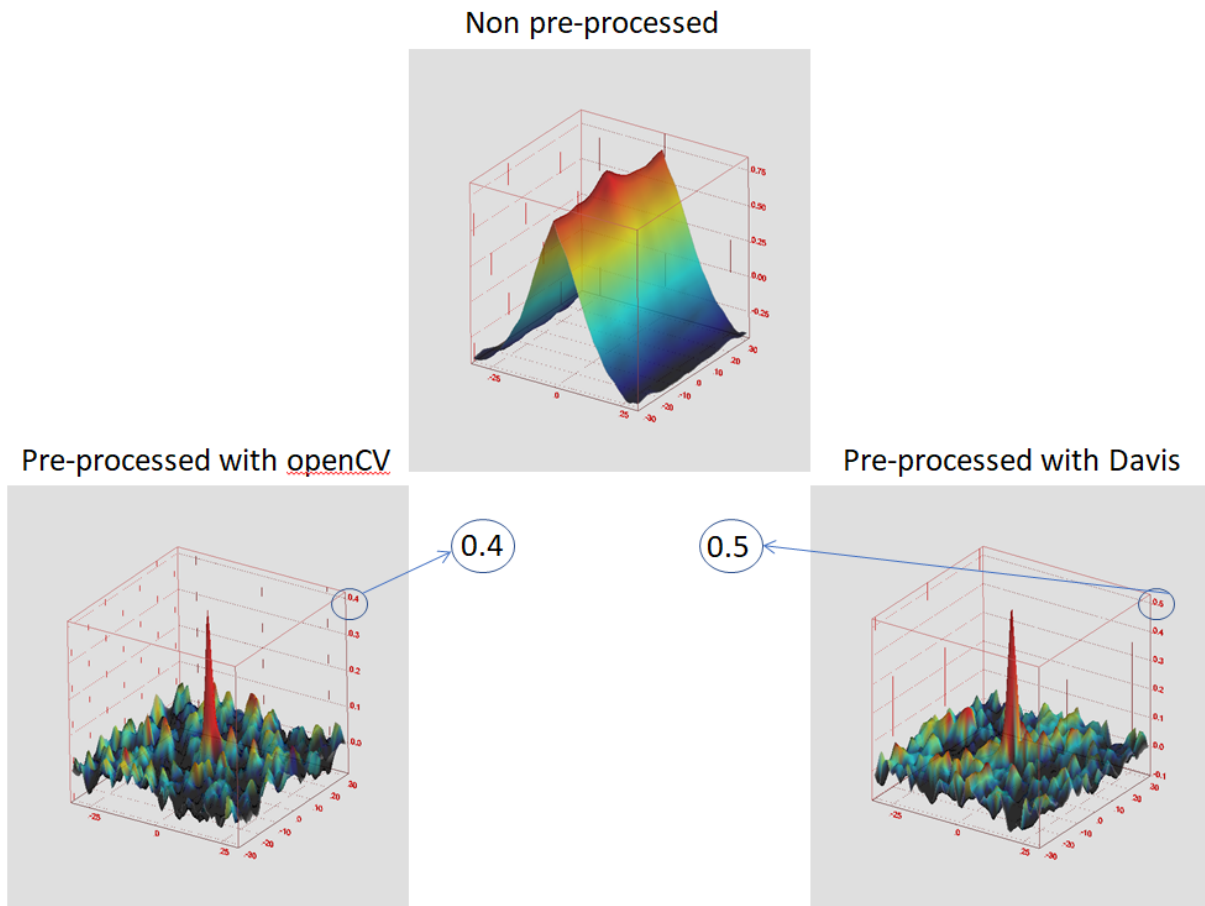


Figure 3.16: Comparison of correlation map for the raw image and between the software DAVIS 8.4 and the OpenCV

By looking into the images in Figure 3.15, its not clear which software performed well in our case. So, it is better to observe the correlation map. Lets check the correlation map of the same region that has been marked in the Figure 3.17 for comparing the software. In Figure 3.16, both the software produced similar kind of results. But while producing the peak, DAVIS 8.4 has a value of 0.5 whereas the OpenCV has a value of 0.4. These results of SOBEL with these two software, the DAVIS 8.4 shown better results compared with the OpenCV. So, for SOBEL filter, the DAVIS 8.4 software will be used in our work. Now looking back into the problem of the SOBEL filter, by observing the correlation map in Figure 3.17, in the presence of bright areas, the particles were not able to cross-correlate properly. This can be observed from the top correlation map where it was not able to make a proper peak. After pre-processing the image with sobel, the particles were able to cross-correlate properly which in turn creates a peak. This means that the instantaneous velocity evaluated in the region marked are correctly calculated.

It can also be observed from the bottom correlation map is that this image has lot of noise and this noise has not been removed with the help of the sobel. Since noise is a highpass signal, the sobel allows the noise to pass through. So after the highpass filter, it is necessary to pass the image through a denoising filter.

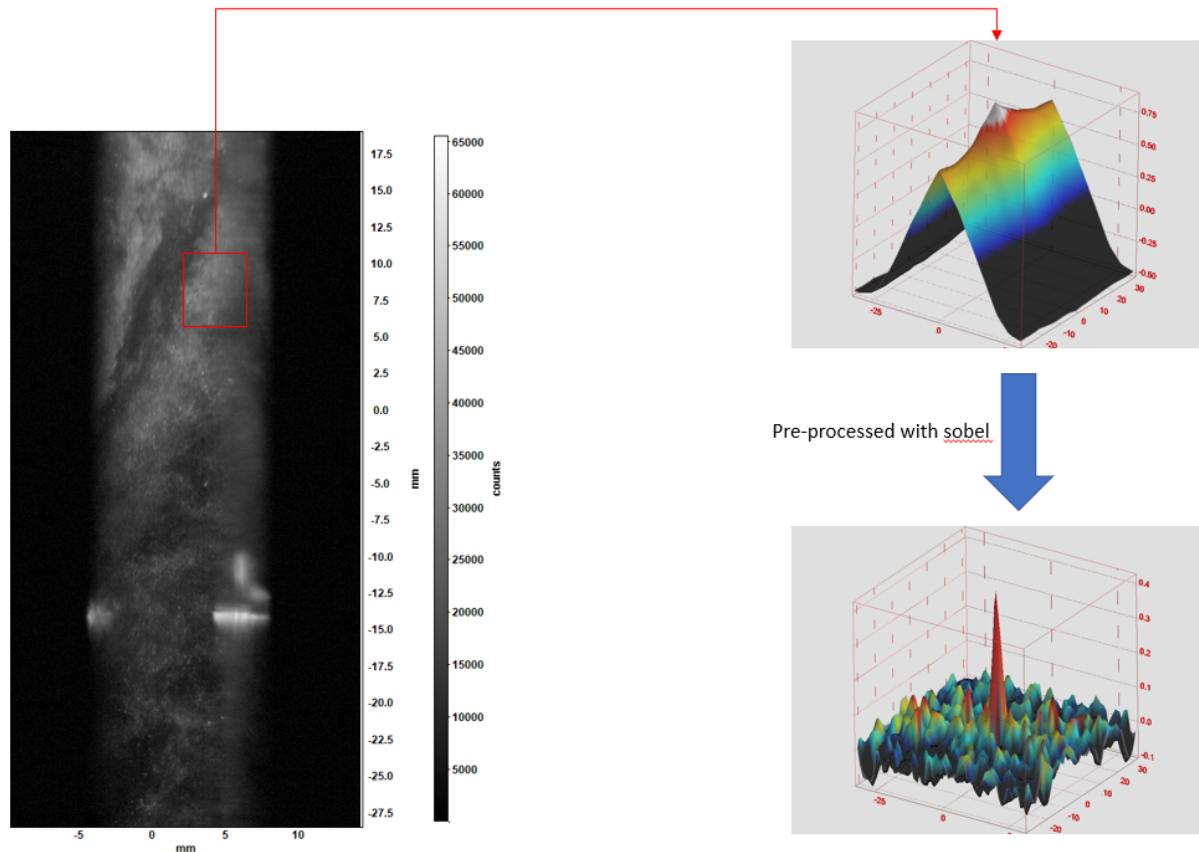


Figure 3.17: Correlation map of the region marked on the raw image(left image is the raw image) and the same map after applying the sobel filter

3.2.2. Temporal

Temporal is also one of the highpass filter for the background removal [24]. This temporal filter works on the basis of Discrete Fourier Transform (DFT). As described in the previous method, this filter also allows the high frequency signal to pass through and blocks the low frequency signal.

From the Figure 3.18, in the raw image there are lot of bright regions and few background reflections. In particular, in the marked region, it can be noticed that there are two background reflections one from the rotor blade and the other from the test section. After applying this filter, in the cropped image, it is clearly observed that both the reflections has been removed with the help of this filter. let's have a look at correlation map also.

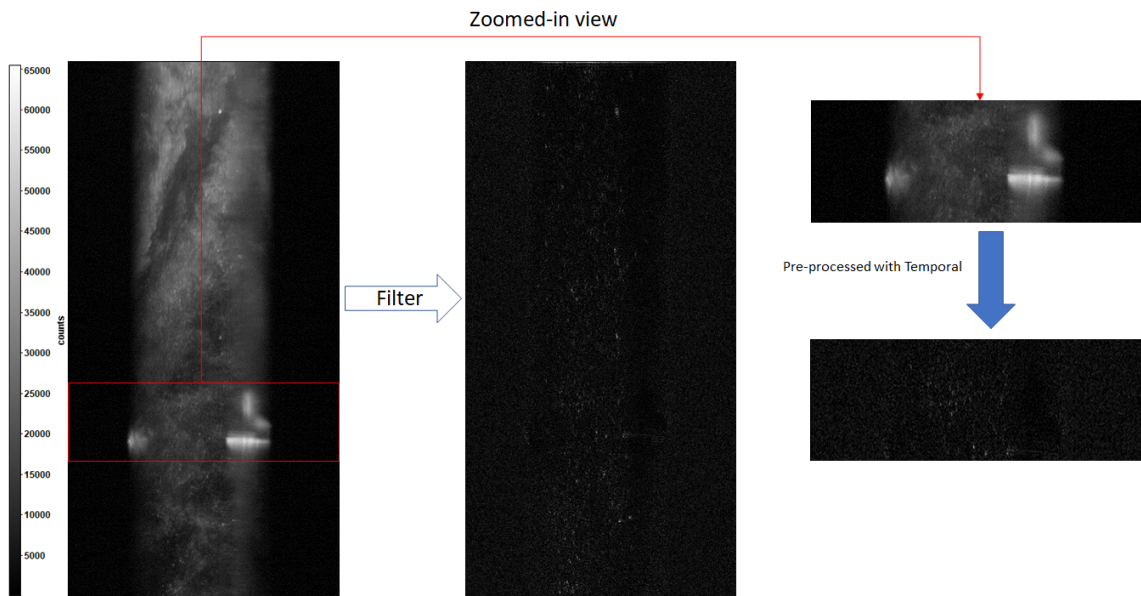


Figure 3.18: Representation of the complete and cropped image before and after applying the temporal filter

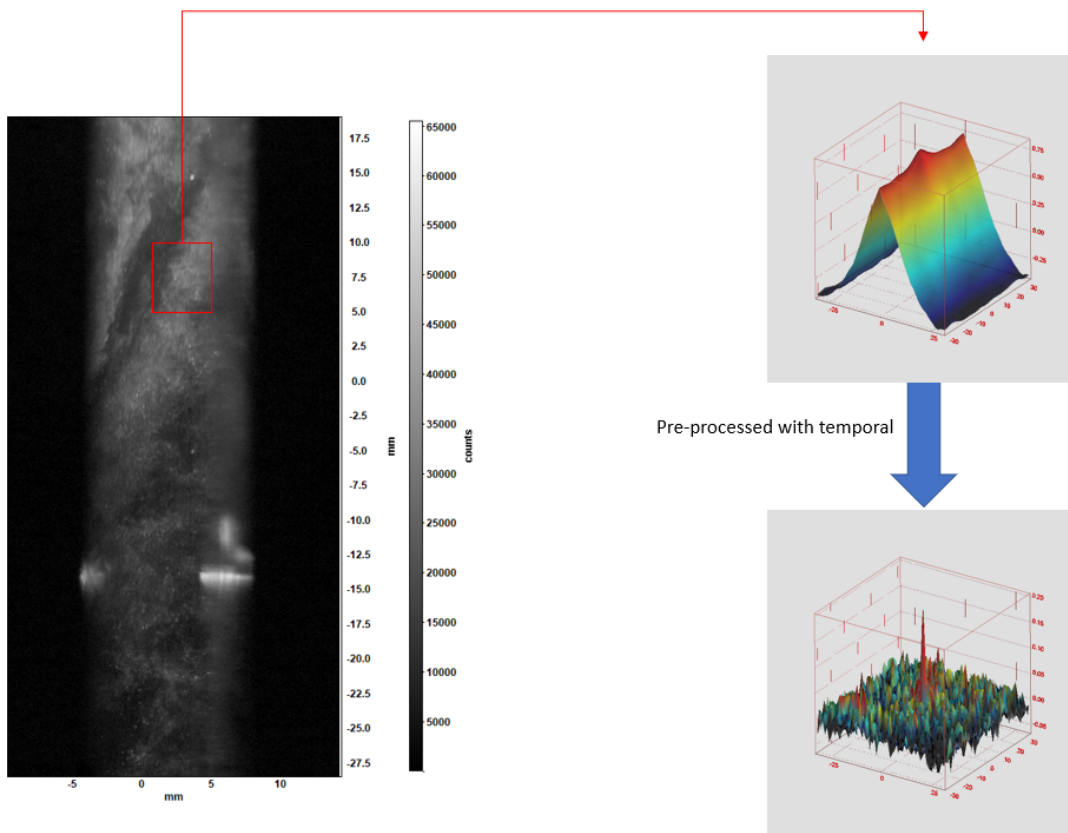


Figure 3.19: Correlation map for the marked region in the left image (raw image) before and after applying the temporal filter

In the correlation map from Figure 3.19, this filter was able to create a peak when compared with the raw image. But this filter is reducing the height of the peak drastically and the noise in the image is getting intensified. And also in few regions there are few unnecessary peaks that might mislead the calculations for the instantaneous velocity. So it is better to look into this filter with combinations of other filter for its best performance.

3.2.3. Proper Orthogonal Decomposition (POD)

While the highpass filter is suitable for high repetition rate systems, when this is not the case, it is still possible to assume that there exists a temporal basis function which correctly describes the variation of the background among the snapshots. The idea is that the background signal should exhibit a certain coherence in space and time which can be correctly captured with a principle component analysis of the acquired sequence of the particle images. This filter is followed by the article written by Mendez et al. (2017) [16]. The proposed method for the PIV image enhancement relies on the proper orthogonal decomposition (POD) of the image sequence to construct a reduced order model (ROM) which only retains the PIV particle pattern.

According to the author, after the images has been loaded into the code, the user has the flexibility for the quantity of modes that has to be removed. According to the users input, the code decides the quantity of particles that has been recovered in percentage. In our case, till the removal of 4 modes, there is no loss of particles. And If we remove eleven modes, we obtain a result with 98 percentage particle recovery. This code provides two types of output. Firstly, it provides the reconstructed image after removing the modes and secondly, it provides the image that has been removed from the reconstructed image.

In Figure 3.20, the left most image is the raw image. The middle and the right most images are the reconstructed image with 100 percent particle recovery and the background respectively. So, here in the reconstructed image, it can be clearly observed that the bright regions as well as few background reflections has been removed from the original image. The removed part from the raw image is shown in the right most image.

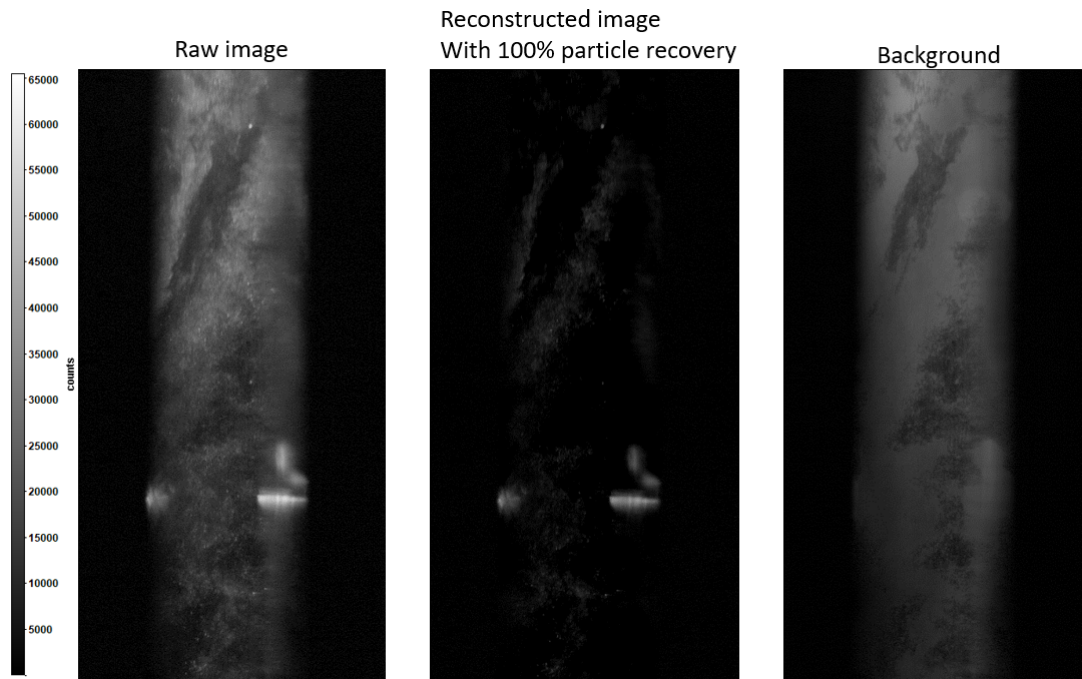


Figure 3.20: Left side image is the raw image, middle image is the reconstructed image with 100 percent particle recovery and the right most image is the background that has been removed from the raw image

It is strange to notice that even after the removal of bright regions as well as few of the background reflections, the correlation map has not improved significantly in Figure 3.21. One of the reasons for this might be the noise in the image. But the major reason is that, during the calculations of the displacements, the PIV cross-correlation also observes the patterns in the image. These patterns due to high density regions were observable during the cross correlation and was useful during the calculations of displacements in turn for the instantaneous velocity.

Let's observe the reconstructed image with 98 percent particle recovery in Figure 3.22 in order to support the above-mentioned conclusion regarding the correlation map.

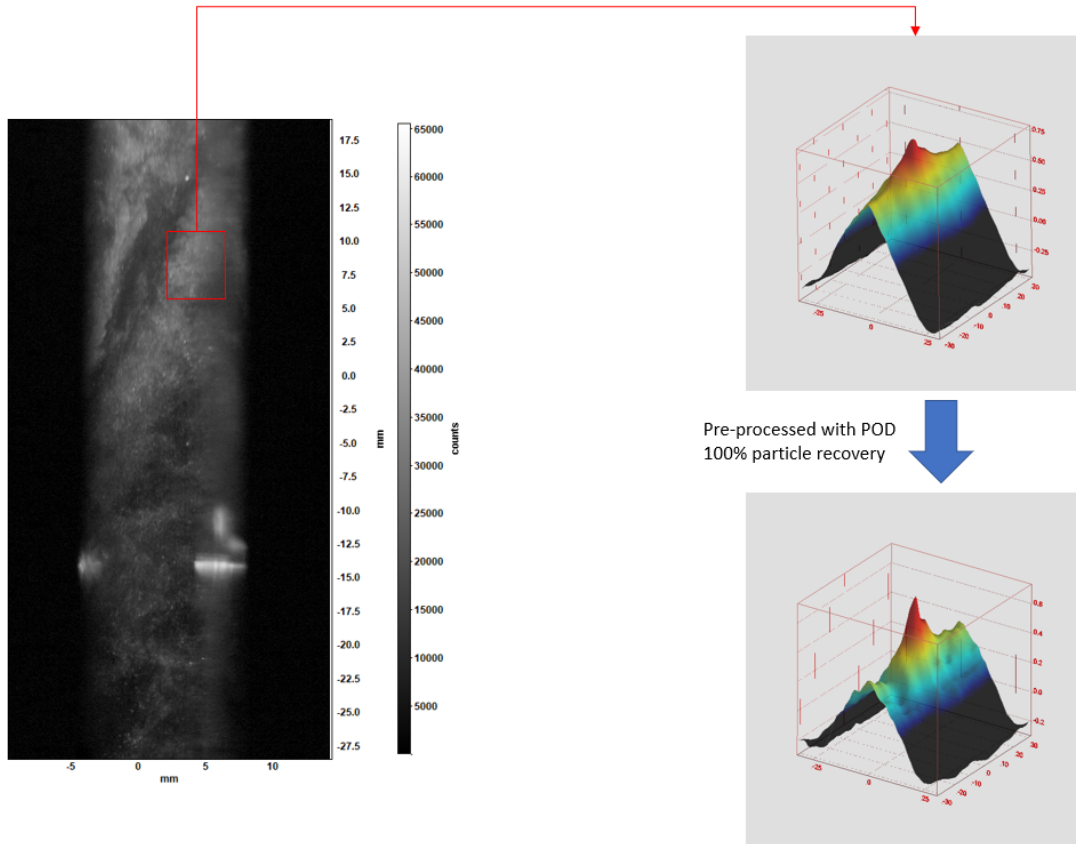


Figure 3.21: correlation map of the marked region in the left image(raw image) before and after the POD filter applied

When compared with the 100 percent particle recovery, the background has been removed in a better way and also the bright regions in the image. Here the image is losing 2 percent of particles for the better cross-correlation and for better background removal. As a result, this betterment is observed in the correlation map when compared with the 100 percent particle recovery. In 98 percent of particle recovery, the map is able to produce the peak. But this peak can not justify the proper cross correlation of the right particles because the peak is not so narrow (for example as shown in the left side of the Figure 1.4) and it is bit wider. Due to this there may be an influence of background reflections in the image.

As a result, it can be strongly said that the particle displacement in the correlation map depends on the patterns in the image. With this proper orthogonal decomposition (POD), the particles were able to cross correlate properly but the patterns are not able to do a proper cross correlation.

And hence, the combinations of multiple pre-processing filters can provide a conclusion for whether to use POD or not for this case.

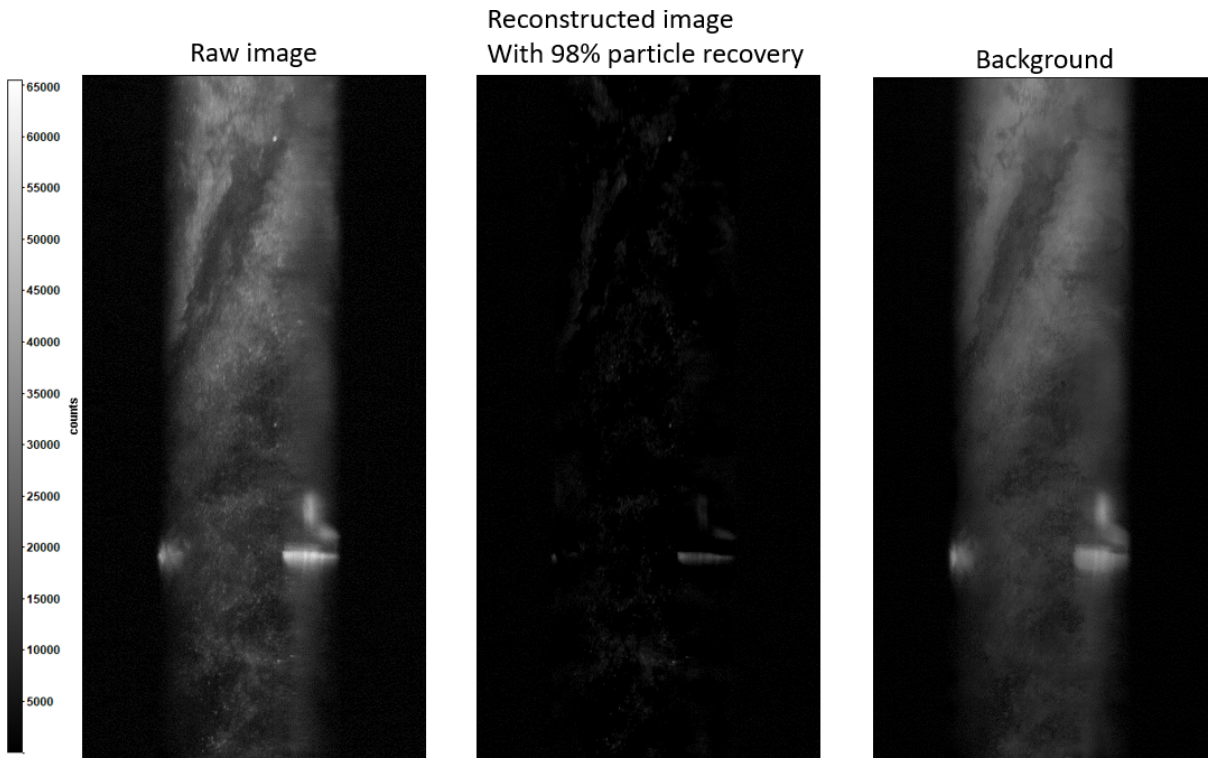


Figure 3.22: Left side image is the raw image, middle image is the reconstructed image with 98 percent particle recovery and the right most image is the background that has been removed from the raw image

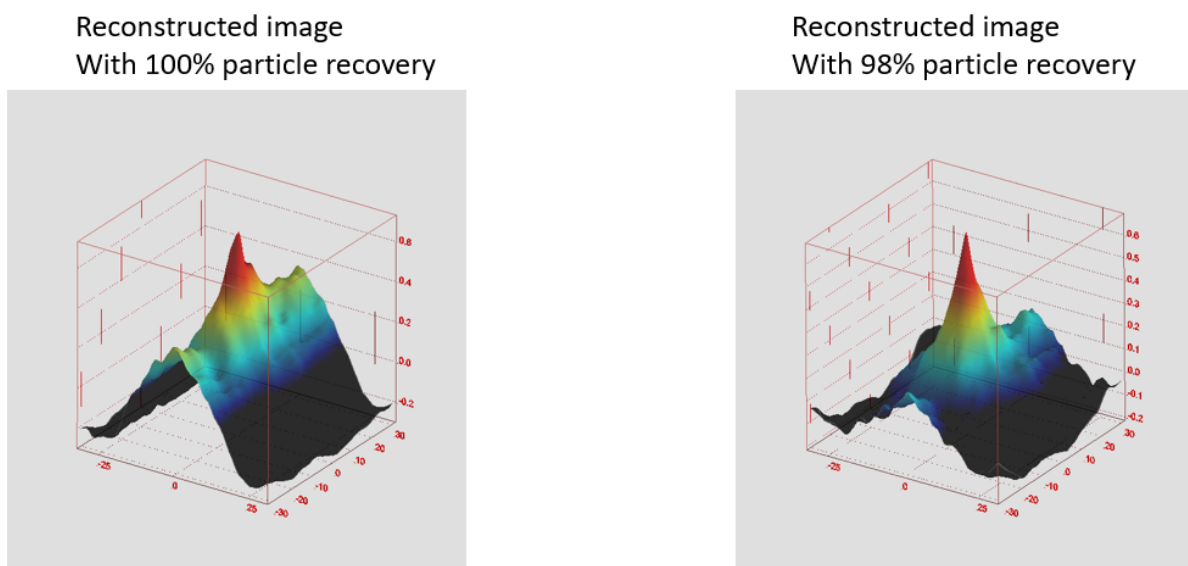


Figure 3.23: Comparison of correlation map between 100 percent particle recovery and 98 percent particle recovery with POD filter

3.3. Denoising (Smoothing)

Usually the Denoising or Smoothing filter plays a major role in PIV images because in general the PIV images have lot of noise in it. And also due to different pre-processing steps that involve local enhancement of the image quality also intensifies the noises in the image. All together considered, it is important to have Denoising filter for a PIV image. The following Denoising filters are used in the present context. Lowpass (Bilateral) and Lowpass (Gaussian) [25].

3.3.1. Bilateral and Gaussian

Both the gaussian and the Bilateral filter smoothens the image with different algorithms. The PIV images usually have lot of noises in the image when captured. And also, during the Min/Max intensity normalization or during the CLAHE, the enhancement happens locally for each window. During this process, if there exists any noise in the image, these pre-processing methods intensifies the noise in the image locally to the next level. So, whenever these enhancement methods are used, it is mandatory to smoothen the image for better cross-correlation.

In bilateral filter, the image is subjected to smoothing by taking into consideration the edges as well [27]. But when it comes to gaussian, the image is smoothed perfectly but the edges are not given importance. The Gaussian filter takes the neighbourhood around the pixel and finds its Gaussian weighted average. This Gaussian filter is a function of space alone, that is, nearby pixels are considered while filtering. It doesn't consider whether a pixel is an edge pixel or not. So it blurs the edges also, which we don't want to do in our case.

Bilateral filtering also takes a Gaussian filter in space, but one more Gaussian filter which is a function of pixel difference is also added. The Gaussian function of space makes sure that only nearby pixels are considered for blurring, while the Gaussian function of intensity difference makes sure that only those pixels with similar intensities to the central pixel are considered for blurring. So it preserves the edges since pixels at edges will have large intensity variation.

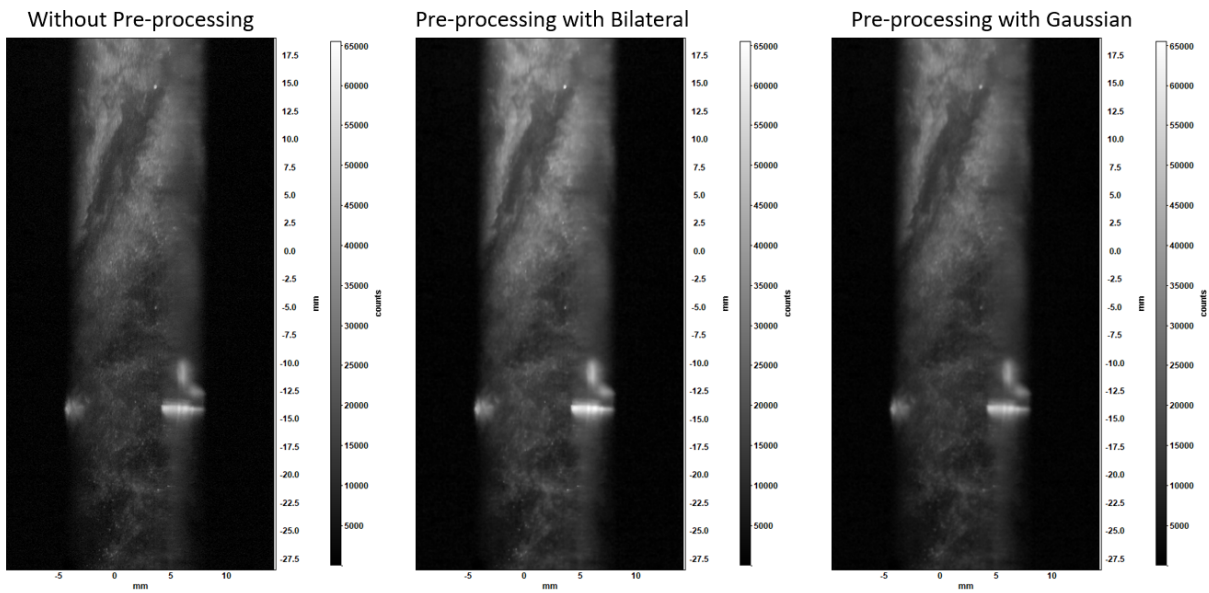


Figure 3.24: left image is the raw image, middle one is pre-processed with Bilateral filter and the right most in pre-processed with Gaussian filter

This actually makes a great impact in the present case because, the edges that are formed due to the smoke as well as particles plays an important role in the calculation of the displacements. This bilateral filter is imposed with the help of OpenCV whereas the gaussian filter is imposed with the help of DAVIS 8.4.

In the Figure 3.24, the difference between the gaussian filter and the bilateral filter is that, in bilateral filter, the edges are detectable whereas the gaussian just smoothed the whole image without giving importance to the edges.

From Figure 3.25, it is very clear that both the bilateral (b) and the gaussian (c) have smoothed the raw image. But the fact with respect to the definitions of both these filters, b should produce better results than c. This can be concluded while looking into the combinations of these pre-processing filters in order to have the better output of the data considered.

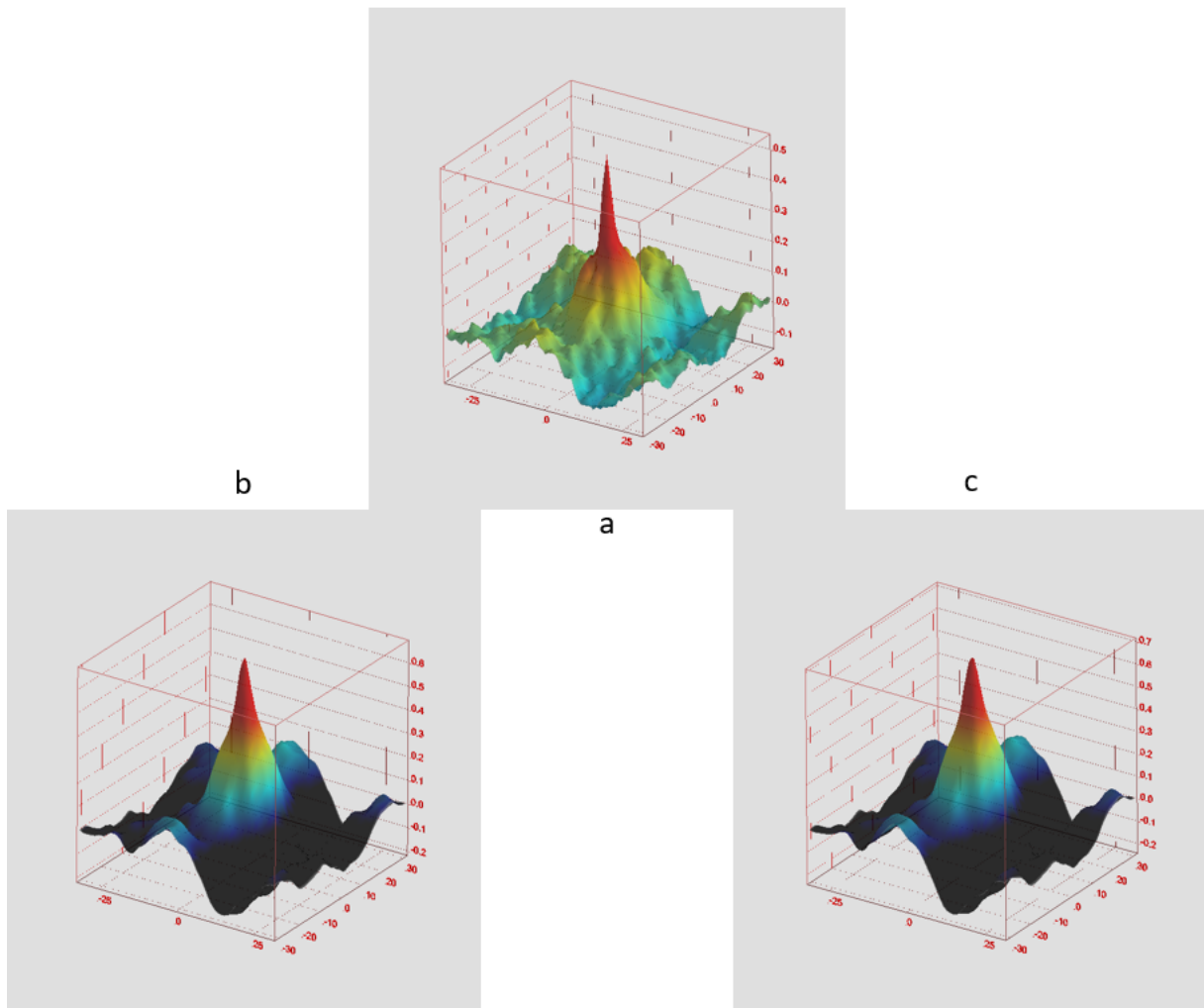


Figure 3.25: Correlation map comparison between the Bilateral filter and the Gaussian filter of the raw image

3.4. Combinations of Pre-Processing filters

To obtain the best PIV result or the best instantaneous velocity, it is not possible just by using any random pre-processing filter. If an image set is considered, the contrast enhancement is very important in order to observe the particles. Since most of the PIV setup consists of rotating or fast-moving objects as well as the metal surfaces in the test section as background, when the laser sheet falls on these fast-moving objects or on the metal surfaces, there will be a lot of reflections from those surfaces that are captured by the digital image. So, a high pass filter is also very important in order to eliminate these background reflections. In both the filters mentioned above, either they increase the noise in the image or they don't contribute to the reduction of noise. So, it is also very mandatory to use the denoising filter since the PIV images always have noise in the

image.

The following combinations are analyzed in order to have the best combination to obtain the better PIV image sets so that they provide the most accurate instantaneous velocity.

- CLAHE + Lowpass (Bilateral)
- CLAHE + Lowpass (Bilateral) + Highpass (Sobel)
- CLAHE + POD with 100 percent particle recovery + Lowpass (Bilateral)
- CLAHE + POD with 98 percent particle recovery + Lowpass (Bilateral)

The first combination is just to observe the contrast enhancement and lowpass without the highpass filter. For lowpass filter, with few comparisons between the bilateral and the gaussian, the gaussian just smoothens the image where as the bilateral smoothens the image by taking the edges into consideration. Because of the mentioned reason earlier, the bilateral produced better results compared to the gaussian. And also, for POD filter it is better to use CLAHE in advance in order to produce the contrast enhancement before the removal of the background.

3.4.1. CLAHE+Lowpass(Bilateral)

In this combination, it is possible to observe how the contrast enhancement and denoising works without the background removal. Initially, the contrast enhancement happens and then the reduction of noise. It is not performed the opposite way because, during the denoising step, it is not that this filter completely eliminates the noise rather it tries to reduce it.

So, if the denoising filter occurs first and then the contrast enhancement, if at all there are few noises that are not completely filtered get intensified during the contrast enhancement. It is always important to apply the contrast enhancement first and then the denoising.

From Figure 3.26, It is clear that the CLAHE has done the contrast enhancement. But it should also be noted that by the definition of CLAHE, this filter intensifies the noise locally in the image. Now after the contrast enhancement with CLAHE, the image has to undergo denoising. This is being done by the lowpass (Bilateral).

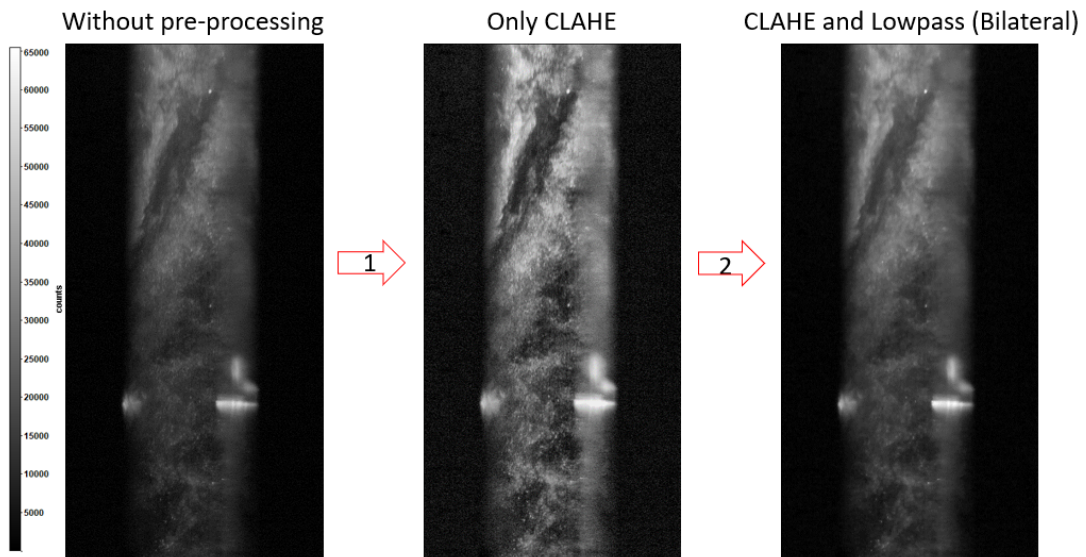


Figure 3.26: Left most image is the raw image, middle image is pre-processed with only CLAHE and the right most image is the combination of CLAHE and Lowpass (Bilateral)

During the enhancement of contrast and denoising, it is observed in Figure 3.27 that from a to b the peak has been improved from 0.4 to 0.8. And also, the image has been smoothed. Since the peak is not sharp, which means that the same particles are not cross-correlating. This is because of the effect that the background removal filter is not applied. Due to this, during the cross-correlation, the particles are not able to find the same particles in the next image. This bias is happening due to the presence of bright regions or spots in the image. So, in conclusion, it is important to have the background removal filter for this present case and also for most of the PIV experimental case.

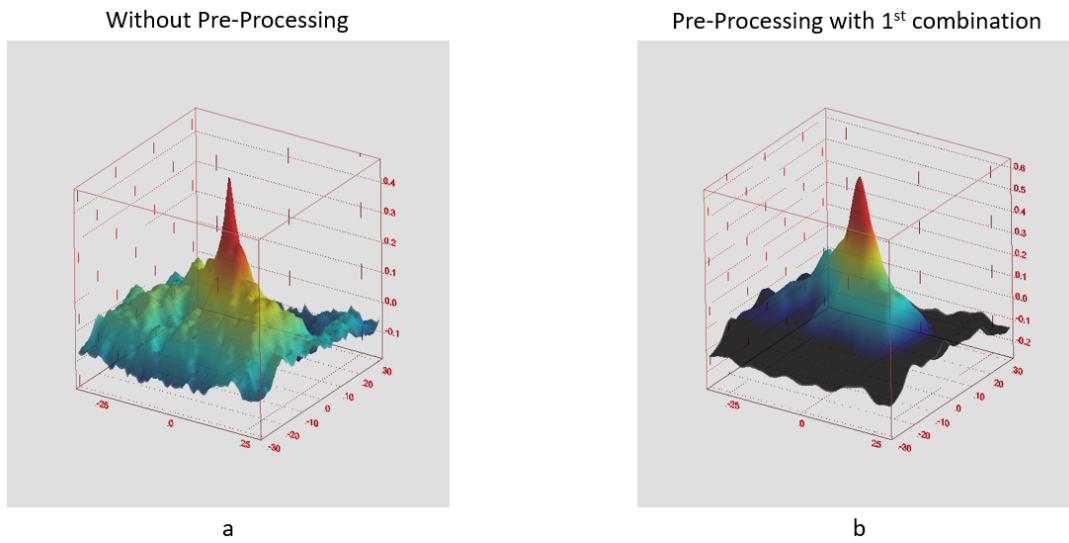


Figure 3.27: Comparison of correlation map between the raw image and the combination CLAHE and Lowpass (Bilateral)

3.4.2. CLAHE + Lowpass (Bilateral) + Highpass (Sobel)

As mentioned in the previous combination, background removal was one of the major filters in order to obtain the better results for instantaneous velocity in the PIV calculations. Because of that, in the previous combination, the particles were not able to cross-correlate properly with the same particles in the next image. This was observed in the correlation map.

Here, after applying the denoising filter to the contrast enhanced image, the background removal (Sobel) is being applied. From the description of the previous sections, the highpass (Sobel) filter will allow the noise to pass through the filter since the noise is a high frequency signal. The final image is one of the best outputs seen so far (from Figure 3.28, the right most image). The final image's contrast has been enhanced, the noise has been filtered and even the background signal has been removed. In this way, the particles and patterns in the image cross-correlate properly with the same particles and patterns in the next image in order to compute the best instantaneous velocity.

In Figure 3.29, the correlation map also shows a better result. In Figure 3.29, from a to b, the image was not able to cross-correlate properly. This is due to the background reflections present in the image. After applying the highpass (Sobel), the peak in the correlation map is observable.

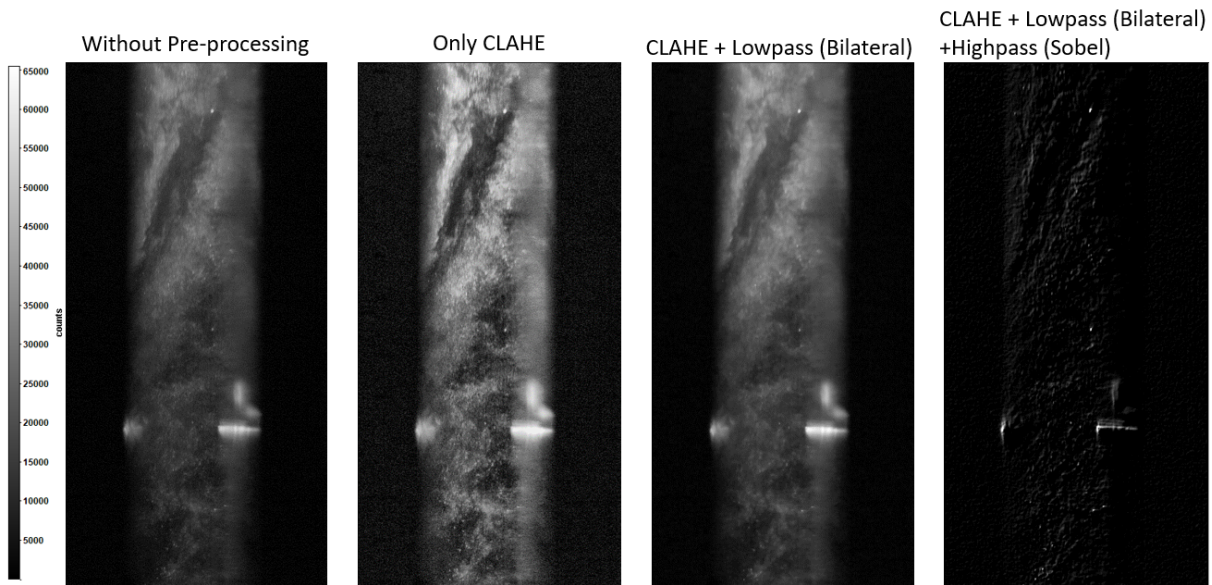


Figure 3.28: From left side, 1st image is the raw image, 2nd image is pre-processed image only with CLAHE, 3rd image is a combination of CLAHE and Lowpass (Bilateral) and finally 4th image is the combination of CLAHE, lowpass (Bilateral) and Highpass (Sobel)

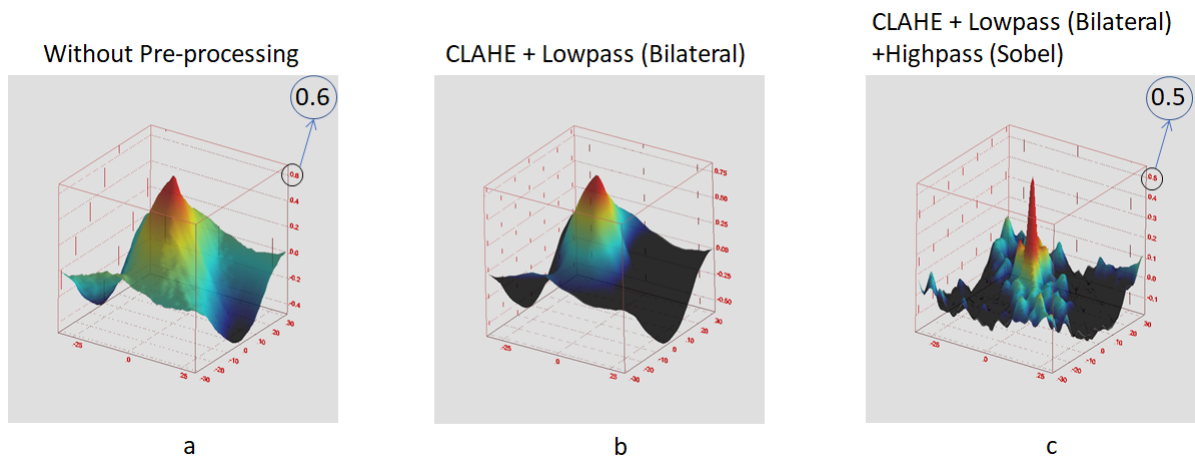


Figure 3.29: Correlation map comparison for raw image, Combination (CLAHE + Lowpass (Bilateral)) and the combination (CLAHE + Lowpass (Bilateral) + Highpass (Sobel))

In Figure 3.29, it is observed that the peak has been dropped from 0.6 to 0.5. But having 0.5 with proper cross-correlation is better than having 0.6 as a greater peak. Figure 3.30 gives the better comparison in terms of the instantaneous velocity. In the figure without pre-processing, it is observed that at the marked region, the instantaneous velocity components are missing or PIV was not able to compute the velocity components at those regions. In general, the displacements in the PIV is calculated with the help of

particles that are being displaced from one region to the other in the same set of image pairs. And the particle displacement and the time taken for the particle to travel such a distance provides the instantaneous velocity .

The reason for velocity components not been computed is that, presence of bright area or background reflection in that location. Due to the presence of background reflection, there was no subsequent motion of particles in that short time period range. Because of this, it produced a null velocity in those locations. After applying the filter for background removal (with this present combination) the reflections in the raw image has been removed. Due to which the it was properly able to cross correlate the particles which in turn able to track the displacement of the particles.

This present combination produced best result of the PIV data that has been extracted. But it is also important to look into the combination that has proper orthogonal decomposition also. Because, POD based filter is also one of the best ways to remove the background. With no loss of particles or with very minimal loss of particles, this POD based filters are a best way to obtain better results.

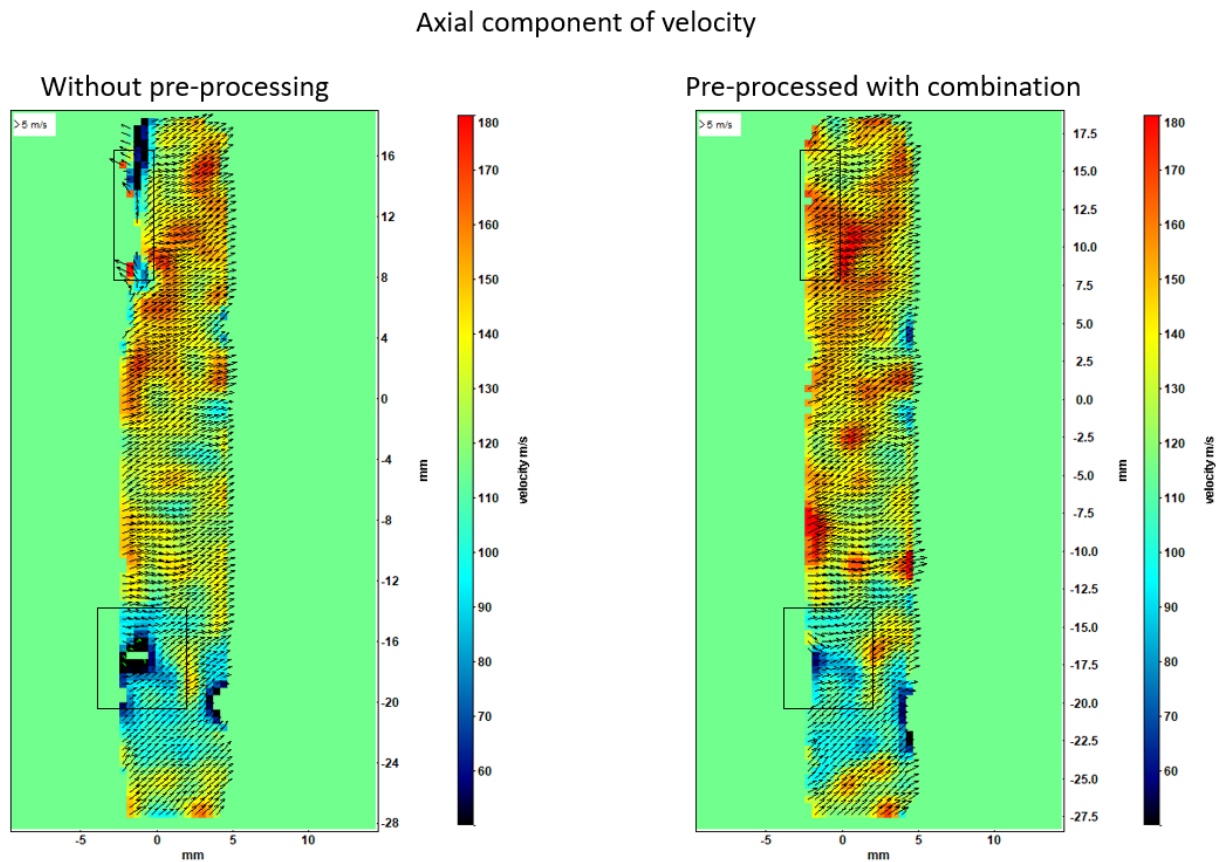


Figure 3.30: Comparison of Axial component of velocity for the raw image and the combination (CLAHE + Lowpass (Bilateral) + Highpass (Sobel))

3.4.3. CLAHE + POD with 100 percent and 98 percent particle recovery + Lowpass (Bilateral)

In this combination, the reason for having smoothing filter at the end instead of having before the background removal is that, POD based filter is Insensitive to the noise. From Figure 3.31, it is very clear that the images in a as well as in b exactly remains the same. This shows that the POD is insensitive to the noise. So instead of having the smoothing in the middle, it is better to have at the end because if somewhere in the process of pre-processing, if there is an intensification of the noise, then this lowpass filter at the end might be very useful.

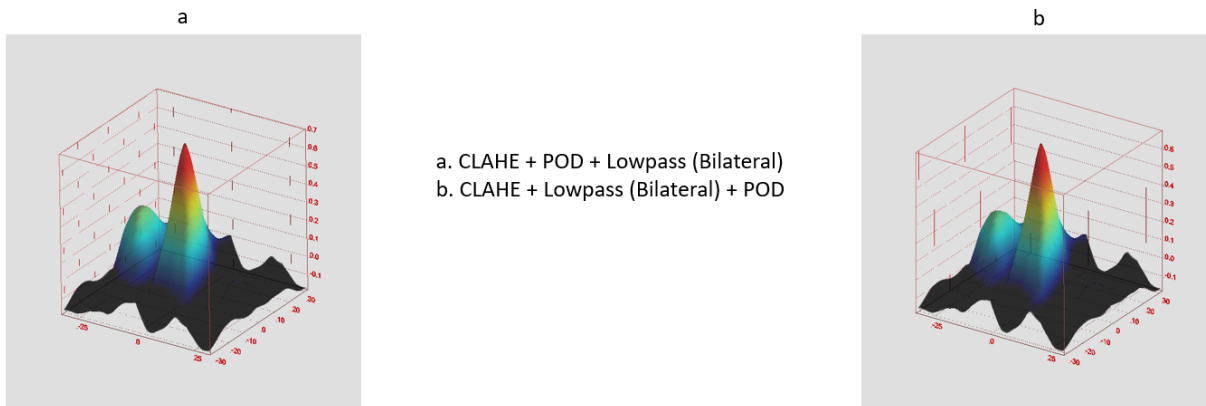


Figure 3.31: Comparison of correlation map for two different combinations; (a) Combination (CLAHE + POD + Lowpass (Bilateral)); (b) Combination (CLAHE + Lowpass (Bilateral) + POD)

From Figure 3.32, it observed that how gradually the raw image is getting pre-processed. As it is observed from the previous combination, in the first step, the contrast has been enhanced. In the coming steps the POD filter is being applied followed by the lowpass filter. Here in this figure, it is observed that the background has been removed with 100 percent particle recovery. Due to this complete particle recovery and the background removal, now the particles will be able to cross correlate properly. This will be clearly observed with the correlation maps in the following figures.

From Figure 3.33, it is important to notice that, the raw image is producing a high value of correlation peak than the pre-processed image. But the fact is that, even though the raw image produced high peak than the pre-processed image, the pre-processed image has the better results than the raw image. In the raw correlation peak of the raw image, there is a lot of background reflection due to which the cross correlation is happening between the reflections and not exactly the particles. So this may increase the peak but it is not best result. In the correlation map of pre-processed image, it is able to observe multiple peaks in the image.

This is due to the background reflection. Since the POD is applied with 100 percent particle recovery, the background reflection is not being eliminated properly.

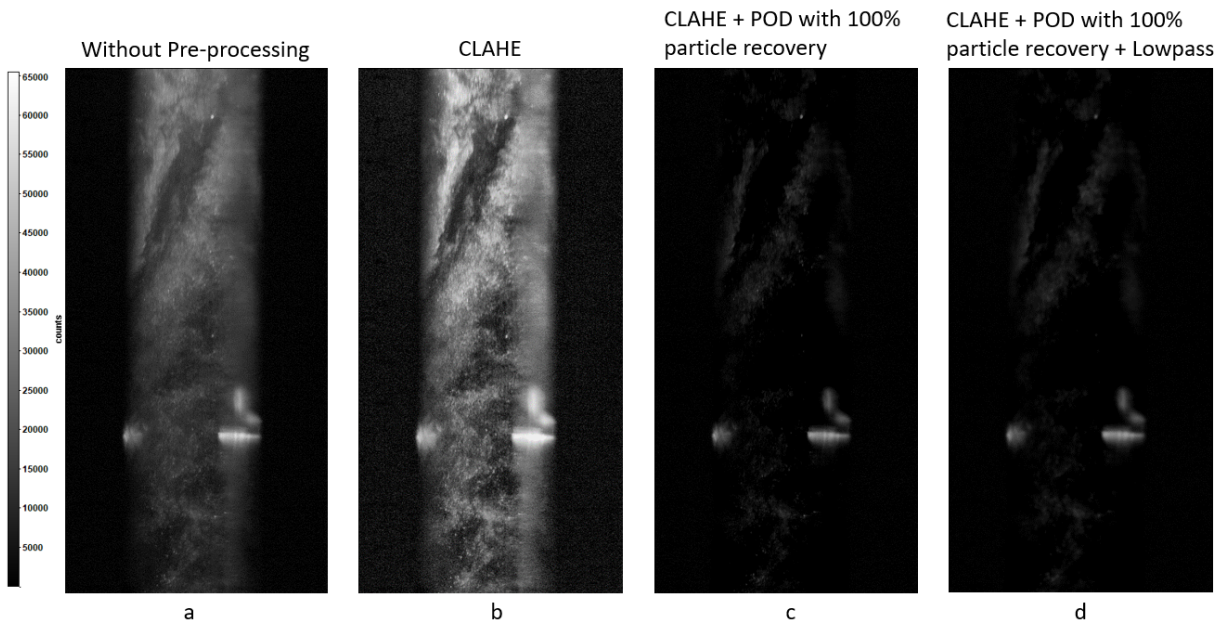


Figure 3.32: From left side, 1st image is the raw image, 2nd image is pre-processed image only with CLAHE, 3rd image is a combination of (CLAHE + POD with 100 percent particle recovery) and finally 4th image is the combination of (CLAHE + POD with 100 percent particle recovery + Lowpass (Bilateral))

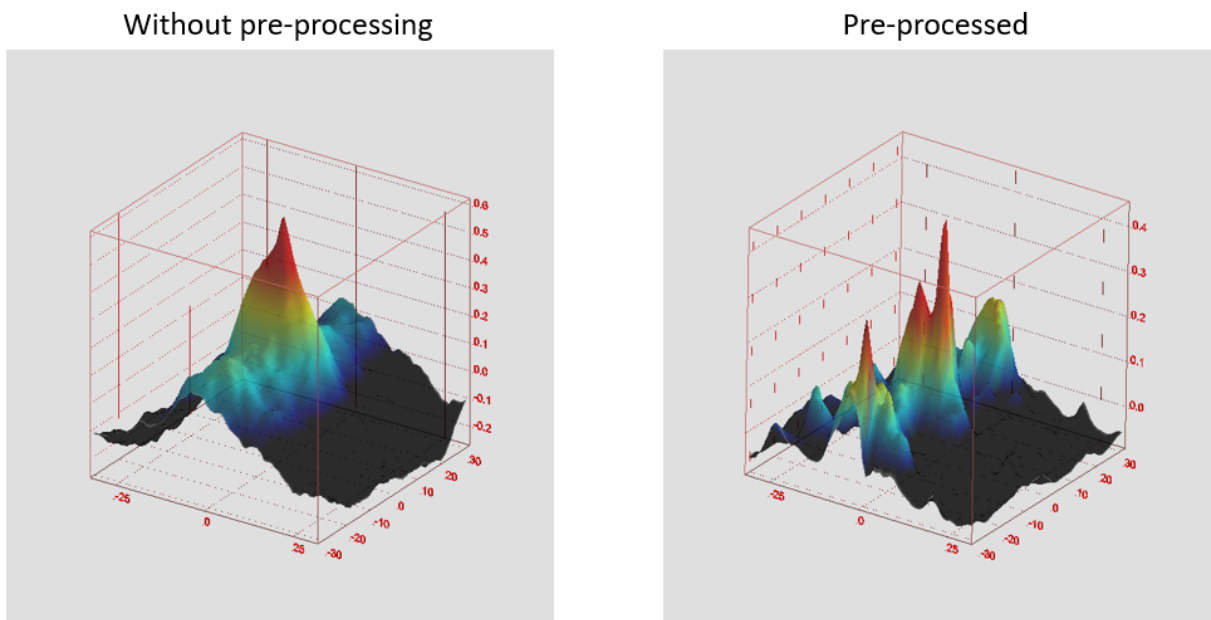


Figure 3.33: Comparison of correlation map between the raw image and the combination (CLAHE + POD with 100 percent particle recovery + Lowpass (Bilateral))

Now the POD is applied with 98 percent particle recovery which means that during the

process of removal of background reflection, 2 percent of particles has been lost. But by losing a few percent of particles, the unnecessary peaks have been eliminated. This is being observed in the Figure 3.34 (c). In Figure 3.34, the comparison between the 100 percent and 98 percent particle recovery is made with raw data. In b, there are unnecessary peaks that are being eliminated in c. In c, by losing 2 percent of particles, the background has been removed in a very effective way so that it was able to eliminate all the other peaks which was forming due to the background reflection and even the correlation between the non-same particles. Hence as a result, combination with 98 percent recovery was able to produce better results than the combination with 100 percent particle recovery.

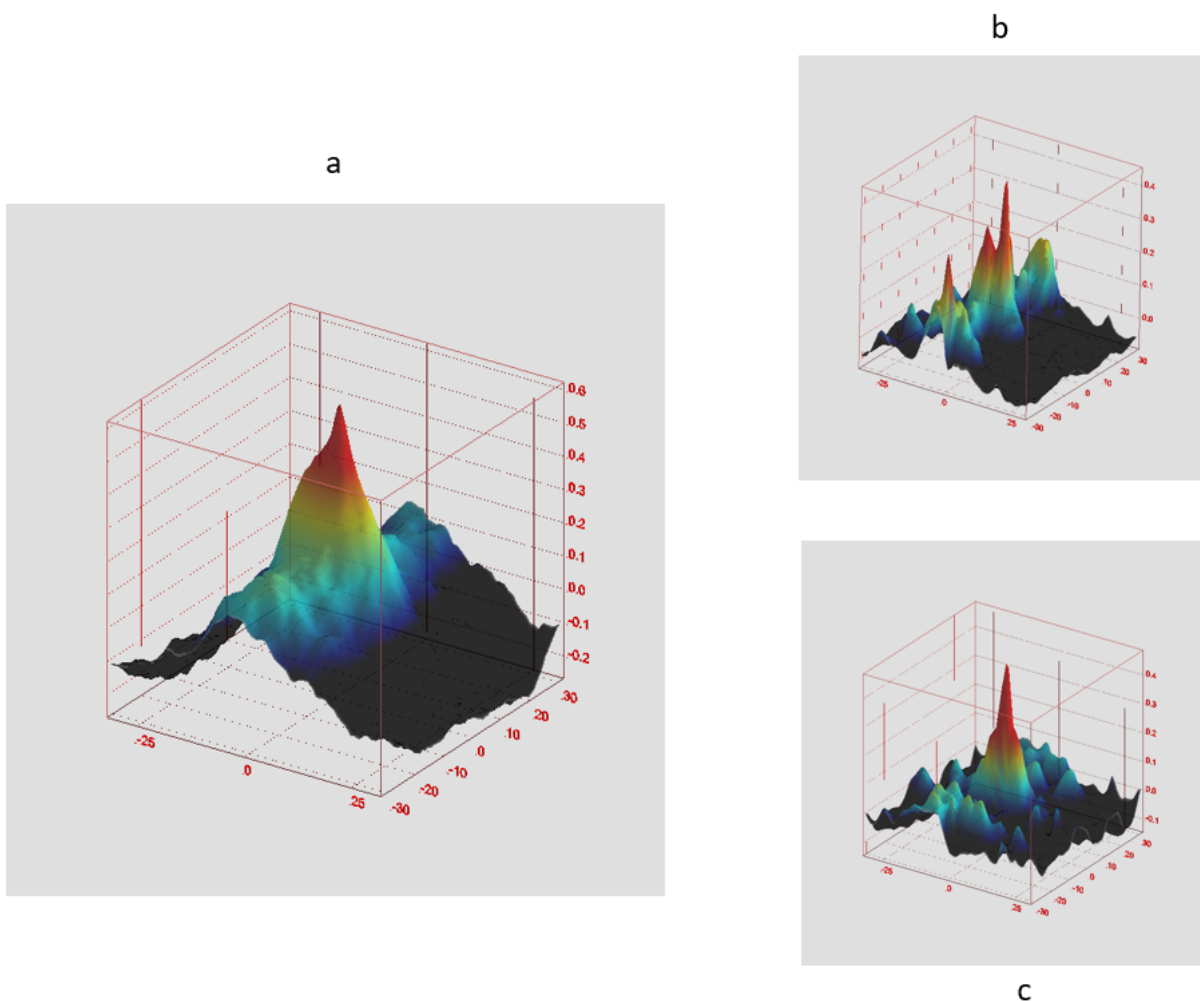


Figure 3.34: Comparison of correlation map; (a) raw image; (b) Combination (CLAHE + POD with 100 percent particle recovery + Lowpass (Bilateral)); (c) Combination (CLAHE + POD with 98 percent particle recovery + Lowpass (Bilateral))

Different combinations has been analyzed and now it is time to compare these different combinations and check for the best one.

3.5. Conclusion for Pre-Processing of PIV images

Different individual pre-processing filters and different combinations of multiple filters has been analyzed. Now, the comparison between the combinations mentioned in the previous sections has to be done. These comparisons has been made in order to observe for the best combination that provides the best result for the pre-processing that is being done on the raw data.

We will look into two examples in which one has a background reflection in the captured image 3.35(a) and the other 3.35(b) has the region where the density of particles is low such that in that region the particles where not able to cross correlate properly.

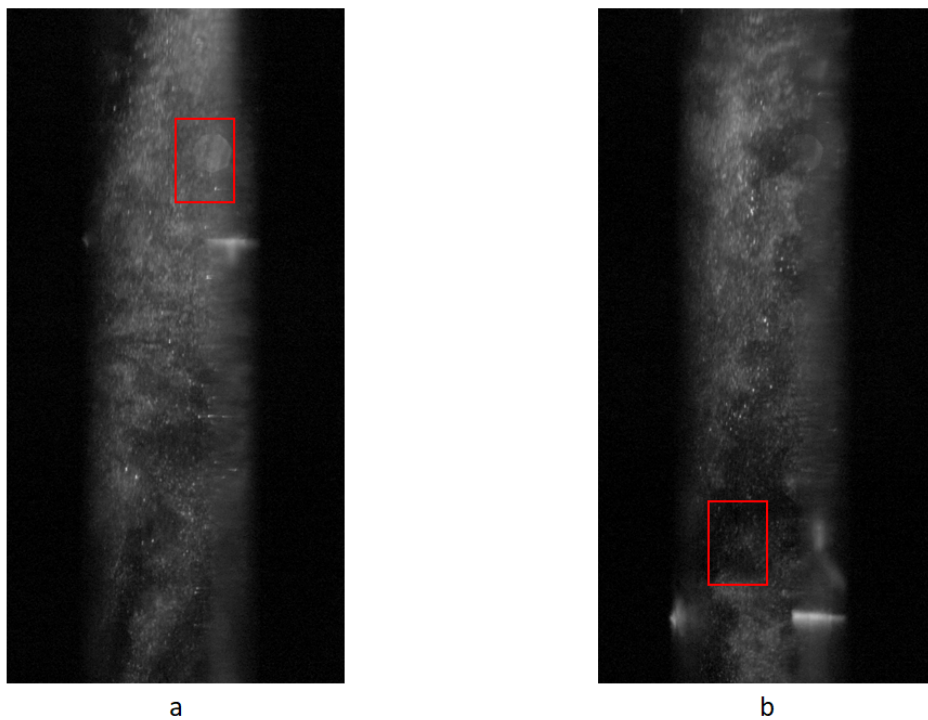


Figure 3.35: (a) raw image representing a background reflection ; (b) raw image representing the region where the density of the particles is low

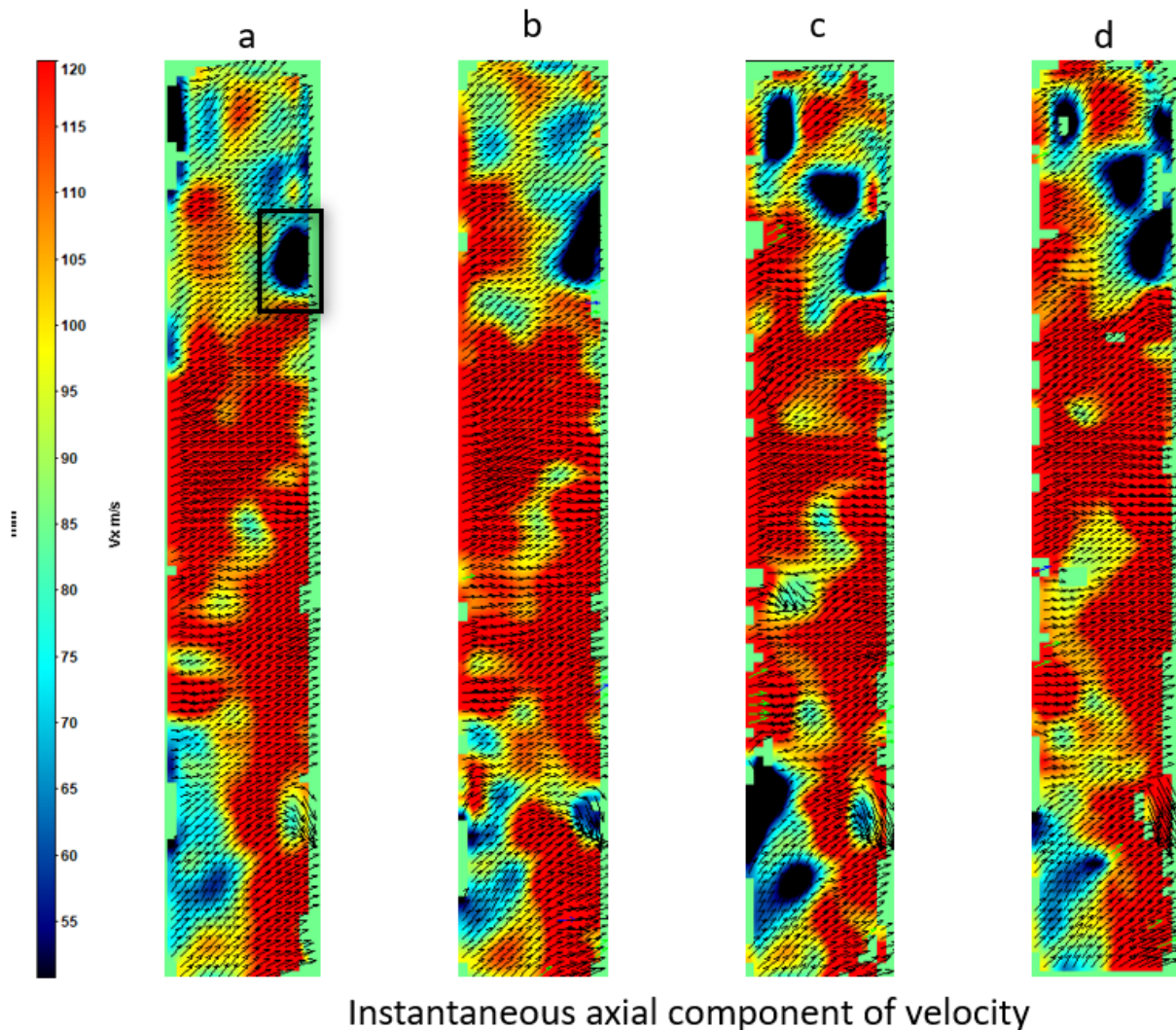


Figure 3.36: Comparison of instantaneous axial component of velocity; (a) raw image; (b) combination (CLAHE + Lowpass (Bilateral) + Highpass (Sobel)); (c) Combination (CLAHE + POD with 100 percent particle recovery + Lowpass (Bilateral)); (d) Combination (CLAHE + POD with 98 percent particle recovery + Lowpass (Bilateral))

Firstly the example of a region where there is a presence of background reflection is considered. In Figure 3.36(a) in the marked region, there is a background reflection due to the test section. Since there is a reflection, the particles were not able to cross correlate properly due to which it resulted in a very low velocity and even the correlation map provided the poor results (Figure 3.37(a)). The background reflection has to be eliminated for which the combinations mentioned in the previous sections has to be used. In Figure 3.36, all three combinations have provided the results by removing the background reflection. In order to check for the best combination, the cross correlation map also needs to be compared. One important point needs to be noted is that, in few regions of the

instantaneous velocity after pre-processing the image has lost few vectors. But in reality, it is not the pre-processed image that has lost few vectors but it is the raw image that produced few incorrect vectors by cross correlating the background reflection and bright spots in the image.

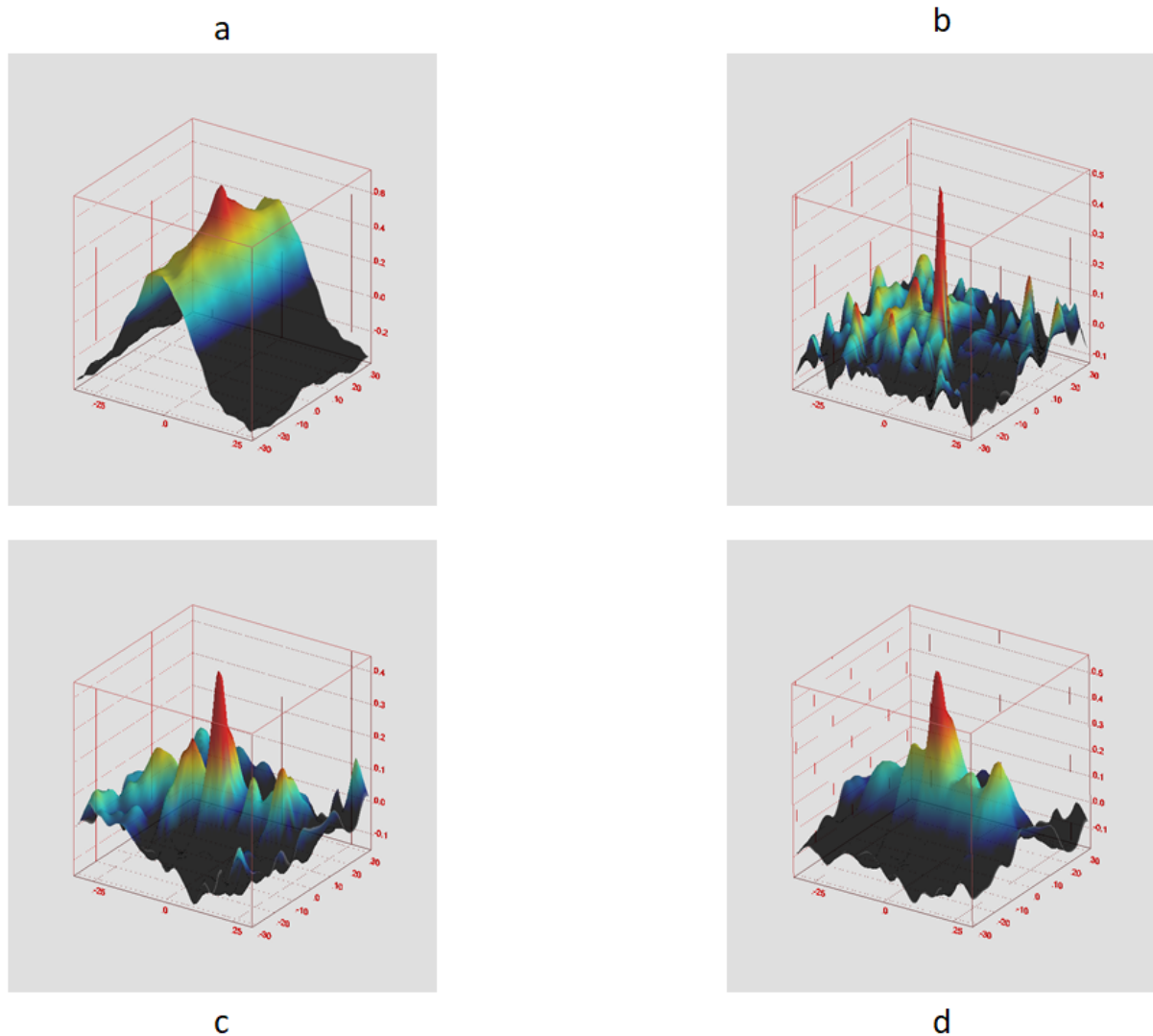


Figure 3.37: Comparison of correlation map for different combinations; (a) raw image; (b) combination (CLAHE + Lowpass (Bilateral) + Highpass (Sobel)); (c) Combination (CLAHE + POD with 100 percent particle recovery + Lowpass (Bilateral)); (d) Combination (CLAHE + POD with 98 percent particle recovery + Lowpass (Bilateral))

Now by observing the correlation map in the Figure 3.37(a), the raw data is not able to cross correlate properly. All the three Figure 3.37 (b), (c), (d) are able to produce better results than the raw data. When the figure (c) and (d) are compared, the combination with 98 percent particle recovery is able to produce better results than the 100 percent

particle recovery. And when all the three combinations are compared, the combination (b) produced the best output. It was able to produce a proper peak as well as all other unnecessary peaks have been suppressed. This means that in combination (b), all the particles were able to cross correlate properly by removing the background. Hence, in this example, the combination (b) produced the best results.

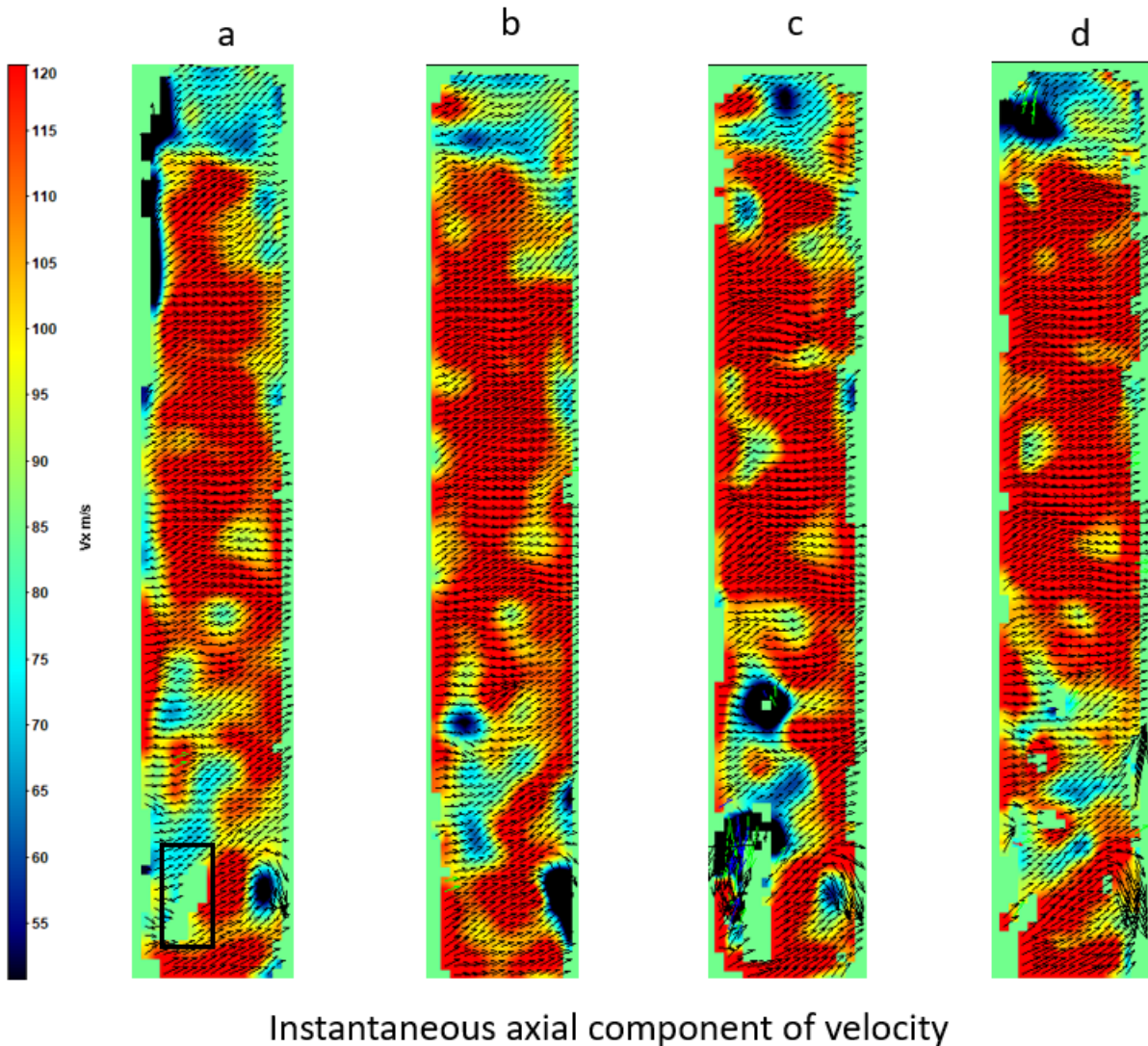


Figure 3.38: Comparison of instantaneous axial component of velocity; (a) raw image; (b) combination (CLAHE + Lowpass (Bilateral) + Highpass (Sobel)); (c) Combination (CLAHE + POD with 100 percent particle recovery + Lowpass (Bilateral)); (d) Combination (CLAHE + POD with 98 percent particle recovery + Lowpass (Bilateral))

Let's look into another example. In this example, there is a region (which is marked in the Figure 3.38(a)) where the construction of instantaneous velocity was not done properly and hence the vectors are being missing in that region. Once again all the three

combinations are being used for the best results. Combination (b) and (d) were able to construct the vectors in which (c) produced slightly less vectors. The combination (c) was not able to produce the vectors. The correctness of this reconstruction has to be verified with the help of the correlation map. Let's look into Figure 3.38. The raw data isn't produced any peak in the marked region which is obvious that the data is missing in that region. The combination (c) with 100 percent particle recovery shows a similar result as that of the raw data.

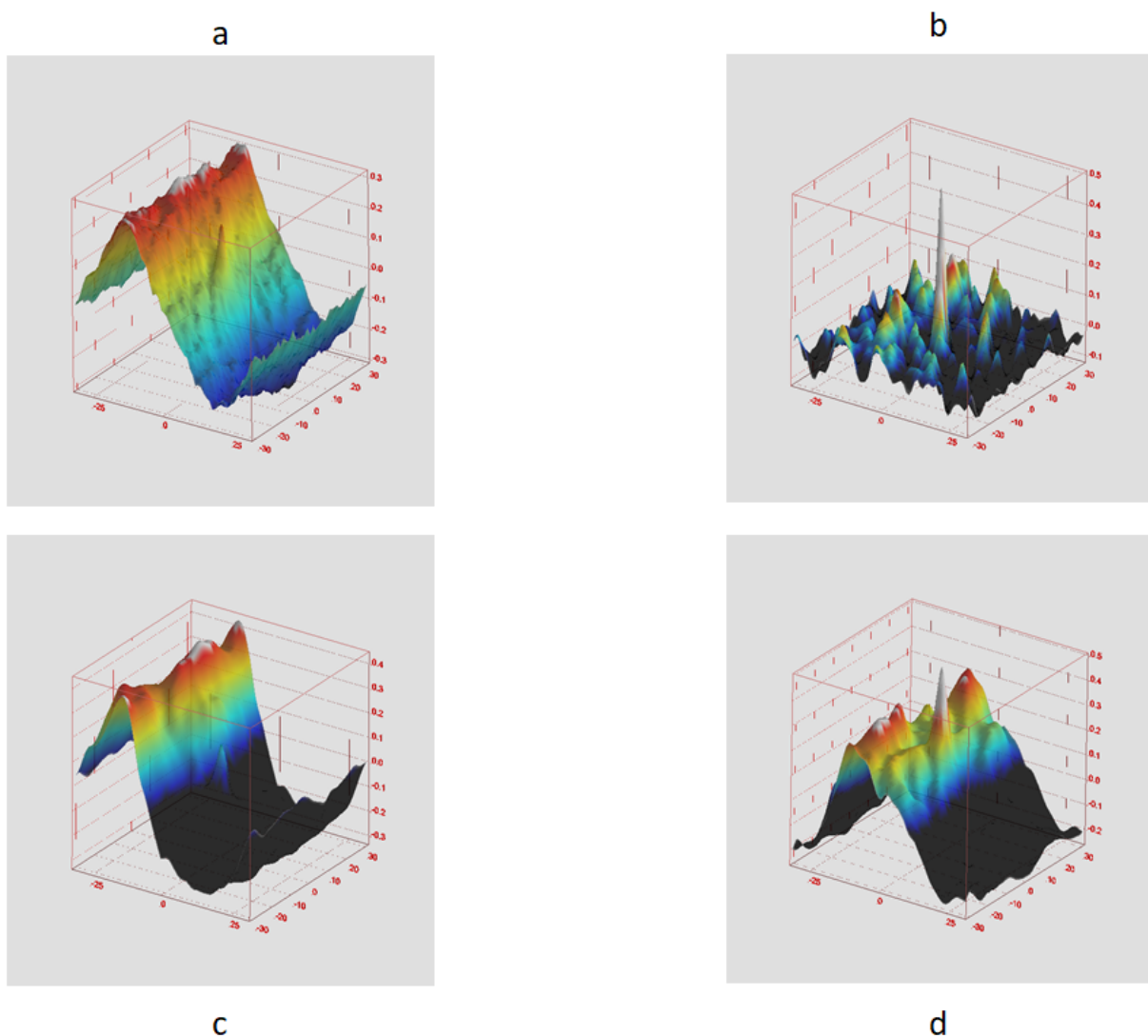


Figure 3.39: Comparison of correlation map for different combinations; (a) raw image; (b) combination (CLAHE + Lowpass (Bilateral) + Highpass (Sobel)); (c) Combination (CLAHE + POD with 100 percent particle recovery + Lowpass (Bilateral)); (d) Combination (CLAHE + POD with 98 percent particle recovery + Lowpass (Bilateral))

And also the combination (d) with 98 percent particle recovery also doesn't show any

improvement in that marked region. The combination (b) was able to produce a proper peak. This means that the combination (b) was able to cross correlate properly. Important point to be noted is that in the PIV instantaneous velocity calculation, the cross correlation not only depends on the particles but also the patterns in the image. Here in this example, during the calculation of the velocity, in few regions, there is high density of particles where instead of tracking the individual particles, the pattern corresponding to those accumulation of particles are to be tracked. This POD technique completely removed those patterns from the PIV images assuming it as a background. Due to this the cross correlation was not able to track the patterns in the image. But the SOBEL High pass filter removed those accumulation of particles assuming it to be background but retained its edges. This can be observed in Figure 3.40. Due to this the combination (b) was able to cross correlate the edges and reconstruct the missing vectors in the marked region.

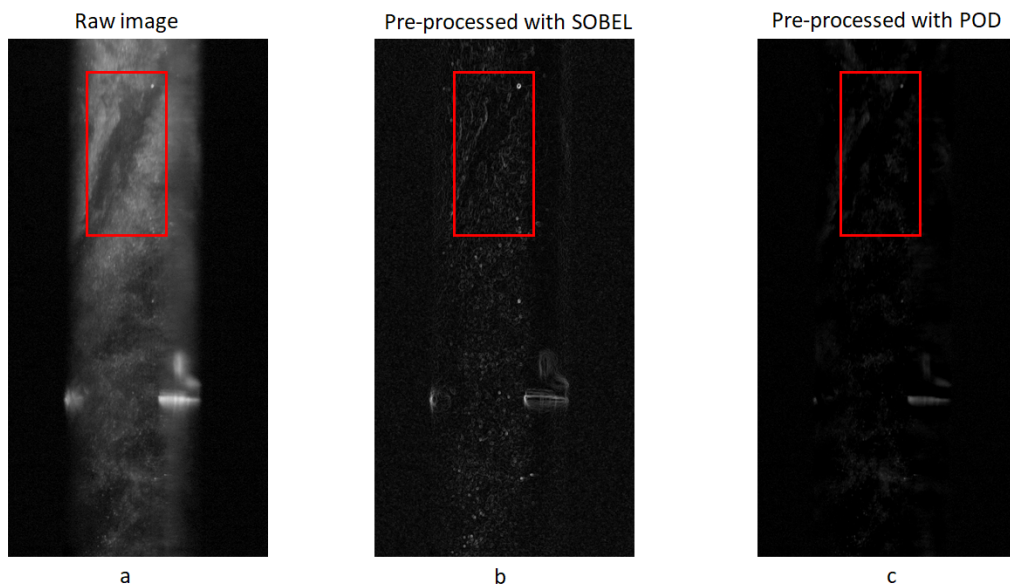


Figure 3.40: Figure representing the comparison between the raw (a) and the SOBEL(b), POD(c) for the retaining the pattern in the image after Pre-processing

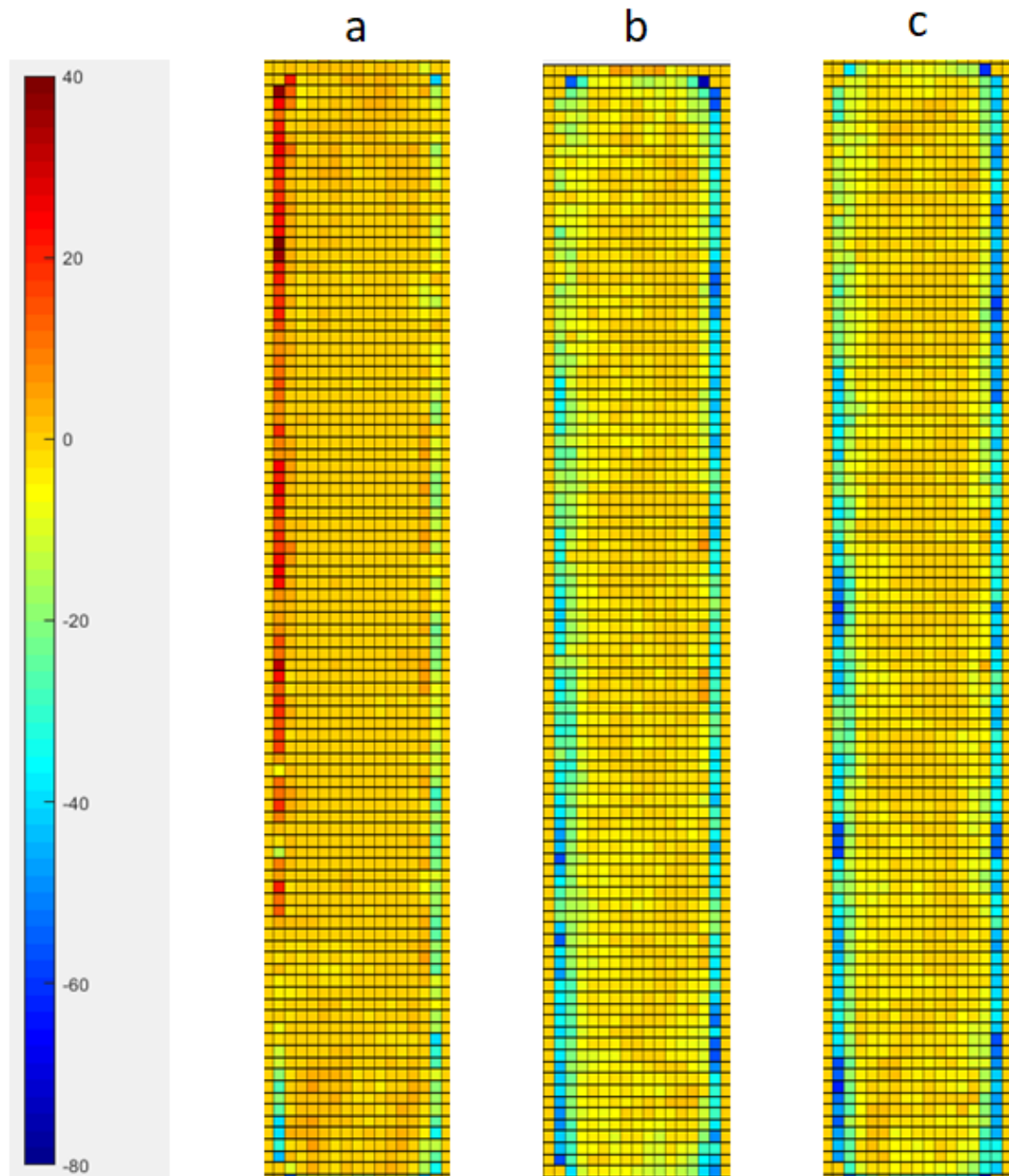


Figure 3.41: Comparison for improvement of number of vectors in different combinations; (a) combination (CLAHE + Lowpass (Bilateral) + Highpass (Sobel)); (b) Combination (CLAHE + POD with 100 percent particle recovery + Lowpass (Bilateral)); (c) Combination (CLAHE + POD with 98 percent particle recovery + Lowpass (Bilateral))

Figure 3.41 is the average data from all the images that has been evaluated for the

calculation of instantaneous velocity. It is observed that the combination (a) improved the number vectors with minimal loss of vectors whereas the combination (b) and (c) lost many vectors.

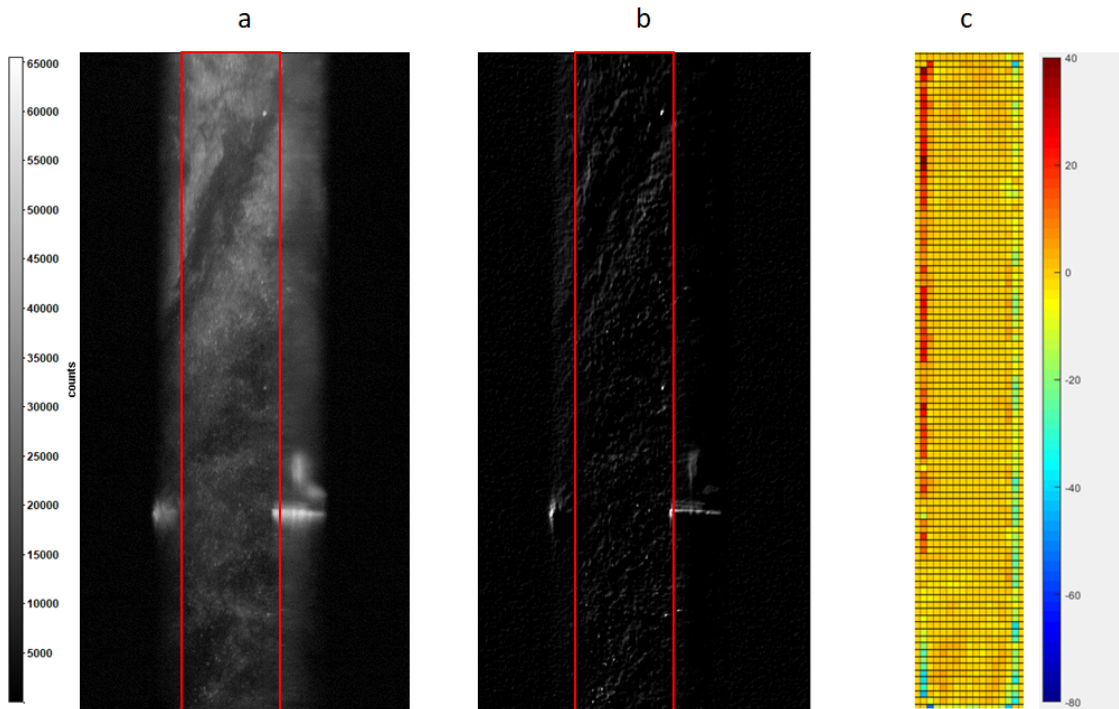


Figure 3.42: (a) Instantaneous raw image without pre-processing; (b) Image after pre-processing; (c) number of vectors improved for a set of images

From Figure 3.42, the pre-processing part can be concluded. The first figure shows the instantaneous raw image without any pre-processing. From the previous discussions, it can be observed that the image without pre-processing provides poor results. The second figure has been enhanced a lot (we have seen this in the second combination). And finally the third figure is the number of vectors that has been improved collectively from a set of around 600 images.

Hence, we can conclude that the combination CLAHE + Lowpass + Highpass(SOBEL) produced the best result both at the background reflection as well as at the missing vectors.

4 | PIV image Processing

After the image pre-processing has been done, the next step is the PIV processing for the evaluation of instantaneous velocity [7] [1]. The software used here for PIV processing is “DAVIS 8.4 (LaVision)”. A test matrix is being formed such that different parameters like single pass or multi-pass, initial and final window size, initial and final window overlap percentage and peak to peak threshold are adjusted to obtain the best PIV setting for best PIV evaluation.

Before looking into the conclusion for PIV setting, we will look into the characteristics of PIV evaluation while using multiple passes and the requirement of multiple passes. Initially, it is better to tabulate the entire required matrix (Table 4.1) that is going to be evaluated. In the table, different PIV settings are adjusted such that one of the combinations provides the best PIV evaluation. These each and every row is given as an input in the DAVIS 8.4 software and the instantaneous velocity is obtained for each set of images.

4.1. Multi-pass filter

We will start with the requirement of multiple passes instead of single pass. From Table 4.1(3), there is only one pass being used due to which the number of vectors that are obtained is very less. Case 4 and case 5 use three passes for the same evaluation. Note that in the later examples, it will be observed that the initial overlap ratio doesn’t make any difference in the PIV evaluation. So from the previous note, it is clear that case 3 and case 4 are same except in the number of passes. From here, it can be concluded that for better evaluation of instantaneous velocity, multiple passes are required. And also the correlation map of the region marked in the Figure 4.1 (all the cases) throws the same results. This means that by increasing the number of passes, the cross correlation between the particles are not effected but by having a single pass leads to lot of missing vectors.

	Pre-processing	Multi-pass	Initial window size	Final window size	Initial overlap%	Final overlap %	PTP threshold	Max/Min Vx	Max/Min Vy	Universal outlier detection	Residual to remove	Filter region
3	Raw	1	96	NIL	87	NIL	1.05	80 +80	0 +-140	Median	2	5x5
4	Raw	3	96	32	50	75	1.05	80 +80	0 +-140	Median	2	5x5
5	Raw	3	48	32	75	87	1.05	80 +80	0 +-140	Median	2	5x5
11	Pre-pro	1	96	NIL	87	NIL	1.05	80 +80	0 +-140	Median	2	5x5
12	Pre-pro	3	96	32	50	75	1.05	80 +80	0 +-140	Median	2	5x5
13	Pre-pro	3	96	32	75	87	1.05	80 +80	0 +-140	Median	2	5x5
14	Pre-pro	3	96	32	87	75	1.05	80 +80	0 +-140	Median	2	5x5
15	Pre-pro	3	64	48	50	87	1.05	80 +80	0 +-140	Median	2	5x5
16	Pre-pro	3	64	32	75	75	1.05	80 +80	0 +-140	Median	2	5x5
17	Pre-pro	3	96	48	50	75	1.05	80 +80	0 +-140	Median	2	5x5
18	Pre-pro	3	48	32	50	75	1.05	80 +80	0 +-140	Median	2	5x5
19	Pre-pro	3	48	32	75	87	1.05	80 +80	0 +-140	Median	2	5x5
20	Pre-pro	4	48	32	75	87	1.05	80 +80	0 +-140	median	2	5x5
21	Pre-pro	4	96	32	50	75	1.05	80 +80	0 +-140	median	2	5x5
22	Pre-pro	7	96	32	50	75	1.05	80 +80	0 +-140	Median	2	5x5
23	Pre-pro	3	96	32	50	87	1.05	80 +80	0 +-140	Median	2	5x5
24	Pre-pro	3	96	32	50	75	1.10	80 +80	0 +-140	Median	2	5x5
25	Pre-pro	3	96	32	50	75	1.15	80 +80	0 +-140	Median	2	5x5
26	Pre-pro	3	96	16	50	75	1.05	80 +80	0 +-140	Median	2	5x5

Table 4.1: Table representing the test matrix that has to be evaluated

By increasing the number of passes much further to a higher value also increases unnecessary computational efforts but not the better results. This can be observed from Figure 4.2. In Figure 4.2, except the number of passes, all other PIV settings remain exactly the same for the three cases. It is clearly observed that the number of passes from three to four and even to seven didn't much change the vectors. Even the correlation map remains exactly the same. This means that the velocity vectors got converged at number of passes equal to three. So further increasing the passes didn't much change results.

4.2. Initial and Final window sizes

Next, the initial and final window sizes are considered. The cross correlation algorithm used in DAVIS 8.4 for PIV evaluation, initial window size is taken for the first pass and for the remaining passes, the final window size is considered. So the initial window size is like the initial value for the remaining iterations (passes). That is the reason the initial window size doesn't make changes in the final result and the final window size does.

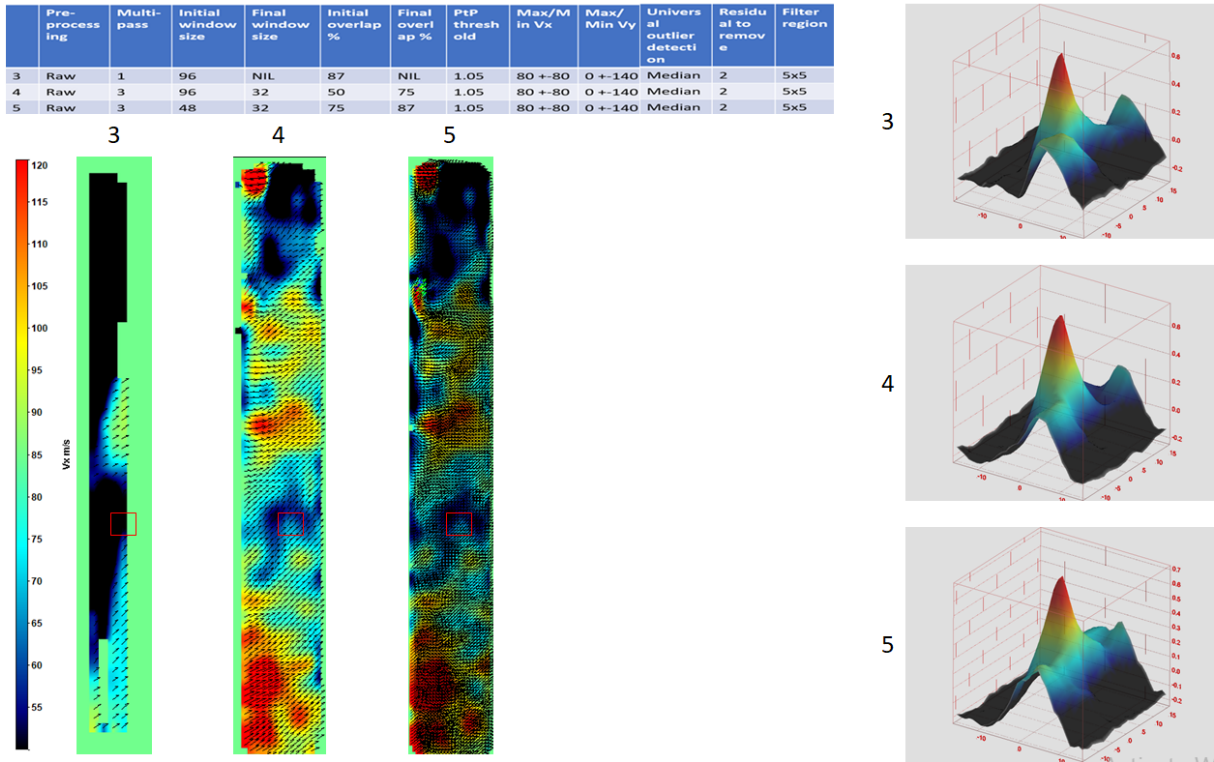


Figure 4.1: Comparison of Instantaneous axial component of velocity and the correlation map for the case 3,4 and 5

4.3. Initial and Final overlap percentage

Now Figure 4.3 speaks about the initial and final overlap percentage. Case 12 and 14 has same final overlap percentage but different initial overlap percentage. This shows that the initial overlap percentage doesn't change the result and this is also like the initial condition for the remaining iterations. Case 12 and 13 has same initial overlap percentage but different final overlap percentage. It is observed that the number of vectors in the case 13 has been increased. The correlation map for all the three cases remains exactly the same shows that the cross correlation is happening correctly in all the three cases. So, it is observed that by changing the initial overlap percentage doesn't alter the result wherein the final overlap percentage increases the number of vectors. This is just an overview of the overlap percentage and further conclusions are drawn in the following subsections.

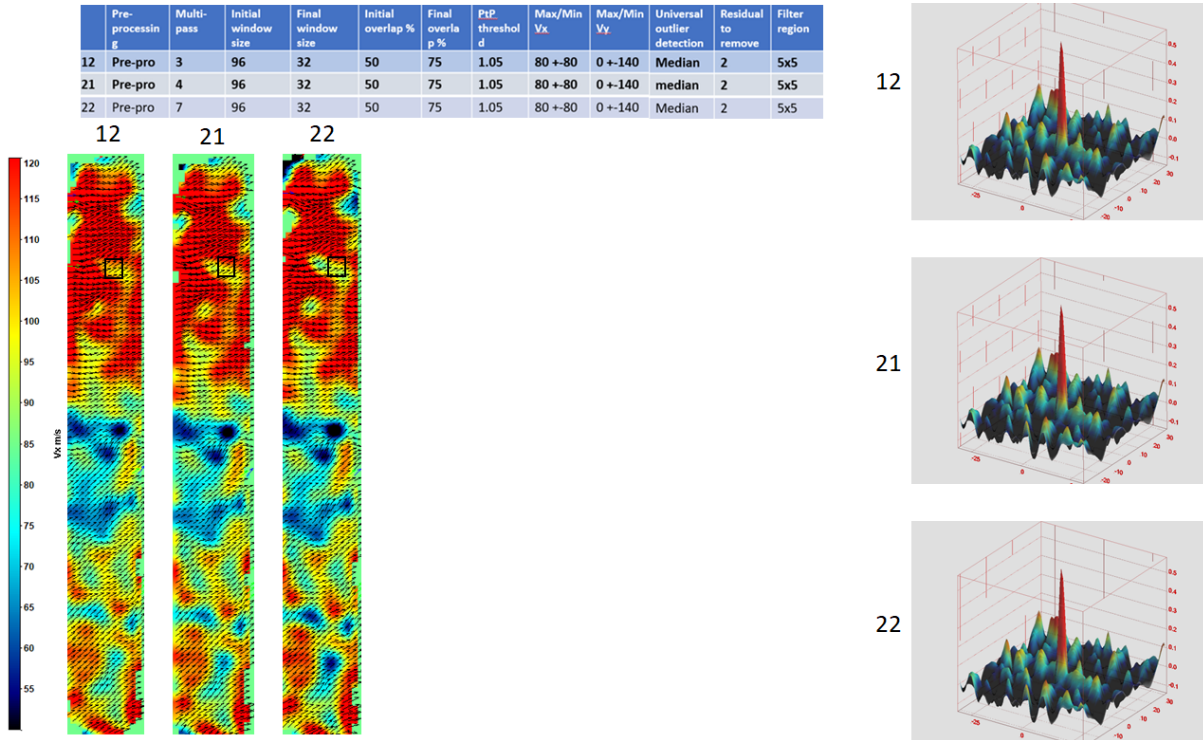


Figure 4.2: Comparison of Instantaneous axial component of velocity and the correlation map for the case 12, 21 and 22

4.4. Conclusion for the best PIV settings

Till now, we observed the behavior of the PIV settings. Now let's conclude the PIV setting which provides the best evaluation of the instantaneous velocity.

4.4.1. Conclusion for the Initial and the Final window size

Let's begin with the Initial and final window size. Start with a large interrogation sample that is known to capture the full dynamic range of displacements within the field of view by observing the one-quarter rule. One quarter rule is a common guideline, which states that the maximum displacements of the particle images should be equal to or less than one quarter of the interrogation window extend in the direction of the particle image shift. In the case of multi-pass evaluation, the one-quarter rule still applies but only for the first pass. The reason behind one quarter rule is that, if the data of length N contains a signal (that is displacements) exceeding half the window size $N/2$, then the correlation peak will be folded back into the correlation plane to appear on the opposite side. For a displacement $dx_{,true} > N/2$, the measured value will be $dx_{,meas} = dx_{,true} - N$. The proper solution to this problem is to either increase the interrogation window size, or, if

possible, reduce the laser pulse delay. In this case, the maximum pixel shift is around 3.5 pixels. So, any window size which is greater than the 14 pixels is perfect for the initial window size. In order to capture more number of vectors, it is better to choose the final window size smaller. But if we further reduce the final window size to 16, it is not able to capture the patterns in order to estimate the velocity. Therefore, the initial window size chosen is 96 x 96 pixels and the final window size is 32 x 32 pixels.

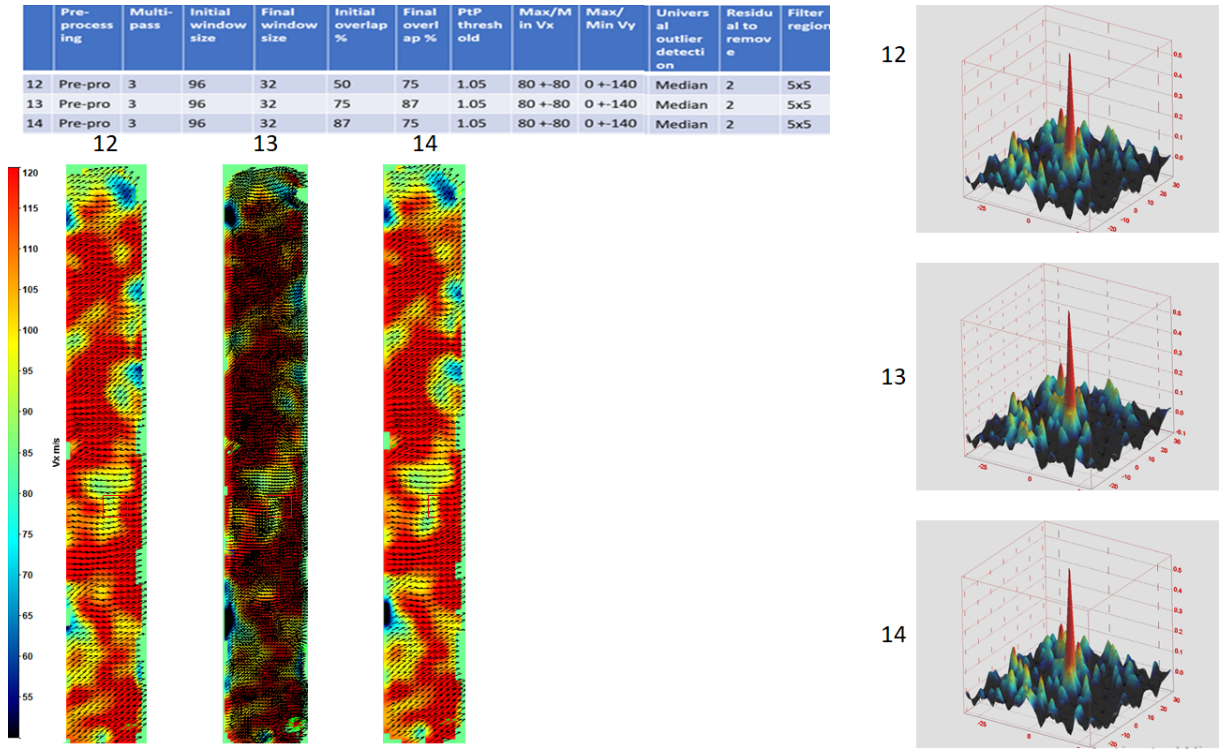


Figure 4.3: Comparison of Instantaneous axial component of velocity and the correlation map for the case 12,13 and 14

4.4.2. Conclusion for the Initial and the Final overlap percentage

Now let's conclude the initial and final overlap percentage. From previous description, it is clear that the initial overlap percentage doesn't affect the number of vectors as well as the correlation map. Since the data from the initial iterations are just used for the final iterations, it is better to keep the initial overlap percentage to 50 percent. It is observable from the previous examples that the final overlap percentage changes the number of vectors. If the comparison between 75 and 87 percent for the final passes are done, then the correlation map remains exactly the same. This means that, by changing the final overlap percent, the number of valid vectors are not increasing rather just the number

of vectors is increasing. And moreover, the disadvantage of increasing the final overlap percentage in our case is that, due to high overlap percentage, the adjacent vectors are correlated and not independent anymore. In case if there is a necessary for more number of vectors by having the same window size, it is better to use 87 percent overlap. Otherwise it is best to use the overlap percentage as 75. Hence, the initial overlap percentage chosen is 50 and the final overlap percentage is 75.

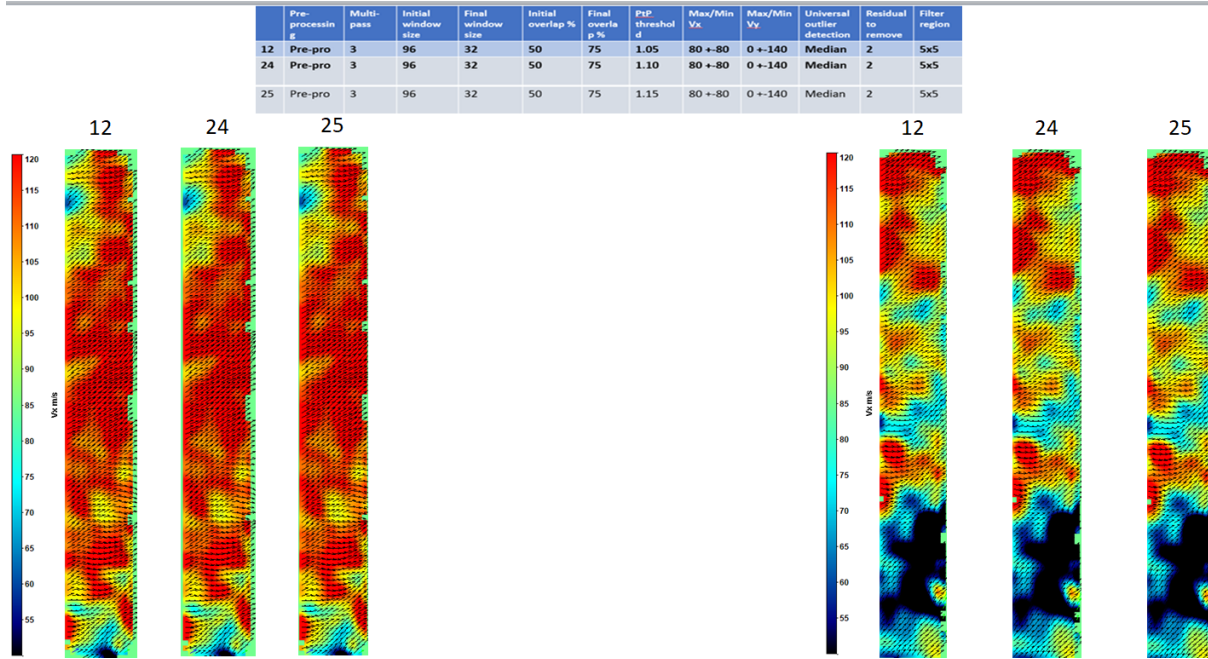


Figure 4.4: Comparison of Instantaneous axial component of velocity for two different frames for the case 12,24 and 25

4.4.3. Conclusion for Peak-to-Peak threshold value

For concluding the peak to peak ratio, it is better to look into two examples. One example comparing the instantaneous velocity and the other is statistical solution for all the frames that has been captured. In Figure 4.4, there are two sets of image (left and right) that has been taken at two different instants of time. Each set of images has three cases in which all the parameters are same except the peak to peak threshold value. By increasing this threshold value, it is clear that the computational efforts (i.e., Computational cost (time)) are getting increased in order to obtain more exact cross correlation. Usually, by increasing the value, which means physically we are filtering out the other peaks which are biasing the displacement vector. But in Figure 4.4, it is very hard to observe any differences (differences like variation in the magnitude of the velocity or in the direction of the vectors) between these three cases. Before concluding, let's look into statistical

analysis for the peak to peak threshold. From Figure 4.5, (a) is the comparison between case 12 and 24 and (b) is the comparison between case 12 and 25.

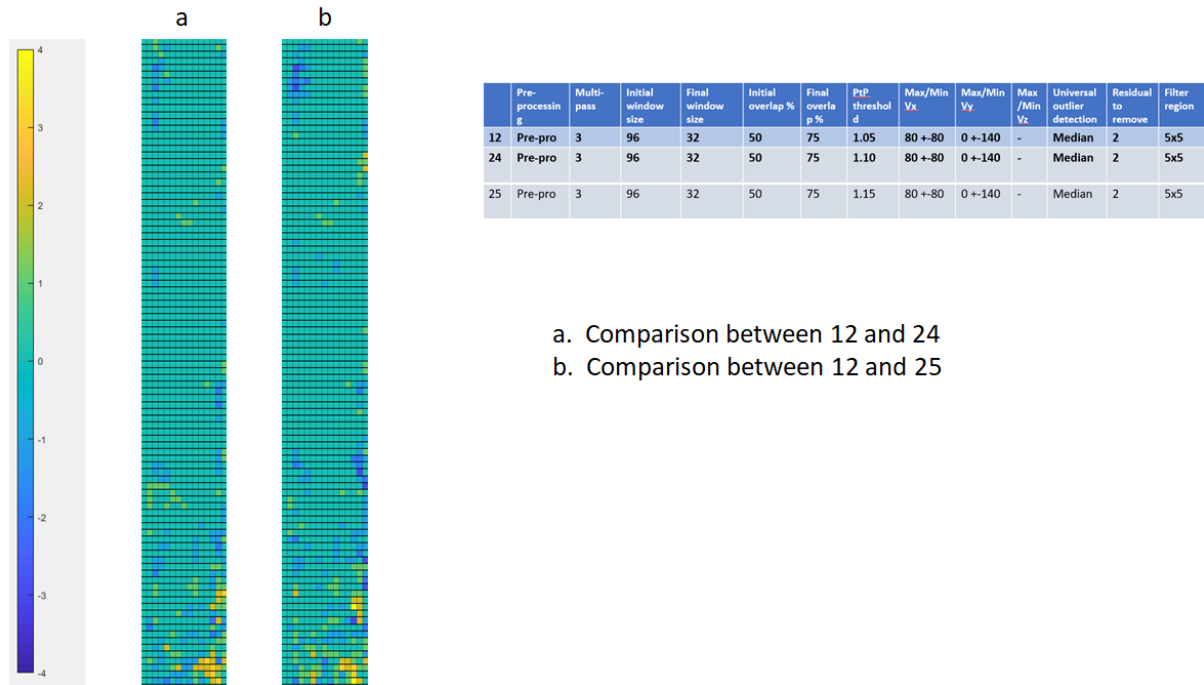


Figure 4.5: Comparison for improvement of number of vectors

Both 4.6(a) and 4.6(b) are the statistical data of all the images that are captures for the PIV evaluation. So, case 4.6(a) is for observing how the number of valid vectors is being increased if the peak to peak threshold value is being altered from 1.05 to 1.10. similarly case 4.6(b) is also for altering the peak to peak threshold from 1.05 to 1.15. It is very hard to observe any improvement of number of vectors in both the cases. There are hardly three to four vectors that have been improved. This means that by increasing the peak to peak threshold value, there is no much removal of vectors which in turn says that the cross correlation is happening properly and all most all the vectors are valid. So, instead of increasing the computational efforts by increasing the peak to peak threshold value, it is better to have the value as 1.05. Therefore, it can be concluded that we can fix the value of 1.05 to the peak to peak threshold value.

Among all the combinations that are present in the test matrix (Table 4.1), case 12 provides the best PIV results. So, hence, finally we have concluded the PIV setting for the best PIV evaluation.

5 | Uncertainty analysis

5.1. Uncertainty due to out-of-the-plane vectors

This is an uncertainty associated with the component of velocity that is in the direction perpendicular to the laser sheet (out-of-the-plane particles). There further more uncertainties that are being discussed in few papers (Two of them are mentioned in these papers [13] [23]). In general uncertainty due to out-of-the-plane components are caused due to two reasons. First reason is the misalignment of the laser sheet with the plane on which the observation is made. The other reason is that, the flow might tend to have a direction that is perpendicular to the plane of observation and since the particles trace the flow direction, these out-of-the-plane particles are observed. However the first reason will be avoided by conducting multiple experiments so that the laser sheet utmost perfectly aligns with the plane of observation. The later one has to be taken into consideration. These out-of-the-plane components are shown in Figure 5.1.

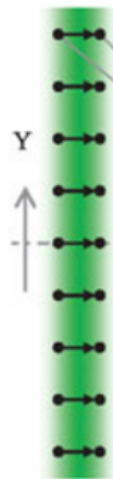


Figure 5.1: Thickness of the laser sheet representing the out-of-the-plane vector components

In general these components are observed with the help of a pin-hole camera. These

observed components of velocity are plotted in a digital plane in order to compute the uncertainty caused. The complete out-of-the-plane components those are present in the laser sheet are 2 dimensionally plotted in a digital plane.

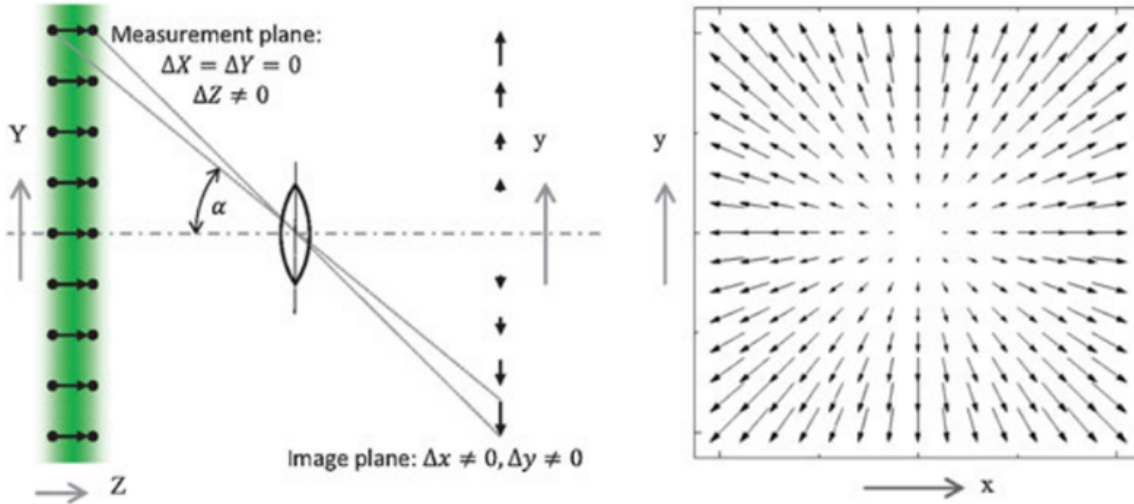


Figure 5.2: Illustration of an out of plane particle displacement and zero in-plane shift. A camera with the optical axis in negative Z direction will observe a particle image shift in x and y direction even if only motion in Z direction is present. The particle displacement is biased and the magnitude and direction depends on the observation angle α with respect to the optical axis. This image has been taken from [19]

In Figure 5.2, it can be observed that a pin-hole camera is being placed between the laser sheet and the digital plane. In the laser sheet, there exist components of vectors that are perpendicular to the laser sheet. This component of vector is being observed by the pin-hole camera and it is being plotted in the digital plane. Left image gives an idea how out-of-the-plane components are plotted for a single cross-section in the laser sheet in a 1 dimensional digital plane. The right side image describes the complete out-of-the-plane components representation in a digital plane. This is the generalized description how the uncertainty is evaluated. Now let's evaluate the uncertainty in our case.

From Figure 5.3, the length of the out of the plane component in the laser sheet is given as \mathbf{x}_2 . One important assumption has been made for the simplicity is that, what ever may be the length of the vector, but the nose of the vector will be placed on the frontal region of the laser thickness for the purpose of calculations. This length of the vector is plotted on the digital plane and that value is computed as \mathbf{x}_4 .

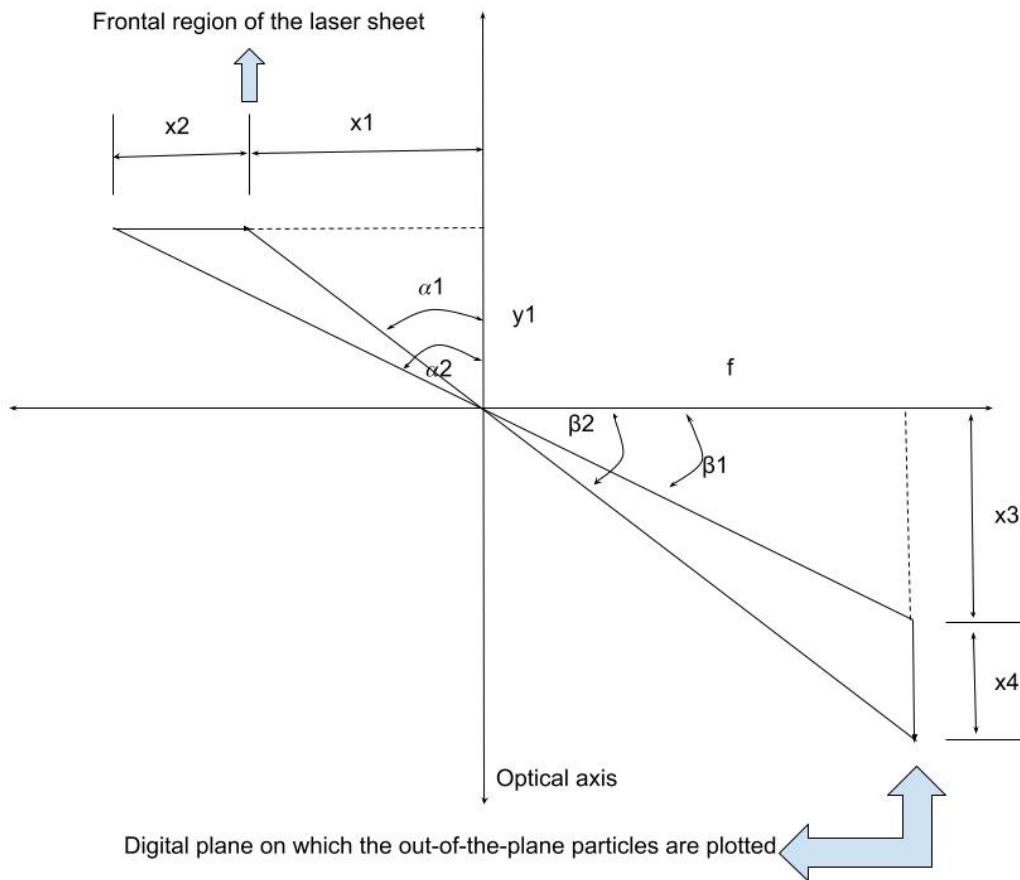


Figure 5.3: Sketch representing, how a single out of the plane component is plotted in the digital plane (observing the laser sheet thickness from side view)

The component x_1 is known from the given data, it is the distance from the nose of the vector component to the optical axis in the same plane. In the same way, x_2 is the length of the vector and y_1 is the perpendicular distance from the vector head to the optical axis. Hence, the values x_1 , x_2 and y_1 are known. Now α_1 and α_2 can be easily computed. After the computation of α_1 and α_2 , β_1 and β_2 can be calculated. Now since, the values of β_1 and β_2 are known, x_3 and x_4 can easily be computed. This figure shows calculations only for a certain cross-section of the laser sheet. But for obtaining the uncertainty for the entire laser sheet, it is important to consider the vectors for the complete laser sheet.

Now let's look into Figure 5.4. It is the top view of the previous figure. The dotted arrow gives the same representation of the out-of-the-plane displacement vector shown in Figure 5.3 but from the top view where, as since it is a top view, the component of the vector that is plotted on the digital plane in Figure 5.3 is perpendicular to the displacement vector (that is, goes perpendicular into the page). Here, the value γ provides the complete

movement of vectors along the whole laser sheet. Since the value x_1 and d are known, the angle γ can be computed easily. The value x_6 gives the x coordinate in the digital plane. This calculation is simple because x_6 as well as f is known. Point to be noted is that, if γ becomes 90 deg, then the x_1 turns out to be just d . which means that the vector is exactly in the plane that is origin to the optical axis.

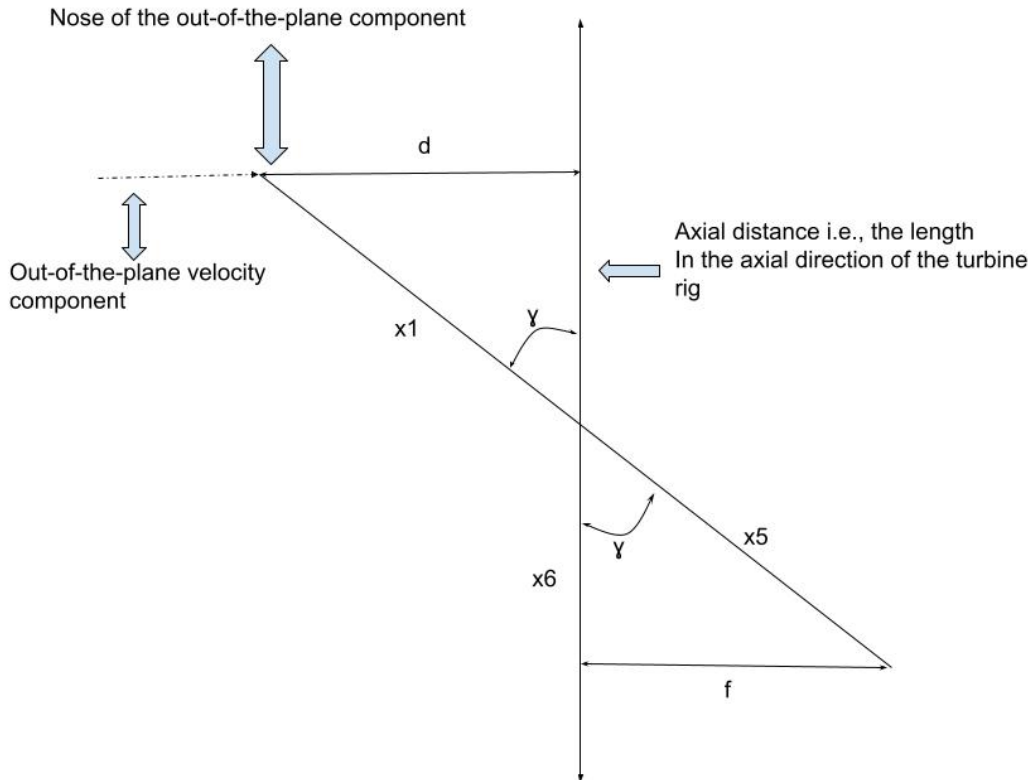


Figure 5.4: Sketch representing the same laser sheet thickness but observing it from the top view

Now it is also very important to note that all the out-of-the-plane vectors that are in the cross sectional plane of the optical axis (that is., the plane perpendicular to the laser sheet that coincides with the optical axis) might not provide any rotation of vectors that are plotted in the digital plane. But all other vectors provide a rotation of angle ϕ to the vectors in the digital plane. This can be clearly observed in Figure 5.5.

This angle ϕ gives the amount of rotation that is happening to the vectors in the digital plane. Consider a vector in the laser sheet. When the length of the vector is projected on the digital plane when it is passed through the optical axis, it is rotated with an angle

of ϕ . When the calculated angle is equal to zero, this means that the selected vector is in the cross-section that is in-line with the optical axis. The velocity in the digital plane is obtained with the help of x_4 multiplied with the time period. So, the u component of velocity in the digital plane is given by (velocity in the digital plane) times the $(\sin \phi)$. Similarly, the v component of velocity is given by (velocity in the digital plane) times the $(\cos \phi)$. It looks easy when it is being computed for a single vector. But it requires high computational efforts in order to calculate for the entire frame and for a set of 332 images (in our case).

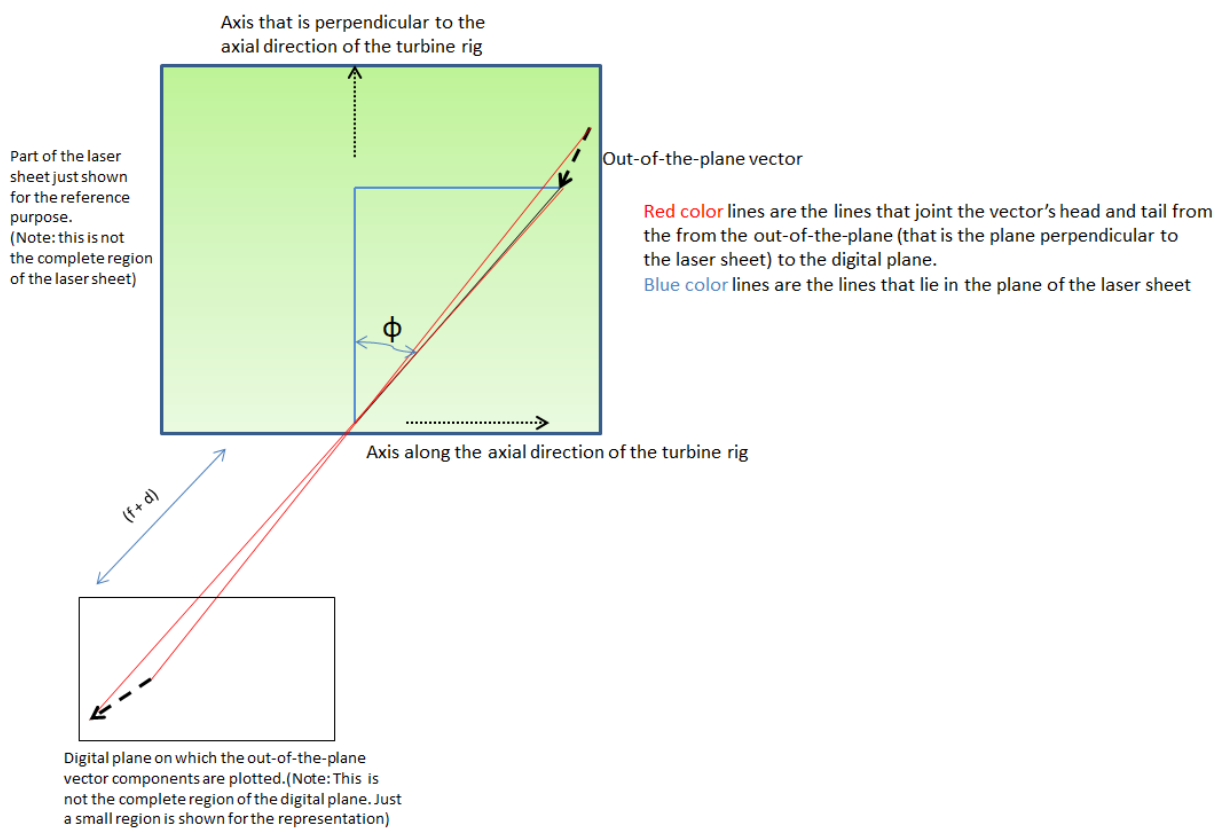


Figure 5.5: Sketch representing how the out-of-the-plane components show a rotation in the digital plane

calculated quantities	Description
1	Tangential coordinate
2	Axial coordinate
3	Out of the plane velocity component in the laser sheet
4	α_1 is the angle between \mathbf{x}_1 and \mathbf{y}_1 (from Figure 5.3)
5	α_2 is the angle between $(\mathbf{x}_1 + \mathbf{x}_2)$ and \mathbf{y}_1 (from Figure 5.3)
6	β_1 is angle between \mathbf{x}_3 and f (from Figure 5.3)
7	β_2 is the angle between $(\mathbf{x}_3 + \mathbf{x}_4)$ and f (from Figure 5.3)
8	γ is the angle between the \mathbf{x}_1 and the axial coordinate of the laser sheet (from Figure 5.4)
9	\mathbf{x}_5 is the distance between the optical center and the tail of the velocity component in the digital plane (from Figure 5.4)
10	\mathbf{x}_6 is the Y coordinate in the digital plane (from Figure 5.4)
11	\mathbf{x}_7 is the X coordinate in the digital plane ($\mathbf{x}_7 = \mathbf{x}_3 + \mathbf{x}_4$)
12	Axial component of velocity in the digital plane(U component)
13	Tangential component of velocity in the digital plane(V component)
14	ϕ gives the amount of twist in that happens the plane that joins the optical center to the nose and tail of the out of the plane velocity component (from Figure 5.5)
15	Magnitude of velocity in the digital plane

Table 5.1: Table showing the quantities that has been evaluated, for uncertainty due to the out of the plane components

Above table gives the detailed description of all the quantities that are being evaluated for the uncertainty. With the help of all the quantities that are being evaluated, now the out of the plane components can be plotted. Figure 5.6 is the graph that represents the out of the plane components that are present. The plot contains the magnitude of out of the plane vectors plotted against the axial and tangential co-ordinates as X and Y-axis respectively. The graph has been scaled up 5 times in order to be visualized. This can be observed in Figure 5.7. This Figure 5.7 is the zoomed in portion of the graph Figure 5.6. The original size of the vector as well as the scaled up size of vector is being shown.

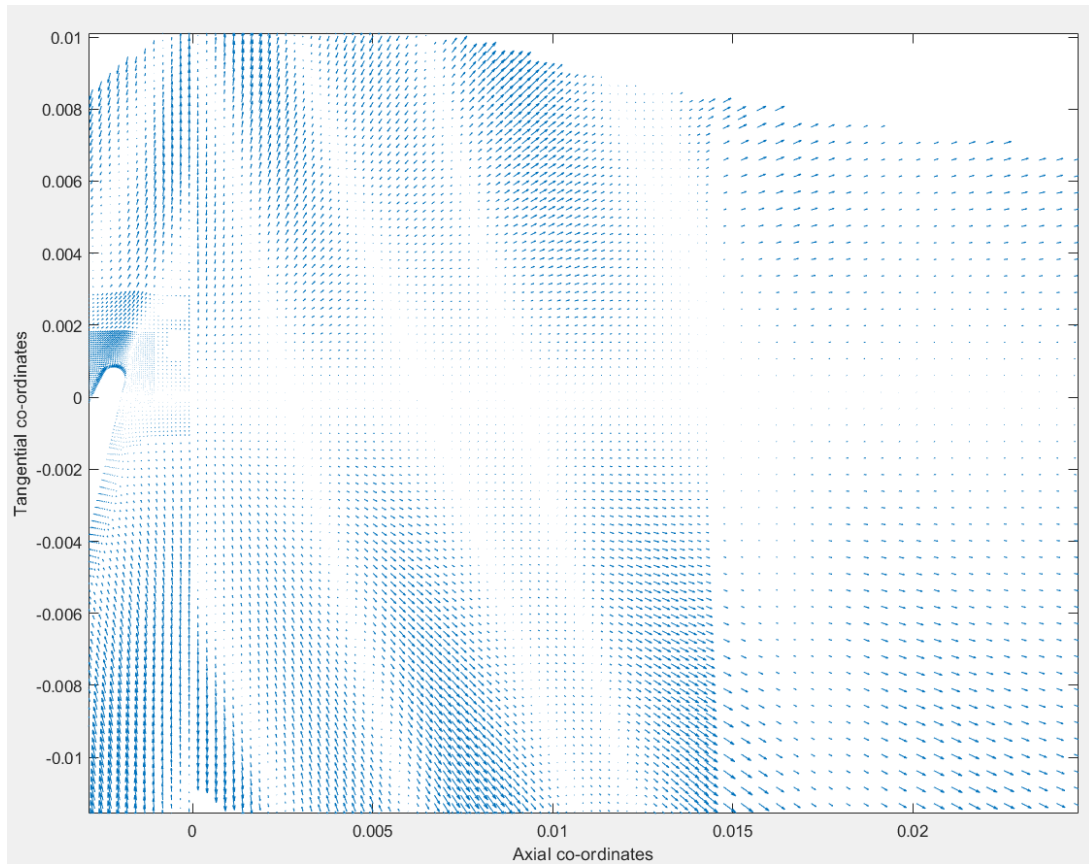
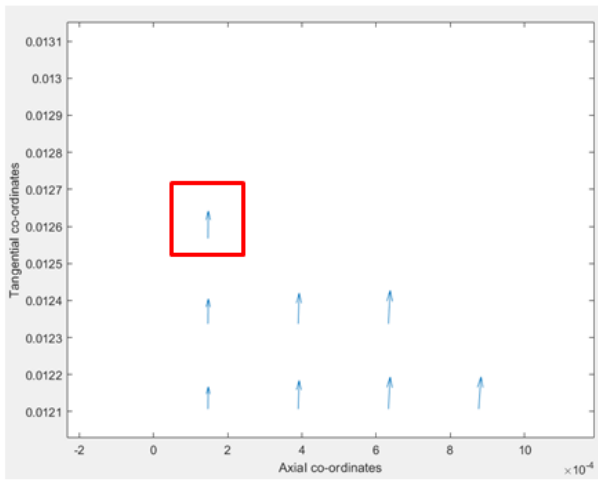


Figure 5.6: Graph representing the out of the plane components in a two dimensional plane having a scaling factor of the length of the vectors as 5. (X-axis = axial direction, Y-axis = tangential direction)

Before going further, let's summarize the work that has been done in this uncertainty analysis of the out of the plane vectors. All the components that are out of the plane in the laser sheet is being observed by the pin hole camera. These vectors that are being observed has to be calculated in order to know the quantity of uncertainty present in our work. This can be observed with the help of a graph. In the previous Figure 5.2, a two-dimensional section of sheet was observed with the help of a pin hole camera for the out of the plane components and those out of the plane components are being plotted in a two-dimensional graph. In the same way, having all the details required for the analysis, a two-dimensional plot has been made in Figure 5.6. This graph represents the uncertainty associated with the out of the plane components in the laser sheet.



These are the co-ordinates and the values of velocities in the marked region. Just the vector has been scaled-up five times so that it can be more clearly visible in the complete graph.

$X = 0.000146738 \text{ m}$
 $Y = 0.0125674 \text{ m}$
 $U = 4.54331e-05 \text{ m/s}$
 $V = 0.00389112 \text{ m/s}$

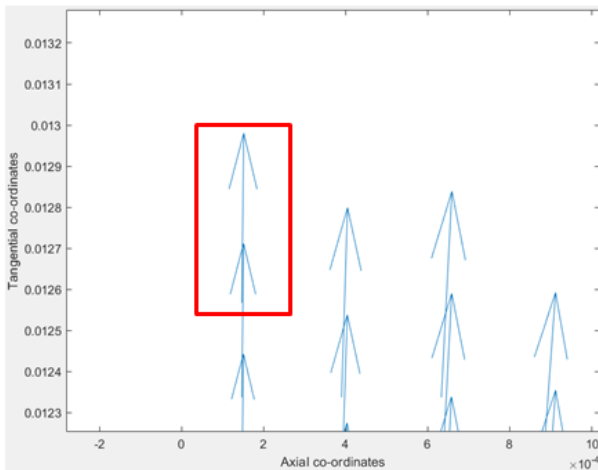


Figure 5.7: Graphs in the figure just represent the scaled up length of the vector when compared with the original vector.

Hence, the uncertainty associated with the out of the plane components has been evaluated.

6 | Comparison with CFD predictions and available experimental data

In the present section, the comparison between the PIV results, experimental data and the CFD data has been done. Here the CFD data is obtained from the Reynolds averaged Navier Stokes simulation (RANS). The experimental data is acquired from the 4 hole probe [5]. The axial component of velocity and the tangential component of velocity are being considered for the comparison. Different regions for the evaluation has been chosen due to the design of the experiment. The 4 hole probe measurement is taken at a distance of $C_{ax} = 1.48$ whereas the RANS and the PIV are compared at three locations $C_{ax} = 1.05, 1.10$ and 1.15 .

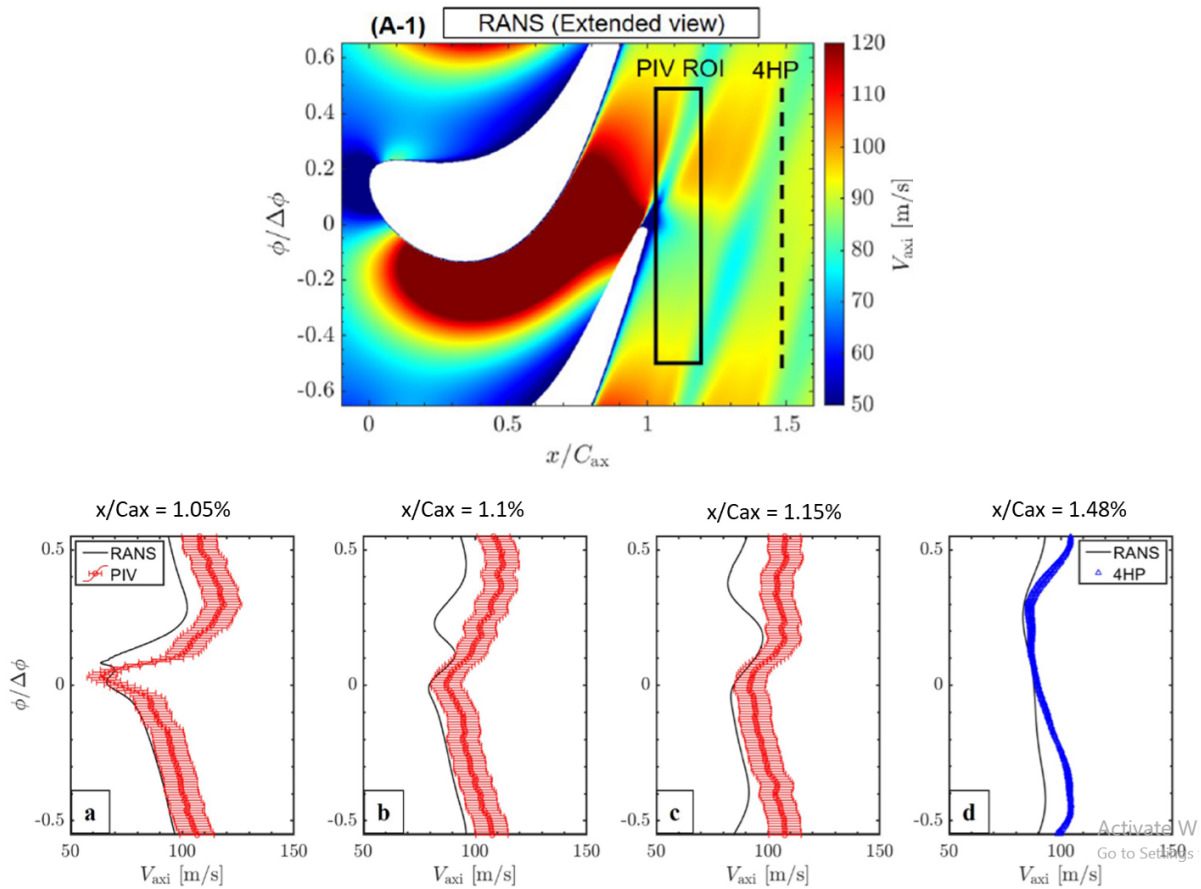


Figure 6.1: In the top left, axial component of velocity with representation of the region that corresponds to the PIV and to the 4 hole probe; in the top right, 1st contour corresponds to the RANS and the last contour corresponds to the PIV; Bottom figures corresponds to the comparison of velocity profiles at different sections

In Figure 6.1, the axial component of velocity is taken into consideration for the purpose of comparison. The black rectangular box indicates the region of interest for PIV evaluation. The dotted line just after the PIV region indicate the section for the 4 hole probe. The contour represented in the figure is the data from the RANS. The region of interest of the PIV is chosen for comparing with the CFD data. The next two contours in the top right is the comparison between the PIV evaluation and the CFD data. There is a slight difference in the evaluation of the result between these two methods. The velocity profiles are compared at different axial locations in the bottom plots of the Figure 6.1. It is observed that the PIV results and the RANS results show a little deviation in their pots but it shows quite similar global trend.

Various reasons for such discrepancy can be deviation of PIV measurement plane from the

annular slice, the error of measurement plane alignment and also the filtering in the PIV result might be considered. On the other hand, the RANS prediction has a limit for its accuracy. The limit of turbulence model may not rigorously treat the progressive mixing of the rotor wake with the surrounding high momentum flow towards downstream.

When comparing the RANS with the 4 hole probe, it shows a global trend similar but there is a discrepancy in the velocity profile.

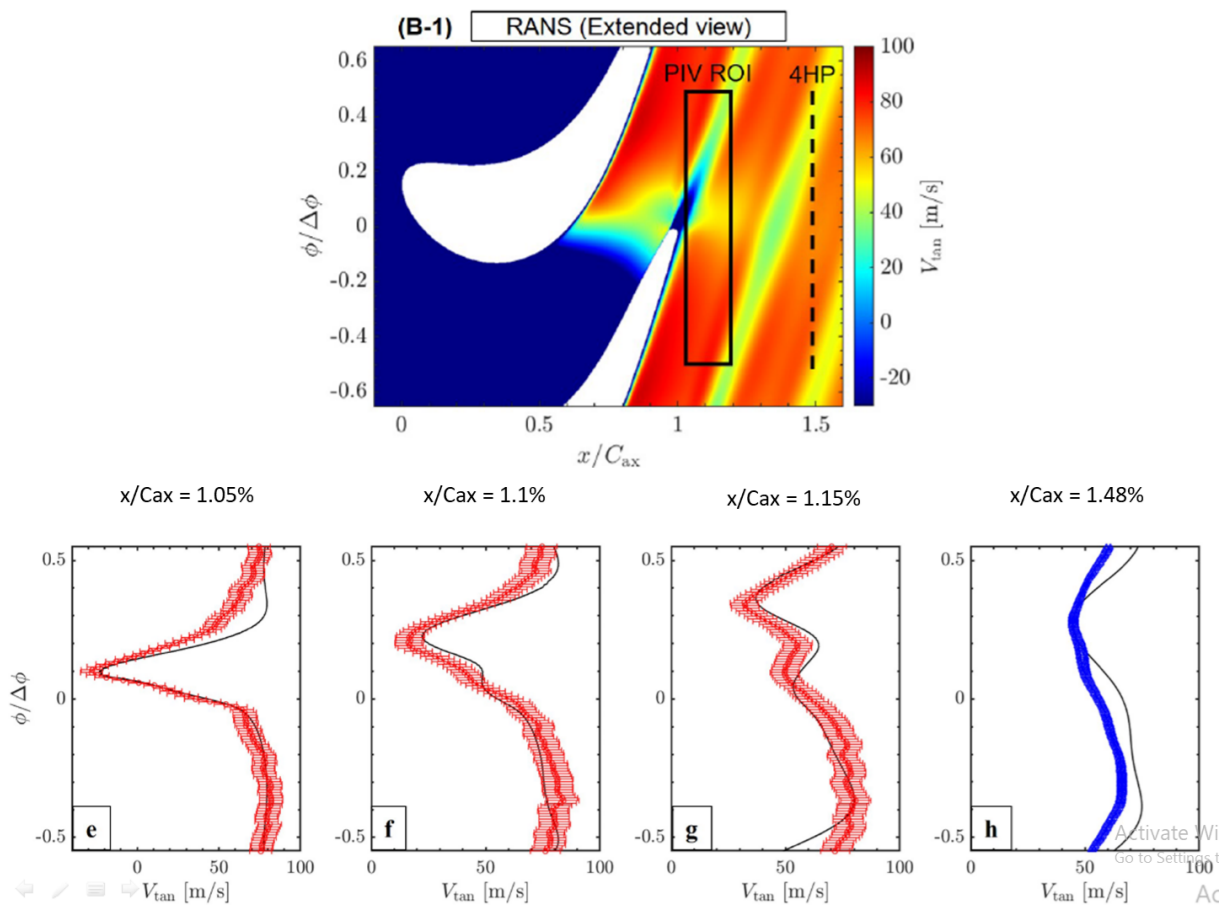


Figure 6.2: In the top left, tangential component of velocity with representation of the region that corresponds to the PIV and to the 4 hole probe; in the top right, 1st contour corresponds to the RANS and the last contour corresponds to the PIV; Bottom figures corresponds to the comparison of velocity profiles at different sections

In the same way in Figure 6.2, the tangential component of velocity is compared. If the contour of the tangential component of velocity is compared between the PIV data and the RANS data, it almost gives the same result. Similarly, let's look into the velocity profile at different sections as mentioned in the above description. The velocity profiles of the RANS data provide almost exact results compared with the PIV results. This is

an excellent agreement between the PIV result and the RANS data for the tangential component of velocity. If the 4 hole probe is being used, this also provides a similar trend to RANS but not the exact match as the PIV provides. Overall, the discrepancy between PIV and RANS results is comparable with the one between 4 hole probe and RANS, indicating PIV measurements provided reasonable velocity estimation.

7 | Conclusion

A set of 662 images has been captured and since those images had lot of background reflections, low contrast and the noises in the image, the best image pre-processing has been derived from these filters CLAHE, Min/Max intensity normalization, sobel, temporal, POD, Gaussian and bilateral. Few of these filters might show better performance individually but when the overall combinations are considered for better results, the combination CLAHE, sobel and the Gaussian shown the best output of results. Later a test matrix containing parameters like, initial and final window size, initial and final overlap percentage, number of passes, peak to peak threshold etc., for the purpose of PIV evaluation. These parameters are altered in such a way so that, it should be able to remove the outliers in the velocity field and should be able reconstruct few vectors that has been biased due to the background reflections. The best combination has been commented in the chapter 4. And finally these results has been compared with the CFD (RANS) and 4 hole probe measurement technique. In conclusion, considering the factors that has been discussed in chapter 6, the PIV has a great potential in obtaining the instantaneous fields in such kind of test rig.

Bibliography

- [1] R. J. Adrian. Particle-imaging techniques for experimental fluid mechanics. *Annual review of fluid mechanics*, 23(1):261–304, 1991.
- [2] R. J. Adrian and J. Westerweel. *Particle image velocimetry*. Number 30. Cambridge university press, 2011.
- [3] V. Andreoli, S. Lavagnoli, G. Paniagua, and V. F. Villace. Robust model of a transient wind tunnel for off-design aerothermal testing of turbomachinery. *Measurement*, 82:323–333, 2016.
- [4] S. Bhattacharya, R. A. Berdanier, P. P. Vlachos, and N. L. Key. A new particle image velocimetry technique for turbomachinery applications. *Journal of Turbomachinery*, 138(12):124501, 2016.
- [5] M. Boerner, M. Bitter, and R. Niehuis. On the challenge of five-hole-probe measurements at high subsonic mach numbers in the wake of transonic turbine cascades. *Journal of the Global Power and Propulsion Society*, 2:453–464, 2018.
- [6] C. Brücker. Piv in two-phase flows. *Lecture series*, 1:1–28, 2000.
- [7] P. Bryanston-Cross, D. Udrea, G. Guenette, A. Epstein, and E. d’Hoop. Whole-field visualisation and velocity measurement of an instantaneous transonic turbine flow. In *ICIASF’97 Record. International Congress on Instrumentation in Aerospace Simulation Facilities*, pages 278–286, 1997. doi: 10.1109/ICIASF.1997.644690.
- [8] P. J. Bryanston-Cross, C. E. Towers, T. R. Judge, D. P. Towers, S. P. Harasgama, and S. T. Hopwood. The Application of Particle Image Velocimetry (PIV) in a Short-Duration Transonic Annular Turbine Cascade. *Journal of Turbomachinery*, 114(3):504–509, 07 1992. ISSN 0889-504X. doi: 10.1115/1.2929173. URL <https://doi.org/10.1115/1.2929173>.
- [9] T. Corpetti, D. Heitz, G. Arroyo, E. Mémin, and A. Santa-Cruz. Fluid experimental flow estimation based on an optical-flow scheme. *Experiments in fluids*, 40(1):80–97, 2006.

- [10] H. Huang, H. Fiedler, and J. Wang. Limitation and improvement of piv. *Experiments in fluids*, 15(4):263–273, 1993.
- [11] D. Inman, D. G. Cuadrado, V. Andreoli, J. Fisher, G. Paniagua, P. A. N. Aye-Addo, L. Bhatnagar, F. Lozano, T. Meyer, and M. Bloxham. Particle Image Velocimetry in a High-Pressure Turbine Stage at Aerodynamically Engine Representative Conditions. *Journal of Engineering for Gas Turbines and Power*, 143(6), 03 2021. ISSN 0742-4795. doi: 10.1115/1.4049448. URL <https://doi.org/10.1115/1.4049448>. 061031.
- [12] M. Kegalj and H.-P. Schiffer. Endoscopic piv measurements in a low pressure turbine rig. *Experiments in Fluids*, 47(4), 2009.
- [13] S. J. Kline. Describing uncertainty in single sample experiments. *Mech. Engineering*, 75:3–8, 1953.
- [14] H. Maas, A. Gruen, and D. Papantoniou. Particle tracking velocimetry in three-dimensional flows. *Experiments in fluids*, 15(2):133–146, 1993.
- [15] R. Mejia-Alvarez and K. Christensen. Robust suppression of background reflections in piv images. *Measurement Science and Technology*, 24(2):027003, 2013.
- [16] M. Mendez, M. Raiola, A. Masullo, S. Discetti, A. Ianiro, R. Theunissen, and J.-M. Buchlin. Pod-based background removal for particle image velocimetry. *Experimental Thermal and Fluid Science*, 80:181–192, 2017.
- [17] K. E. Meyer and J. Westerweel. Advection velocities of flow structures estimated from particle image velocimetry measurements in a pipe. *Experiments in fluids*, 29(1):S237–S247, 2000.
- [18] S. M. Pizer, E. P. Amburn, J. D. Austin, R. Cromartie, A. Geselowitz, T. Greer, B. ter Haar Romeny, J. B. Zimmerman, and K. Zuiderveld. Adaptive histogram equalization and its variations. *Computer vision, graphics, and image processing*, 39(3):355–368, 1987.
- [19] M. Raffel, C. E. Willert, J. Kompenhans, et al. *Particle image velocimetry: a practical guide*, volume 2. Springer, 1998.
- [20] A. M. Reza. Realization of the contrast limited adaptive histogram equalization (clahe) for real-time image enhancement. *Journal of VLSI signal processing systems for signal, image and video technology*, 38(1):35–44, 2004.
- [21] D. Schanz, S. Gesemann, and A. Schröder. Shake-the-box: Lagrangian particle tracking at high particle image densities. *Experiments in fluids*, 57(5):1–27, 2016.

- [22] D. Schanz, A. Schröder, S. Gesemann, F. Huhn, M. Novara, R. Geisler, P. Manovski, and K. Depuru-Mohan. Recent advances in volumetric flow measurements: High-density particle tracking ('shake-the-box') with navier-stokes regularized interpolation ('flowfit'). *New Results in Numerical and Experimental Fluid Mechanics XI*, pages 587–597, 2018.
- [23] A. Sciacchitano. Uncertainty quantification in particle image velocimetry. *Measurement Science and Technology*, 30(9):092001, 2019.
- [24] A. Sciacchitano and F. Scarano. Elimination of piv light reflections via a temporal high pass filter. *Measurement Science and Technology*, 25(8):084009, 2014.
- [25] L. G. Shapiro, G. C. Stockman, et al. *Computer vision*, volume 3. Prentice hall New Jersey, 2001.
- [26] D. Tisserant and F. A. E. Breugelmans. Rotor Blade-to-Blade Measurements Using Particle Image Velocimetry. *Journal of Turbomachinery*, 119(2):176–181, 04 1997. ISSN 0889-504X. doi: 10.1115/1.2841096. URL <https://doi.org/10.1115/1.2841096>.
- [27] C. Tomasi and R. Manduchi. Bilateral filtering for gray and color images. In *Sixth international conference on computer vision (IEEE Cat. No. 98CH36271)*, pages 839–846. IEEE, 1998.
- [28] H. Wang, G. He, and S. Wang. Globally optimized cross-correlation for particle image velocimetry. *Experiments in Fluids*, 61(11):1–17, 2020.
- [29] Z. Xue, J. J. Charonko, and P. P. Vlachos. Signal-to-noise ratio, error and uncertainty of piv measurement. 2013.

A | Appendix A

This appendix is used for giving the codes that has been used for the purpose of Image pre-processing. Image pre-processing has been done with the help of matlab, python and DAVIS 8.4. The POD based filter is completely derived in matlab as mentioned in this article [16]. The image pre-processing for Min/Max Intensity Normalization, Sobel highpass filter and Gaussian smoothening is done with DAVIS 8.4 software. The CLAHE and the Bilateral smoothening filter has used python with openCV package. The codes for the python, and matlab has been shown in the following slides.

A.1. Code for Contrast Limited Adaptive Histogram Equalization (CLAHE)

In this section, the Python code for the CLAHE has been written. This was actually written in Anaconda Navigator:spider.

The inital step is to import all the packages that are required for the CLAHE.

```
# -*- coding: utf-8 -*-
"""
Created on Thu Dec  9 15:10:23 2021

@author: srinivasan
"""

import cv2
import glob
#from skimage.filters import gaussian
from skimage import img_as_ubyte
import numpy as np
from matplotlib import pyplot as plt
```

```
import os.path
```

After importing the required packages, the path should be defined. The folder which contains all the images that has to be pre-processed with CLAHE should be shown in this path.

```
path = "0_inputForCLAHE/*.*"
```

Now here, each and every image gets pre-processed for CLAHE with this code

```
img_number = 1
```

```
for file in glob.glob(path):
```

```
    #print(file)
```

```
    img = cv2.imread(file,-1)
```

```
    clahe = cv2.createCLAHE(clipLimit=2.0, tileGridSize=(8,8))
```

```
    cl_img = clahe.apply(img)
```

```
    #kkk = cl_img
```

```
    #kkk = cv2.normalize(kkk,None,0, 65535, cv2.NORM_MINMAX, cv2.CV_16U)
```

```
    basename = os.path.basename(file)
```

```
    name = os.path.splitext(basename)[0]
```

```
    cv2.imwrite("0_outputFromCLAHE/"+name+ ".tif",cl_img)
```

And finally, after pre-processing, all the images will be saved to a folder with its corresponding extensions automatically.

A.2. Code for Bilateral smoothening

In the same way, the code for Bilateral is also written Anaconda Navigator:spyder.

Initially all the packages has to be added for the purpose of the bilateral filtering.

```
import cv2
import glob
#from skimage.filters import gaussian
from skimage import img_as_ubyte, io, img_as_float
import numpy as np
from matplotlib import pyplot as plt
import os.path

path = "2_inputForBilateral/*.*)"
img_number = 1

for file in glob.glob(path):
    #print(file)
    img = cv2.imread(file,0)

    bilateral_cv2 = cv2.bilateralFilter(img, 5, 20, 100, borderType=cv2.BORDER_CONS

    kkk = bilateral_cv2
    kkk = cv2.normalize(kkk,None,0, 65535, cv2.NORM_MINMAX, cv2.CV_16U)

    basename = os.path.basename(file)
    name = os.path.splitext(basename)[0]

    cv2.imwrite("2_outputFromBilateral/"+name+ ".tif",kkk)
```

As said in the previous code for CLAHE, the images will be imported first and then the smoothening occurs and at last the images will be saved with the same extension.

When it comes the combination of filters, then these codes can be combined and the outputs from one of the filter is given as a inout for the other filter and the results can be taken out finally.

B | Appendix B

In this appendix, let's look into the working of the sobel operator.

Basically sobel operator is an edge detector. Before looking into the operator, let's look how to model edges mathematically.

B.1. Mathematical modelling of edges in an image

In this section, the complete description of modeling the edges will be discussed. Lets start with an over-simplified example. A gray scale image of 10x1 pixels is considered as shown in the Figure B.1.



Figure B.1: Image representing a gray scale image of 10x1 pixels

From the image, it can be clearly observed at the middle of the scale that, there is a sudden change in the intensity of the scale. This sudden change in the intensity in an image is known as the edge in an image. Figure B.2 (a) represents the pixel intensity graph of the above mentioned gray scale varying between -1 (the lowest intensity-black) and the 1 (the highest intensity-white). Mathematically, we can plot the sudden change in the curve by plotting the slope of the curve. This can be done by taking the first derivative at each point along the curve. Figure B.2 (b), the orange curve is the slope of the graph that has been taken at each point on the curve. It can be observed that the graph reaches a maximum at the middle and then drops. This peak corresponds to the edge which is being represented in the original image (Figure B.1).

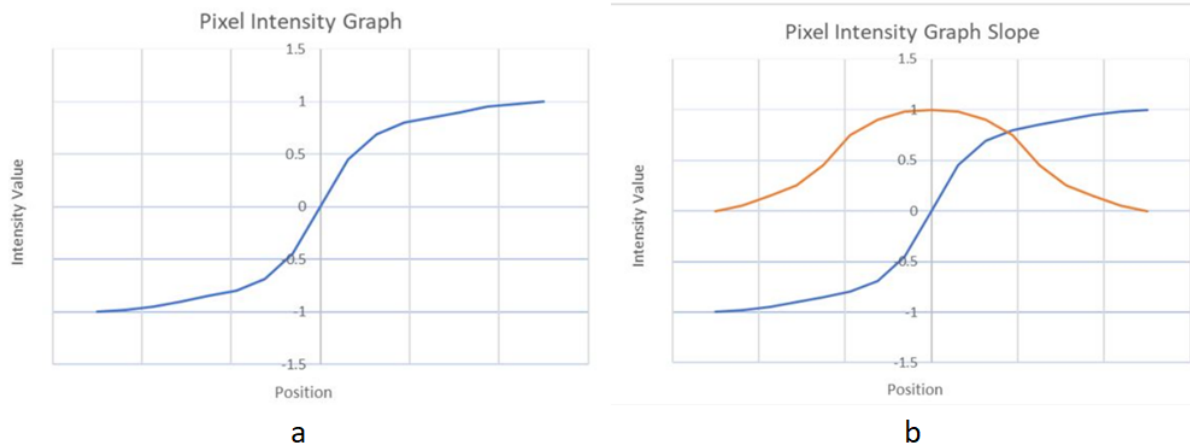


Figure B.2: Graphs representing the Pixel intensity, one (a) just the pixel intensity and the other (b) with its slope

It is very important to note at this point is that, the graph that is shown is a continuous one but the pixel intensity values are discrete. Therefore, in image processing, the first derivatives of an image cannot be evaluated using the standard calculus methods, instead to evaluate the derivatives of the image, a mathematical operation known as convolution has to be used. In the coming section, the convolution operation has been discussed clearly.

B.2. Convolution Operation

In this section, we will see how the convolution operation has been performed given an image as input.

-1	-2	-1
0	0	0
1	2	1

Figure B.3: Figure just showing an example for the Kernel matrix

In order to perform a convolution, the basic mathematical tool that is required known as a Kernel (or just a filter). Kernel is nothing but a matrix. Below in Figure B.3, there is

an example of a kernel of 3x3 matrix. Now, lets see how to estimate the first derivatives of an image by doing a convolution calculation.

Now lets take an image as shown in Figure B.4(a), which is a colour image having a resolution of 6x6. Usually a colour image has three channels(that is red, green and blue). But fo edge detection, only one channel is enough. Mostly in all the algorithms including the sobel, the first step would be to convert the image to a gray scale image. After converting the original image to a gray scale image, it would look like the image in Figure B.4 (b).

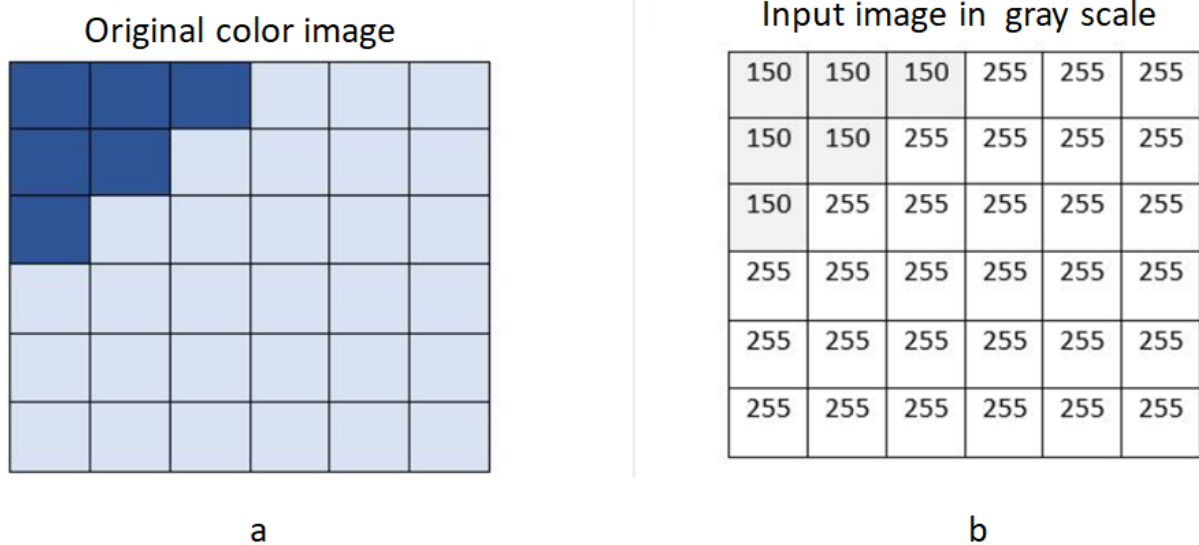


Figure B.4: (a) representing the original image and (b) representing the original image after converting into a gray scale

In order to perform the convolution of the matrix B.4(b) with the matrix B.3, firstly the matrix B.3 should overlay on the upper-left portion of the matrix B.4(b) and then perform an element-wise product. It has been clearly mentioned in Figure B.5(a) and (b). In Figure B.5 (a), there occurs a elemt wise multiplication for the upper-left portion of the gray scale matrix. After multiplying, the result matrix is shown in Figure B.5(b). Now all the elements in the matrix B.5(b) would add up and becomes the first element for the output matrix B.5(c) (that is the matrix after convolution).

Now, the kernel moves to the next portion on the gray scale matrix and a similar matrix is being evaluated and then the elements in that matrix adds up and becomes the second element of the output matrix. In this way, the output matrix gets filled up.

$150 * -1$	$150 * -2$	$150 * -1$	255	255	255
$150 * 0$	$150 * 0$	$255 * 0$	255	255	255
$150 * 1$	$255 * 2$	$255 * 1$	255	255	255
255	255	255	255	255	255
255	255	255	255	255	255
255	255	255	255	255	255

a

-150	-300	-150
0	0	0
150	510	255

b

Output Image			
315			

c

Figure B.5: (a) gray scale matrix with the element wise multiplication for the upper-left portion and (b) shows the upper-left portion after the element-wise multiplication

So, this is how the convolution works and the present section was only to observe the working of the convolution. Now lets look into the sobel operator and how this convolution works with sobel operator.

B.3. Working of sobel operator

The sobel operator uses kernel mentioned in Figure 3.11 and the convolution operation (as described in the previous section) to detect the edges. Lets deeply look into the working of sobel operator.

- Let gradient approximations in x-direction be denoted as G_x .
- Let gradient approximations in y direction be denoted as G_y .

Lets assume a gray scale image as shown in Figure B.6. In order to calculate the G_x and G_y , the center pixel has to be chosen from the original image and to that central pixel, the surrounding 3x3 matrix has to be convoluted with the sobel kernels in both x and y directions.

Original source image in gray scale with intensity values

150	150	150	255	255
150	150	255	255	1
150	255	255	1	1
255	255	1	1	1
255	1	1	1	1

Figure B.6: An example gray scale image with intensities to perform the sobel operator

150	150	150	255	255
150	150	255	255	1
150	255	255	1	1
255	255	1	1	1
255	1	1	1	1

x-direction kernel

-1	0	1
-2	0	2
-1	0	1

150	150	150	255	255
150	150	255	255	1
150	255	255	1	1
255	255	1	1	1
255	1	1	1	1

y-direction kernel

-1	-2	-1
0	0	0
1	2	1

Figure B.7: Figure representing the original image, the matrix to be convoluted and the respective kernel matrices

In Figure B.7, the top 3x3 matrices marked with dark lines are chosen for convolution with the yellow marked region as center. As described in the previous section, the convolution has to be performed for the marked matrix.

As a result, for the matrix with yellow region as center, the gradient approximation in x direction (Gx) and the gradient approximation in y direction (Gy) are 315 and 315 respectfully. Now we need to combine the above obtained values to calculate the magnitude of gradient for the matrix marked with yellow region as center.

$$\text{Magnitude}(G) = \sqrt{Gx^2 + Gy^2}$$

$$\text{Magnitude}(G) = \sqrt{315^2 + 315^2}$$

Now the Magnitude is approximately equal to 445.

This magnitude above is just for the single matrix with the yellow marked region as center. The same has to be performed for all the other 3x3 regions in the image.

And once all those calculations has been completed, **the pixels with the highest magnitude (G) are likely part of an edge.**

So, this is the working of a sobel operator.

C | Appendix C

In this appendix, let's look into how the histogram equalization started, its advantages and disadvantages and how the histogram equalization evolved till CLAHE.

C.1. Histogram Equalization

As discussed in the subsection 3.1.2, histogram equalization is nothing but stretching the histogram of an image which are concentrated to its complete scale. Lets understand this with examples.

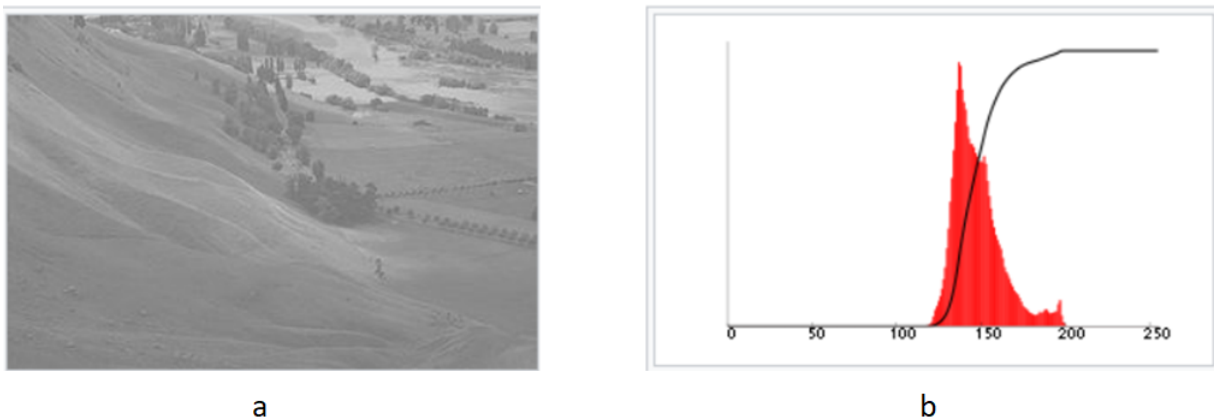


Figure C.1: (a) Image before histogram equalization, (b) Histogram of the chosen image (red-histogram, black-cumulative histogram)

In the Figure C.1(a), the image needs the enhancement of contrast. This is because the details in the image is very hard to notice. The Figure C.1(b) represents the histogram of the Figure C.1(a). It is seen that the histogram is concentrated to a certain region. Due to this, the details in the image are unnoticeable. So, in this histogram equalization technique, the graph in Figure C.1(b) is stretched to the complete region of the graph(that is stretched for all the intensities). By doing so, the global contrast of the image has been enhanced. This allows for areas of lower contrast to gain a higher contrast.

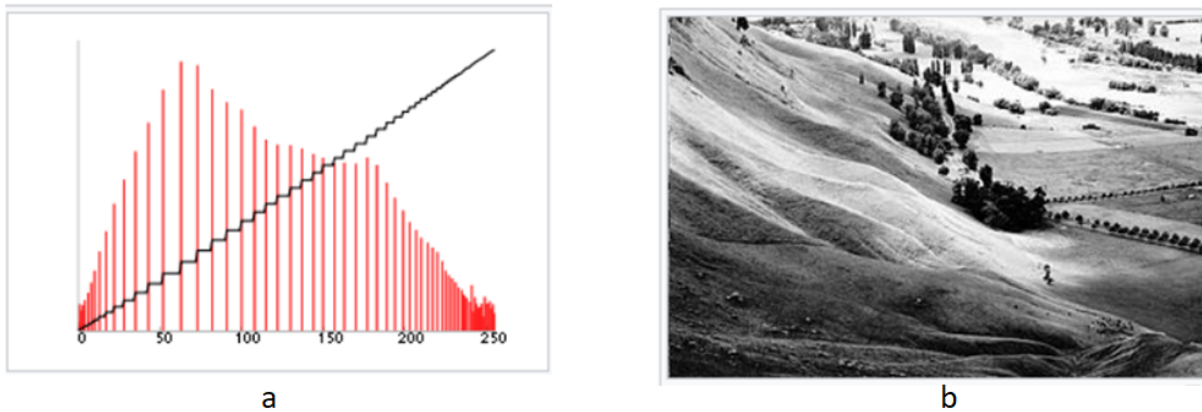


Figure C.2: (a) Histogram of the chosen image after stretching (red-histogram, black-cumulative histogram), (b) Image after histogram equalization

The Figure C.2(a) represents the histogram after stretching out the intensity range. This can result in a better image than the original one. This can be observed in Figure C.2(b). Now the details in the image are observable. But the major disadvantage of this equalization technique is that, since the equalization happens with the histogram of the complete image, this either produces too bright regions or too dark regions in the image. Because of this, few accurate details that are required might be missing in the image.

C.2. Adaptive Histogram Equalization

To overcome the above mentioned limitation, the adaptive histogram equalization method has been introduced. Instead of looking into the histogram of the complete image (as happened in the histogram equalization method), this method looks into the histogram of the local regions and try to stretch it locally. Lets see how this works.

Initially, the complete image will be split into number of windows according to the user. Then the histogram is drawn for each window for the complete image. And those local histograms for each window will be equalized locally. Due to this, too bright regions or too dark regions in the pre-processed image can be avoided. Lets look with the help of an example.

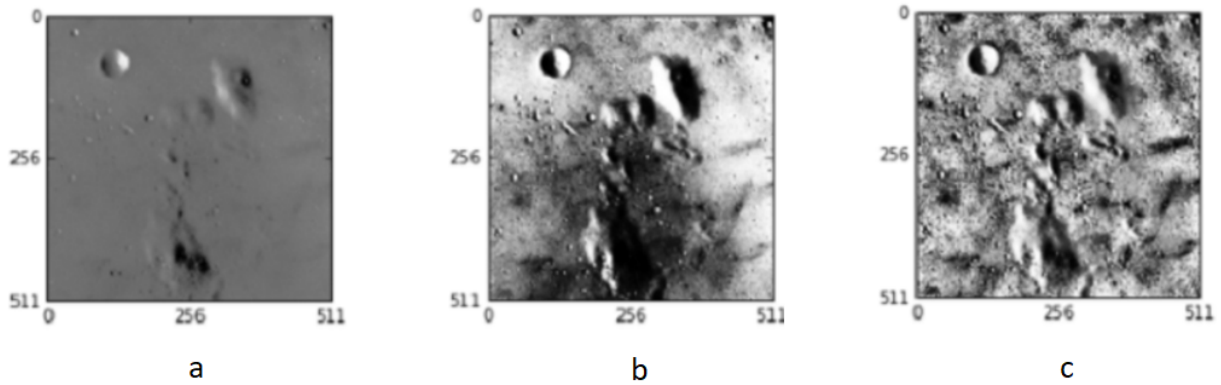


Figure C.3: (a) Original image; (b) Image enhanced with histogram equalization; (c) Image enhanced with adaptive histogram equalization.

Now Figure C.3(a) represents the original image. In this image it is really hard to find any details. Hence this image has to be enhanced in order to obtain any kind of information. Figure C.3(b) is the image enhanced with histogram equalization. Here some information can be captured since there are few available details after enhancement. But as we discussed in the earlier, there are too bright and dark regions in the image due to which there might be few more details that are missing. Finally Figure C.3(c) is enhanced with adaptive histogram equalization. Here there are lot more details that are observable. point to be noted is that, the original image with lot of missing information in it is now able to provide more details when enhanced with the adaptive histogram equalization. The major two drawback of this adaptive histogram equalization is that, its slow speed and the over-enhancement of noise locally [18]. To overcome this issue, the adaptive histogram equalization has been updated with the Contrast Limited Adaptive Histogram Equalization (CLAHE).

C.3. Contrast Limited Adaptive Histogram Equalization (CLAHE)

Contrast Limited Adaptive Histogram Equalization (CLAHE) differs from Adaptive Histogram Equalization in its contrast limiting. In order to limit the drastically enhanced contrast as well as the noise, this limitation applies to the adaptive histogram equalization. This also speeds up the filter. Here in this section we will just observe an image as an example and discuss about it.

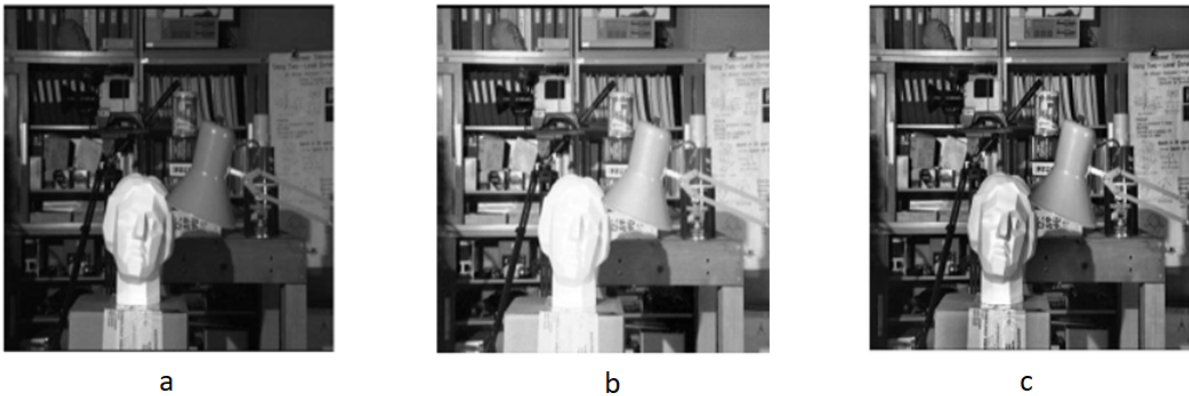


Figure C.4: (a) Original image; (b) Image enhanced with adaptive histogram equalization; (c) Image enhanced with contrast limited adaptive histogram equalization.

Figure C.4(a) is the original image that require contrast enhancement. Figure C.4(b) is the image after enhancing with adaptive histogram equalization. since there is no limitation for the contrast, it can be observed that at few regions the contrast has been over amplified. because of that, few information are not that clear to observe. Then Figure C.4(c) is the image enhanced with CLAHE. Here since, there is a limitation of how much the contrast has to enhance, the image doesn't have any over amplification of the contrast.

This CLAHE is one of the most important filter for enhancing the contrast and this filter is used in many fields. Coming to PIV, since most of the images require the enhancement of contrast, this CLAHE is one of the most important filter.

The code that is used for this filter is being written in Appendix A.

List of Figures

1.1	Position of tracers particles at two different instants of time, t1 and t2. Picture taken from [19]	2
1.2	Experimental arrangement for planar PIV in a wind tunnel. This image has been taken from [19]	5
1.3	Representation of an interrogation window in a complete image and the detection of peak for those two interrogation windows after cross-correlating. (The image has been taken from seika digital images)	6
1.4	Example representing the correlation map for describing the primary peaks and the peak ratio. The image has been taken from [29]	8
1.5	Figure representing the displacement peak and the peak due to noise in the raw image. The image has been taken from the article [28]	9
2.1	Schematic representation of the short-duration compression tube turbine test facility at Von Karman Institute for fluid dynamics. The image has been taken from [3]	12
2.2	Sectional view of the test section that is being marked in the red box . . .	13
2.3	Overview of optical access containing test section downstream of rotor row	14
2.4	Image of the calibration scale used for PIV evaluation	16
3.1	Figure representing the raw images(a-d) captured at the first four consecutive time intervals.	20
3.2	Conceptual example of contrast normalization using min/max intensity normalization for a one-dimensional signal. Picture for the PIV book by Adrian and Westerweel (2011).	21
3.3	image (a) is the raw image captured and image (b) is the image after applying the filter Min/Max intensity Normalization	22
3.4	The red box drawn on the raw image(left-side figure is the raw image) is observed closely before and after applying the Min/Max intensity Normalization	23

3.5	Left-side image is the raw image. In the right-side, the correlation map is observed for the marked region with red box before and after applying the filter Min/Max intensity Normalization	24
3.6	Left-image is the histogram drawn for a random image and Right-side image is the histogram equalized plot for the same image. Note that this histogram is randomly chosen just to observe how the histogram equalization works	25
3.7	The left side image is the raw image and the right side image is the image filtered with CLAHE	26
3.8	Left image is the raw image and the right side images are the raw image and the pre-processed image with CLAHE in the marked region	27
3.9	Correlation map of the region marked on the raw image(left image is the raw image) and its correlation map after the filter CLAHE	28
3.10	(a) correlation map of the raw image. (b) correlation map of the image pre-processed with Min/Max intensity Normalization. (c) Correlation map of the image pre-processed with CLAHE	29
3.11	The two convolution kernels that the sobel filter depends on.	31
3.12	Diagonal kernel that is being used for the sobel filter in our case. Data has been taken from the DAVIS user manual	31
3.13	Left side image is the raw image and the right side image is pre-processed with the sobel filter	32
3.14	left image is the raw image and the right side images are the images before and after the sobel filter is applied for the region mention with red box	32
3.15	left image is the raw image, middle image is the pre-processed image with SOBEL (OpenCV) and the right most image is the image pre-processed with SOBEL (DAVIS 8.4)	33
3.16	Comparison of correlation map for the raw image and between the software DAVIS 8.4 and the OpenCV	34
3.17	Correlation map of the region marked on the raw image(left image is the raw image) and the same map after applying the sobel filter	35
3.18	Representation of the complete and cropped image before and after applying the temporal filter	36
3.19	Correlation map for the marked region in the left image(raw image) before and after applying the temporal filter	36
3.20	Left side image is the raw image, middle image is the reconstructed image with 100 percent particle recovery and the right most image is the background that has been removed from the raw image	38

3.21	correlation map of the marked region in the left image(raw image) before and after the POD filter applied	39
3.22	Left side image is the raw image, middle image is the reconstructed image with 98 percent particle recovery and the right most image is the background that has been removed from the raw image	40
3.23	Comparison of correlation map between 100 percent particle recovery and 98 percent particle recovery with POD filter	40
3.24	left image is the raw image, middle one is pre-processed with Bilateral filter and the right most in pre-processed with Gaussian filter	42
3.25	Correlation map comparison between the Bilateral filter and the Gaussian filter of the raw image	43
3.26	Left most image is the raw image, middle image is pre-processed with only CLAHE and the right most image is the combination of CLAHE and Lowpass (Bilateral)	45
3.27	Comparison of correlation map between the raw image and the combination CLAHE and Lowpass (Bilateral)	46
3.28	From left side, 1st image is the raw image, 2nd image is pre-processed image only with CLAHE, 3rd image is a combination of CLAHE and Lowpass (Bilateral) and finally 4th image is the combination of CLAHE, lowpass (Bilateral) and Highpass (Sobel)	47
3.29	Correlation map comparison for raw image, Combination (CLAHE + Lowpass (Bilateral)) and the combination (CLAHE + Lowpass (Bilateral) + Highpass (Sobel))	47
3.30	Comparison of Axial component of velocity for the raw image and the combination (CLAHE + Lowpass (Bilateral) + Highpass (Sobel))	49
3.31	Comparison of correlation map for two different combinations; (a) Combination (CLAHE + POD + Lowpass (Bilateral)); (b) Combination (CLAHE + Lowpass (Bilateral) + POD)	50
3.32	From left side, 1st image is the raw image, 2nd image is pre-processed image only with CLAHE, 3rd image is a combination of (CLAHE + POD with 100 percent particle recovery) and finally 4th image is the combination of (CLAHE + POD with 100 percent particle recovery + Lowpass (Bilateral))	51
3.33	Comparison of correlation map between the raw image and the combination (CLAHE + POD with 100 percent particle recovery + Lowpass (Bilateral))	51

3.34	Comparison of correlation map; (a) raw image; (b) Combination (CLAHE + POD with 100 percent particle recovery + Lowpass (Bilateral)); (c) Combination (CLAHE + POD with 98 percent particle recovery + Lowpass (Bilateral))	52
3.35	(a) raw image representing a background reflection ; (b) raw image representing the region where the density of the particles is low	53
3.36	Comparison of instantaneous axial component of velocity; (a) raw image; (b) combination (CLAHE + Lowpass (Bilateral) + Highpass (Sobel)); (c) Combination (CLAHE + POD with 100 percent particle recovery + Lowpass (Bilateral)); (d) Combination (CLAHE + POD with 98 percent particle recovery + Lowpass (Bilateral))	54
3.37	Comparison of correlation map for different combinations; (a) raw image; (b) combination (CLAHE + Lowpass (Bilateral) + Highpass (Sobel)); (c) Combination (CLAHE + POD with 100 percent particle recovery + Lowpass (Bilateral)); (d) Combination (CLAHE + POD with 98 percent particle recovery + Lowpass (Bilateral))	55
3.38	Comparison of instantaneous axial component of velocity; (a) raw image; (b) combination (CLAHE + Lowpass (Bilateral) + Highpass (Sobel)); (c) Combination (CLAHE + POD with 100 percent particle recovery + Lowpass (Bilateral)); (d) Combination (CLAHE + POD with 98 percent particle recovery + Lowpass (Bilateral))	56
3.39	Comparison of correlation map for different combinations; (a) raw image; (b) combination (CLAHE + Lowpass (Bilateral) + Highpass (Sobel)); (c) Combination (CLAHE + POD with 100 percent particle recovery + Lowpass (Bilateral)); (d) Combination (CLAHE + POD with 98 percent particle recovery + Lowpass (Bilateral))	57
3.40	Figure representing the comparison between the raw (a) and the SOBEL(b), POD(c) for the retaining the pattern in the image after Pre-processing . . .	58
3.41	Comparison for improvement of number of vectors in different combinations;(a) combination (CLAHE + Lowpass (Bilateral) + Highpass (Sobel)); (b) Combination (CLAHE + POD with 100 percent particle recovery + Lowpass (Bilateral)); (c) Combination (CLAHE + POD with 98 percent particle recovery + Lowpass (Bilateral))	59
3.42	(a) Instantaneous raw image without pre-processing; (b) Image after pre-processing; (c) number of vectors improved for a set of images	60

4.1	Comparison of Instantaneous axial component of velocity and the correlation map for the case 3,4 and 5	63
4.2	Comparison of Instantaneous axial component of velocity and the correlation map for the case 12,21 and 22	64
4.3	Comparison of Instantaneous axial component of velocity and the correlation map for the case 12,13 and 14	65
4.4	Comparison of Instantaneous axial component of velocity for two different frames for the case 12,24 and 25	66
4.5	Comparison for improvement of number of vectors	67
5.1	Thickness of the laser sheet representing the out-of-the-plane vector components	69
5.2	Illustration of an out of plane particle displacement and zero in-plane shift. A camera with the optical axis in negative Z direction will observe a particle image shift in x and y direction even if only motion in Z direction is present. The particle displacement is biased and the magnitude and direction depends on the observation angle α with respect to the optical axis. This image has been taken from [19]	70
5.3	Sketch representing, how a single out of the plane component is plotted in the digital plane (observing the laser sheet thickness from side view)	71
5.4	Sketch representing the same laser sheet thickness but observing it from the top view	72
5.5	Sketch representing how the out-of-the-plane components show a rotation in the digital plane	73
5.6	Graph representing the out of the plane components in a two dimensional plane having a scaling factor of the length of the vectors as 5. (X-axis = axial direction, Y-axis = tangential direction)	75
5.7	Graphs in the figure just represent the scaled up length of the vector when compared with the original vector.	76
6.1	In the top left, axial component of velocity with representation of the region that corresponds to the PIV and to the 4 hole probe; in the top right, 1st contour corresponds to the RANS and the last contour corresponds to the PIV; Bottom figures corresponds to the comparison of velocity profiles at different sections	78

6.2	In the top left, tangential component of velocity with representation of the region that corresponds to the PIV and to the 4 hole probe; in the top right, 1st contour corresponds to the RANS and the last contour corresponds to the PIV; Bottom figures corresponds to the comparison of velocity profiles at different sections	79
B.1	Image representing a gray scale image of 10x1 pixels	91
B.2	Graphs representing the Pixel intensity, one (a) just the pixel intensity and the other (b) with its slope	92
B.3	Figure just showing an example for the Kernel matrix	92
B.4	(a) representing the original image and (b) representing the original image after converting into a gray scale	93
B.5	(a) gray scale matrix with the element wise multiplication for the upper-left portion and (b) shows the upper-left portion after the element-wise multiplication	94
B.6	An example gray scale image with intensities to perform the sobel operator	95
B.7	Figure representing the original image, the matrix to be convoluted and the respective kernel matrices	95
C.1	(a) Image before histogram equalization, (b) Histogram of the chosen image (red-histogram, black-cumulative histogram)	97
C.2	(a) Histogram of the chosen image after stretching (red-histogram, black-cumulative histogram), (b) Image after histogram equalization	98
C.3	(a) Original image; (b) Image enhanced with histogram equalization; (c) Image enhanced with adaptive histogram equalization.	99
C.4	(a) Original image; (b) Image enhanced with adaptive histogram equalization; (c) Image enhanced with contrast limited adaptive histogram equalization.	100

List of Tables

2.1	Parameters and their quantities that the test facility at Von Karman Institute for fluid dynamics can achieve which are similar to the engine operating conditions	11
3.1	Table representing different image pre-processing with their respective filters	19
4.1	Table representing the test matrix that has to be evaluated	62
5.1	Table showing the quantities that has been evaluated, for uncertainty due to the out of the plane components	74

List of Symbols

Variable	Description	SI unit
\mathbf{u}	solid displacement	m
\mathbf{u}_f	fluid displacement	m
\mathbf{x}_1	distance between the nose of the out-of-the-plane velocity component and the optical axis	m
\mathbf{x}_2	length of the individual out-of-the-plane velocity component	m
\mathbf{x}_3	the perpendicular distance between the optical center and the corresponding vector in the digital plane	m
\mathbf{x}_4	length of the out-of-the-plane vector in the digital plane	m
\mathbf{x}_5	the distance between the optical center and the tail of the velocity component in the digital plane	m
\mathbf{x}_6	the Y coordinate in the digital plane	m
\mathbf{x}_7	the X coordinate in the digital plane ($\mathbf{x}_7 = \mathbf{x}_3 + \mathbf{x}_4$)	m
\mathbf{y}_1	the perpendicular distance between the optical center and the nose of the out-of-the-plane velocity component	m
α_1	the angle between \mathbf{x}_1 and \mathbf{y}_1 (from diagram)	deg
α_2	the angle between $(\mathbf{x}_1 + \mathbf{x}_2)$ and \mathbf{y}_1 (from diagram)	deg
β_1	the angle between \mathbf{x}_3 and \mathbf{f}	deg
β_2	the angle between $(\mathbf{x}_3 + \mathbf{x}_4)$ and \mathbf{f}	deg
γ	the angle between the \mathbf{x}_1 and the axial coordinate of the laser sheet	deg
ϕ	the amount of twist that happens in the plane that joins the optical center to the nose and tail of the out-of-the-plane velocity component	deg

Acknowledgements

Initially, I would like to thank Prof. Gaetani Paolo for providing me with this opportunity. Secondly, I would like to thank my co-advisor Prof. Sergio Lavagnoli for accepting me for doing the thesis at Von Karman Institute for fluid dynamics which is one of the well-known research institutes. Finally, I would like to thank Mr. Mizuki Okada, PhD student at VKI, who continuously guided me during the whole course of my thesis work.

